HSP70: a therapeutic biomarker for treatment of glioma

By

Harshada Shashikant Patil

A thesis submitted to the University of Central Lancashire in partial fulfilment of the requirements for the degree of Doctor of Philosophy.

June 2015

Declaration

I declare that while registered as a candidate for the research degree, I have not been a registered candidate or enrolled student for another award of the University or other academic or professional institution. I declare that no material contained in the thesis has been used in any other submission for an academic award and is solely my own work

Signed

Harshada S Patil

Type of Award **Doctor of Philosophy (PhD)**

School **Pharmacy and Biomedical Sciences**

Abstract

Gliomas are amongst the most malignant, invasive and recurrent forms of brain tumour with very short survival rate due to high chemoresistance. Recently, highly inducible molecular chaperones HSP70 and HSP90 are emerging as important anti-cancer targets. Previously, proteomic analysis had demonstrated that post-induction of HSP70 on HSP90 inhibition undermines the efficacy of treatment. The present study has quantified transcriptional levels and Akt/PKB activity of *Hsp70* and *Hsp90α* in glioma cell lines. In order to evaluate the therapeutic value of both chaperones, HSP70 and HSP90 were targeted in glioma cells U87-MG using VER-155008 and 17-AAG, respectively. Improved efficacy of HSP70 and HSP90 inhibitors was evaluated using a chemosensitivity assay. MicroRNAs (miRNAs) are highly conserved small non-coding RNA molecules (21-24 nucleotides) that regulate simultaneously the expression of hundreds of mRNA targets, and are reported to be aberrantly expressed in glioma. Therefore, miRNA microarray technology was used to evaluate the efficacy of these inhibitory drugs compared with Temozolomide (TMZ) which is used as a standard treatment for glioma. Microarray data identified 154 miRNAs using either stringent or non-stringent parameters. 16 miRNAs were overlapped with treatments, 15 were upregulated, while 13 were overlapped between Temozolomide and VER-155008. In Temozolomide and VER-155008 treatment, Hsa-miR-194p was upregulated by 139 and 63 fold, respectively, Hsa-miR-215 was upregulated 165 and 61 fold, respectively, Hsa-miR-449a was upregulated by 62 and 77 fold, respectively and Hsa-miR-744-5p was upregulated by 63 and 43 fold, respectively. 17-AAG and VER-155008 treatment shown only one miRNA overlapping with 29 and 2 fold change, respectively. Hsa-miR-4636 was the only downregulated miRNA in TMZ and VER treatment with a 32 and 33 fold change, respectively. The miRNA target prediction

software was used for the highly upregulated miRNAs: hsa-miR-194-5p, hsa-miR-215, hsa-miR-449a, hsa-miR-744-5p and hsa-miR-3161 correlating to *Dnmt3a, Alcam, Cdk4, Dnajc16 (Hsp40)* and *R-Ras2* genes, respectively. Gene validation using qRT-PCR suggested no correlation between miRNA-mRNA levels, and thus, challenges the suitability of miRNAs technology as treatment predictors. In conclusion, the result for the protein data showed that HSP70 was inhibited on treatment with Temozolomide, 17-AAG and VER-155008 to 13, 0 and 20 %, respectively, while HSP90 inhibition was 84, 43 and 65 %, respectively, reflecting the affinities of these three compounds towards HSP90 compared to HSP70, and therefore infers that HSP70 could be a stronger therapeutic approach. In conclusion the result of the study has clearly demonstrated that HSP70 can be better therapeutic biomarker for treatment of glioma.

Table of Contents

List of Figures

List of Tables

Acknowledgements

I wish to express my most sincere gratefulness to my supervisors, Dr Leroy Shervington and Dr Amal Shervington, for the immense patience they have shown during the past three years and the constant support and guidance. They have not just guided me with my research, but also taught me to be a better researcher and to make the most of every opportunity. I consider myself extremely lucky for receiving the opportunity to work under the supervision of such wise Gurus.

I would like to thank my RDT Professor Jaipaul Singh for his support and guidance. I appreciate the contribution from all of my colleagues and staff from the Darwin research labs as they have helped maintain lively environment throughout the research. I would like to take this opportunity to specially thank Dr Zarine Khan, Dr Adi Mehta and Ashish Darekar for their invaluable support and for the knowledge they shared with me. I appreciate the support and help provided by the School of Pharmacy and Biomedical Sciences, UCLan.

I would like to thank Mr and Mrs Hariharan for being my family away from home. I am eternally grateful to my parents, Mrs Manisha Patil and Dr Shashikant Patil, and my brothers, Riddhish and Anvay, for being there at every moment and for having faith in me. I cannot possibly conclude without thanking my grandparents, Mrs Lilavati Patil and Dr Pandharinath Patil for inspiring me to always aim higher.

Finally, my earnest gratitude to all the people in my life for it would not have been possible to complete this research without their enormous support.

Abbreviations

Note: All protein names are written in uppercase such as HSP90α or HSP70 while the gene names are italicised with capitalised first letter such as *Hsp90α* or *Hsp70* with exception for *GAPDH*.	
17-AAG	17-aminoallylgeldanamycin
17-DMAG	17-dimethylaminoethylamino-17-demethoxygeldanamycin
3'UTR	3' untranslated region
5'UTR	5' untranslated region
ABC	ATP-binding cassette
ABCA3	ATP-binding cassette Family A member 3
ABCB1	ATP-binding cassette Family B member 1
ABCG2	ATP-binding cassette Family G member 2
ADD70	AIF derived decoy 70
AGE	Agarose gel electrophoresis
Ago	Argonaute
Ago2	Argonaute2
AHA1	Activator of Hsp90 ATPase homologue 1
AIF	Apoptosis inducing factor
ALCAM	Activated leukocyte cell adhesion molecule
APAF-1	Apoptotic protease activating factor 1
ATCC	American type culture collection
ATP	Adenosine 5’-tri-phosphate

Bad	Bcl-2-associated death promoter
BAG-1	BAG family molecular chaperone regulator 1
BCL-2	B-cell lyphoma-2
BCRP1	Breakpoint cluster region pseudogene 1
BMI-1	B lymphoma Mo-MLV insertion region 1 homolog (Oncogene)
bp	base pair
B-Raf	B- rapidly accelerated fibrosarcoma
BSA	Bovine serum albumin
cAMP	Cyclic AMP
CBR	Coomassie blue reagent
CCD	Charged coupled device
CD166	Cluster differentiation 166 protein
CD44	Cluster differentiation 44 protein
Cdc37	Cell division cycle 37
CDK4	Cyclin dependent Kinase 4
CDK6	Cyclin dependent Kinase 6
CDKN2A	Cyclin-dependent kinase inhibitor 2A
cDNA	Complementary DNA
CHIP	C-terminus of Hsc70 interacting protein
CIP	Calf intestinal alkaline phosphatase
CNS	Central nervous system
COX2	Cyclooxygenase 2

cRNA	Complementary DNA
ct	Cycle threshold
CyP40	Cyclophilin 40, an immunophilins
DGCR8	DiGeorge syndrome critical region gene 8 (microprocessor complex)
DMEM	Dulbecco's modified eagle's medium
DMSO	Dimethylsulphoxide
DNA	Deoxy ribonucleic acid
DNMT3A	DNA methyl transferase 3A
DNMT3B	DNA methyl transferase 3B
DSMZ	Deutsche Sammlung von Mikroorganismen und Zellkulturen
ECACC	European Collection of Cell Cultures
EDTA	Ethylenediaminetetraacetic acid
EGFR	Epidermal Growth Factor Receptor
ELISA	Enzyme-linked immuno-sorbent assay
EMEM	Eagle's minimum essential medium
EMT	Epethelial mesenchymal transition
ERK	Extracellular signal regulated kinase
EtBr	Ethidium bromide
FADD	Fas-associated protein with death domain (FADD)
FBS	Foetal bovine serum
FC	Fold change
FDR	False discovery rate

GA	Geldanamycin
GAPDH	Glyceraldehyde-3-phosohate dehydrogenase
GBM	Glioblastoma multiforme
GLUT-1	Glucose transporter 1
GRP78	78 kDa glucose-regulated protein
GRP94	94 kDa glucose-regulated protein
GTP	Guanosine-5'-triphosphate
HCC	Hepato cellular carcinoma
HDJ1	DnaJ (Hsp40) homolog
HER2	Human epidermal growth factor receptor 2
HIF-1α	Hypoxia-inducible factor-1α
HIP	Hsp90 interacting protein
HOP	Hsp70-Hsp90 organizing protein
HRP	Horseradish peroxidase
HSC70	Heat shock cognate 71 kDa protein
HSE	Heat shock element
HSF-1	Heat shock factor-1
HSP	Heat shock protein
HSP27	Heat shock protein 27kDa
HSP40	Heat shock protein 40kDa
HSP60	Heat shock protein 60kDa
HSP70/HSPA8	Heat shock protein 70kDa

HSP90	Heat shock protein 90kDa
HSP90N	Hsp89αΔN, Hsp90 isoforms
HSP90α	Hsp90 isoforms (inducible)
HSP90β	Hsp90 isoforms (constitutively expressed)
HSPBP1	Hsp70-binding protein 1
HSR	Heat shock response
IC_{50}	Inhibitory concentration 50%
IgG	Immunoglobulin G
MAPK AP	MAP kinase-activated protein kinase
MDR	Multi drug resistance
MDR1	Multi drug resistance gene 1
MGMT	O^6-methlyguanine-DNA-methyltransferase
miR	micro RNA (mature)
miRNA	micro RNA
MMP2	Matrix Metalloproteinase 2
mRNA	messenger RNA
MTIC	Methyltriazen-1-yl imidazole-4-carboxamide
NBD	Nucleotide binding domain
NCBI	National center for biotechnology information
NEAA	Non-essential amino acid
NF-κB	Nuclear factor-κB
NSCLC	Non-small cell lung carcinoma

NSG	Next generation sequencing
nt	Nucleotides
p23	protein 23
p53	protein 53
PBS	Phosphate buffer saline
PC	Personal computer
pCp	Cytidine biphosphate
PCR	Polymerase chain reaction
PI3K	Phosphoinositide 3-kinase
PKB	Protein kinase B
PPE	Personal protective equipment
qRT-PCR	Quantitative real time-PCR
Ran-GTP	RAs-related nuclear protein
RDD	miReasy buffer
RIN	RNA Integrity Number
RISC	RNA-induced silencing complex
RNA	Ribonucleic acid
RNAi	interference RNA
ROS	Reactive oxygen species
RPE	miReasy buffer
Rpm	Rotation per minute
R-RAS	Related RAS viral oncogene homogene

rRNA	Ribosomal RNA
RT	Room temperature
RWT	miReasy buffer
SBD	Substrate binding domain
sHSPs	Small Heat shock proteins
siRNA	Small interfering RNA
SMPs	Streptavidin magnetic particles
SNP	Single nucleotide polymorphisms
TAE	Tris-acetate EDTA
TGF-β	Transforming growth factor-β
TMB	Tetramethylbenzidine
TMZ	Temozolomide
TNF	Tumour inducing factor
TRAIL	TNF-related apoptosis inducing ligand
TRBP	Transactivating response RNA-binding protein
TRP	Tetratricopeptide repeat-binding motif
VEGF	Vascular endothelial growth factor
VER	VER-155008
VGFR	Vascular endothelial growth factor
WHO	World health organization

CHAPTER 1

INTRODUCTION

1.1 Molecular chaperones

In the cellular environment, a set of functional proteins are required to maintain the normal functioning of the cell. The amino acid sequences of these proteins fold itself into the native state to accomplish a variety of functions. However, due to the highly crowded nature of the cellular environment, newly synthesised proteins have a high probability of misfolding or aggregating (Houry *et al.,* 2001). It is essential to ensure the efficiency and accuracy of the protein folding process in order to form active protein conformations. Molecular chaperones play key role in several processes (Figure 1.1). Molecular chaperones are proteins that stabilise conformation of unstable polypeptides (proteins) by regulating binding and release cycles, which facilitate the correct conformational folding and prevent aggregation. They are also essential for protein translocation and normal protein turnover (Whitesell *et al.,* 2005).

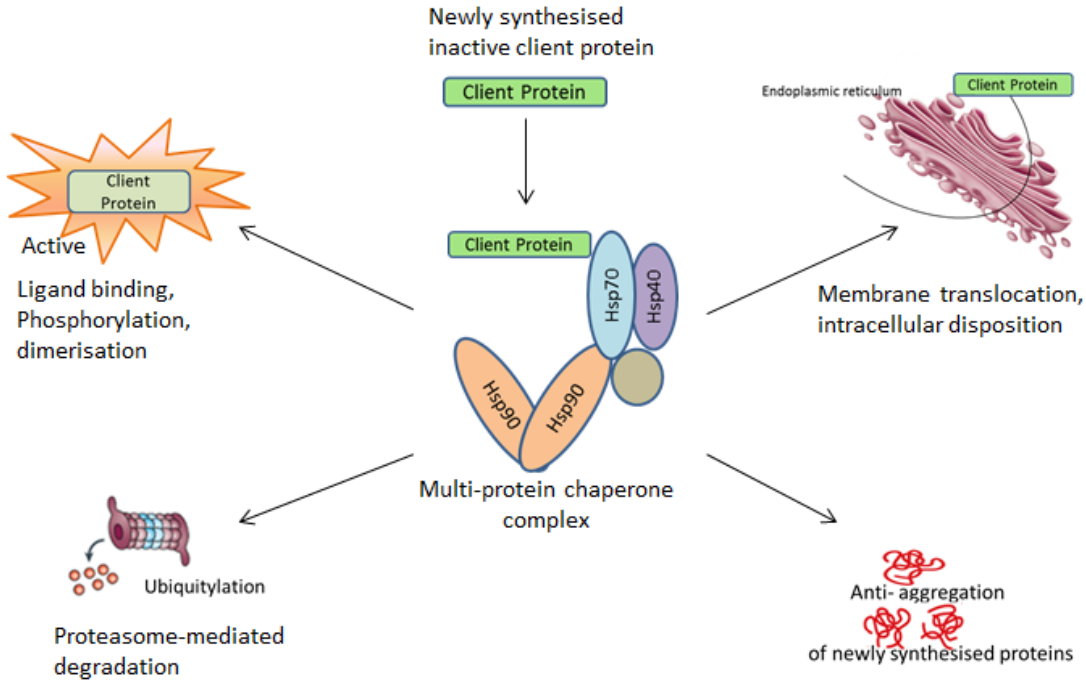

Figure 1.1: Role of molecular chaperones. Above figure describes different role of multiprotein complex (Taken from Whitesell *et al*., 2005).

1.2 Heat Shock Proteins

In stress-like conditions, intracellular milieu induces stress responses inhibiting the activity of housekeeping genes and activating stress genes. This condition results in a group of molecular chaperones being activated. These molecular chaperones are termed stress-proteins or heat shock proteins (HSPs). They are a group of highly conserved and ubiquitous molecular chaperones initially identified on the basis of their amplified synthesis on exposure to elevated temperatures. This observation was first reported by Ritossa in 1962 (Ritossa *et al.,* 1962; Stephanou *et al.,* 2011). They comprise of approximately 5-10% of the total protein content in a normal healthy cell (Soo *et al.,* 2008). A cellular insult such as heat, hypoxia, starvation, sodium arsenite exposure, virus transformation or radiation are associated with induction of protein misfolding or aggregation (Graner *et al.,* 2005). These misfolded or aggregated proteins bind to molecular chaperones causing the release of heat shock factors (HSF), a transcription factor, which activates heat shock element (HSE), located on *Hsp* promotor gene leading to induced HSP concentration. HSPs functions to prevent protein aggregation, induce solubilisation of loose protein aggregates, and escorts denatured polypeptides for proteolytic recycling (Ahner *et al.,* 2005; Calderwood *et al.,* 2006). They participate in refolding of proteins which have been damaged, and sequester damaged proteins and target them for degradation. HSPs are mainly classified and defined according to their molecular weights namely (as shown in Table 1.1): HSP100 (100kDa), HSP90 (90kDa), HSP70 (70kDa), HSP60 (60kDa), HSP40 (40kDa) and small HSPs (sHSP) with a molecular size ranging between 15 to 30 kDa (Soo *et al.,* 2008; Powers *et al.,* 2012). On the basis of location, they accomplish different functions. HSPs with high molecular weights are ATP-dependent as they assist newly synthesised or damaged proteins in ATP-dependent processes, while HSPs of low molecular weight function as ATP-independent proteins

(Soo *et al.,* 2008). The overexpression of both HSP70 and HSP90 has been reported in solid tumours and haematological malignancies. The presence of HSPs also contributes towards the survival of malignant cells by maintaining protein homeostasis and also helps in tolerating genetic alterations. Apart from cancers, HSPs are also expressed in diseases such as Alzheimer's, Huntington's, amyotrophic lateral sclerosis and cardiovascular diseases, thus, targeting HSPs is of therapeutic importance (Mahalingam *et al.,* 2009; McConnell *et al.,* 2013).

HSP70 and HSP90 can be therapeutic targets in glioma therapy since they are found to interact with hallmarks of cancer proposed by Hanahan and Weinberg. These hallmarks are (i) self-sufficient in growth signalling; (ii) insensitivite to anti-growth signalling; (iii) able to evade apoptosis; (iv) sustain angiogenesis; (v) tissue invasion and metastasis; and (vi) limitless replicative potential (Hanahan *et al.,* 2011). This research focuses on HSP70 and HSP90α as they are abundantly present in various cancers.

Table 1.1: Classification and role of heat shock proteins.

Family	Subunits	Location	Functions	References
HSP90	HSP90α, HSP90β, HSP90N and TRAP-1	Cytosol, mitochondria and nucleus	Play a role in signal transduction by interacting with steroid hormone receptors, tyrosine kinases, serine/threonine kinases; refold and maintain proteins *in vitro*; auto-regulation of the heat shock response; role in cell cycle and proliferation.	(Sato *et al.,* 2000)
HSP70	HSC70, HSP72, GRP75 and GRP78	Cytosol and nucleus	Anti-apoptotic activity; refolds and maintains denatured proteins *in vitro*; role in signal transduction, cell cycle, proliferation and intracellular transporting; interacting with nascent chain polypeptides; auto-regulating heat shock response; potential antigen-presenting molecule in tumour cells.	(Goloudina *et al.,* 2012)
HSP60	HSP60	Cytoplasm, mitochondria, nucleus and Endoplasmic reticulum	Refolds and prevents aggregation of denatured proteins *in vitro*; acts as cofactor in proteolytic systems and facilitate protein degradation	(Lim *et al.,* 2005)
HSP40	HSP40	Cytosol	Plays a role as co-chaperone of HSP70 to enhance ATPase activity	(Fan *et al.,* 2003)
HSP27	HSP27	Cytosol and nucleus	Anti-apoptotic activity; Suppresses aggregation and heat inactivation of proteins *in vitro*; anti-apoptotic activity.	(Lim *et al.,*2005)

1.2.1 HSP70

HSP70 (Heat shock protein 70kDa) is one of the major molecular chaperones which is ubiquitous and present throughout prokaryotes to eukaryotes. There are atleast 8 genes found that code for HSP70 family (Barnes *et al.,* 2001; Davis *et al.,* 2013). Isoforms of the HSP70 family are present in different locations in the cell. Their functions differ according to their location. Constitutively expressed isoform heat shock cognate (HSC70) and stress-induced form HSP70 are two major isoforms located mainly in the cytoplasm while other HSP70 isoforms, mortalin is located in the mitochondria and GRP78 is found in the endoplasmic reticulum (Barnes *et al.,* 2001; Chatterjee *et al.,* 2012). They play important roles of chaperoning in *de novo* synthesis (Nicolaı *et al.,* 2010) and function by assisting nascent protein folding, preventing protein aggregation and protein assembly (Massey *et al.,* 2010). They also act as co-chaperones to the major multiprotein complex HSP90 and function by assisting in the substrate loading phase (Davis *et al.,* 2013).

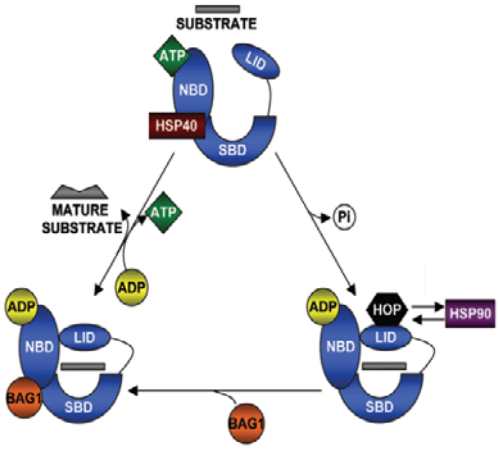

Figure 1.2: Diagrammatic representation of HSP70 conformational activity. (Blue structure represents HSP70, NBD= Nucleotide Binding Domain, SBD = Substrate Binding Domain) (Taken from Powers *et al.,* 2012).

HSP70 proteins comprise of two functional regions, N-terminal nucleotide binding domain (NBD) and a substrate binding domain (SBD) and both of these domains act interdependently. N-terminal NBD (44 kDa) has ATPase activity and binding site for HSP70 co-chaperones. It connects to the C-terminus (27 kDa) which is composed of the SBD and a "lid" region by conserved linkers (Javid *et al.,* 2007). HSP70 forms large multi-protein complexes with various co-chaperones including BAG-1 (BCL2-associated athanogene), HIP (HSC70 Interacting protein), HOP (HSP90/HSP70 Organising Protein), HSP40 (Heat shock protein 40 kDa, HSPBP1 and CHIP (C terminus of HSC70-Interacting Protein) in order to undergo chaperoning (Massey *et al.,*2010). This chaperoning activity is dependent on the ATP hydrolysis cycle (Figure 1.2). HSP70 chaperone complex forms 'open state' when ATP is bound to the NBD and the lid segment of C-Terminus develops low affinity for substrate binding. ATP stimulates peptide binding at SBD inducing conformational change to form 'close state' and thus resulting in increased affinity for peptide substrate binding. This also leads to an increase in the interaction of NBD with co-chaperone HSP40. HSP70 and HSP90 chaperone activity assists substrate maturation by simultaneously interacting with TPR (tetratricopeptide repeat) domain co-chaperones (HOP, CHIP) at the C-terminus of both chaperones. This process is essential for the assembly of both chaperones. To release a peptide substrate, ATP undergoes hydrolysis to form ADP by the interaction of BAG-1 (nucleotide exchange factors) (Jego *et al.,* 2010; Nicolaı *et al.,* 2010; Powers *et al.,* 2012). Thus, along with ATPase activity and peptide binding activity, the HSP70 co-chaperone plays an important role in HSP70 activity and protein substrate specificity (Zylicz *et al.,* 2001). Heat shock proteins are induced due to stress such as heat shock, hypoxia or cancer. In non-stress conditions they play roles as normal molecular chaperones. In normal cellular environments, HSC70 is abundantly expressed while HSP70 is expressed at low basal levels but both are over

expressed in stress conditions which are related with protein misfolding disorders (Nicolaı *et al.,* 2010). Their elevated levels are the outcome of activation of transcription factors HSF-1 and HIF-1α. It has been reported that HSP70 isoforms are overexpressed in various cancers (Beere *et al.,* 2000; Nylandsted *et al.,* 2000). HSP70 is also involved in various pathologic conditions such as neurodegenerative diseases and ischemia, inflammatory processes and immunogenicity. In Multiple Myeloma (MM) cells, HSP70 was found to be strongly upregulated on pharmacological inhibition of HSP90 (Chatterjee *et al.,* 2012). Evidence shows that HSP70 suppresses apoptosis activity and controls cell cycle and cell growth (Beere *et al.,* 2000). HSP70 inhibits apoptosis both upstream via cytochrome-C and Apoptosis–inducing factor (AIF) release and downstream by caspase-3 activation (Guo *et al.,* 2005). HSP70 inhibits apoptosis in U937 lymphoma cells by preventing caspase-3 activation in the presence of active Cytochrome-C (Aghdassi *et al.,* 2007). HSP70 inhibits apoptosis via TRAIL (TNF-related apoptosis inducing ligand) pathway in colon cancer and in cardiomyocytes (Demidenko *et al.,* 2006). In addition, HSP70 has the ability to inhibit apoptosis by caspase independent pathways, preventing DNA fragmentation by interacting with apoptosis inducing factor (AIF) (Li *et al.,* 2000; Guo *et al.,* 2005). Thus, HSP70 with its anti-apoptotic activity encourages cell viability even in malignant cells. As mentioned earlier, various studies have confirmed the expressions of HSP70 in cancers and other diseases. HSP70 acts as co-chaperone to HSP90 forming multi-chaperone complex which is involved in folding and maturation of several key proteins and cancer progression (Shervington *et al.,* 2008).

1.2.2 HSP90

Heat shock protein 90 (HSP90) is one of the most abundant proteins found in both prokaryotes and eukaryotes (Mehta *et al.,* 2011). It is involved in various cellular processes including signal transduction, protein folding, protein degradation. It plays an important role in the folding of newly synthesized proteins and the stabilization and refolding of denatured proteins after stress. The chaperone HSP90 family is further classified as cytosolic HSP90α, HSP90β and HSP90N, endoplasmic reticulum GRP94 and mitochondrial TRAP-1 (Sreedhar *et al.,* 2004). HSP90α expression is highly inducible while HSP90β is considered to be constitutively expressed**.** Under non-stress conditions, it comprises of 1-2 % of total cellular proteins while it increases by 4-6 % under stress conditions (Gallerne *et al.,* 2013). The high expression levels of HSP90α has been associated with tumour progression, enhanced cell cycle regulation and induced cell signalling via tyrosine kinases.

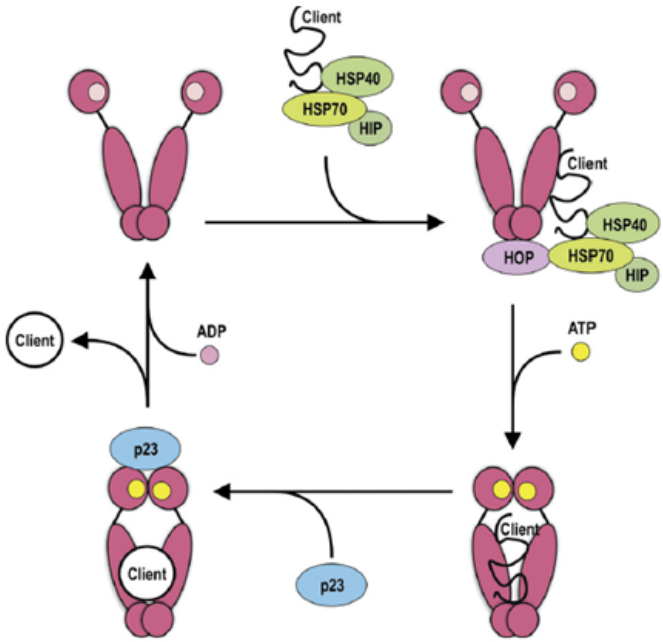

Figure 1.3: Schematic diagram showing the HSP90 ATPase activity. (Pink structure represents HSP90) (Taken from Centenera *et al*., 2013).

HSP90 is a homodimer composed of three functional domains: an N-terminal ATP binding domain, a middle domain having an affinity for client protein binding and C-terminal dimerization domain which regulates ATPase activity as it contains the tetratricopeptide repeat-binding (TRP) motif, EEVD (Javid *et al.,* 2007). Since HSP90 exists as a large multi-chaperone complex, it simultaneously interacts with co-chaperones such as activators of HSP90 ATPase protein 1 (AHA1), HSP70/HSP90 interacting protein (HIP), HSP90 organising protein (HOP), and Tumor protein (p23) to maintain the conformational maturation and stability of key signalling molecules involved in cell proliferation, survival, and transformation via sequential binding or release of involved co-chaperones (Massey *et al.,* 2010). HSP90 chaperone complex cycle involves an open and close state. In the open state, HSP90 in the absence of ATP recruits co-chaperone that assist in client proteins binding. During ATP binding, HSP90 undergoes conformational changes to form the closed state which functions as a clamp that holds client proteins and opens on ATP hydrolysis resulting in client proteins being released (Figure 1.3) (Xiao *et al.,* 2006; Jego *et al.,* 2010). The overexpression of heat shock proteins has been reported in various diseases such as breast cancer, lung cancer, leukaemia, and Hodgkin's disease (Jolly *et al.,* 2000).Over 200 client proteins of HSP90 are involved in this event, maintaining cell survival and thus HSP90 is significant in various cellular functions (Picard *et al.,* 2002; Centenera *et al.,* 2013). Many of the client proteins, such as steroid receptors, epidermal growth factor receptor (EGFR) family members, the MET oncogene, RAF-1 kinases, Akt kinase, BCR-ABL, mutant p53, cyclin dependent kinase 4 (CDK4), hypoxia-inducible factor 1α (HIFα), and matrix metalloproteinase 2 (MMP2), are known to be involved in cancer signalling pathways, thus they are also known as oncoproteins. The role of HSP90 makes it promising target for anti-cancer treatment (Xiao *et al.,* 2006).

1.2.3 HSP70/HSP90 co-chaperones

The heat shock protein families accomplish cellular function along with co-chaperone and clients proteins. The co-chaperones and client proteins are important for maturation of their complexes. HSP70 and HSP90 are involved in various cell survival pathways. HSP90 is a multi-chaperone complex and the HSP70 form co-chaperones to HSP90. Similarly, HSP40 acts as co-chaperone to HSP70 for chaperoning proteins. While BAG-1, HIP, HOP and CHIP are client proteins of HSP70 (Macias *et al.,* 2011), HSP90 has more than 100 known client proteins (Table 1.2) (Picard *et al.,* 2002). HSP90 client proteins are also known as oncoproteins due to their interaction in oncogenic signalling pathways (Xiao *et al.,* 2006). These client proteins bind on to the N-terminal of protein structure (An *et al.,* 2000). The roles of some of these client proteins are as follows:

1.2.3.1 *BAG-1*

BAG-1 promotes cell survival (Townsend *et al.,* 2005). It was the first protein to be identified to regulate cell survival by binding BCL-2. BAG is a nucleotide exchange factor in the HSP70 chaperoning cycle. Most tumours show an elevated overexpression of BAG-1 which leads to inhibition of apoptosis and isolation of the death domain (DD) protein, FADD (Fas-Associated protein with Death Domain), resulting in the inhibition of anoikis (Programmed cell death). It also interacts with RAF pathway to enhance cell survival (Cutress *et al.,* 2002).

1.2.3.2 *AKT*

Akt is present in HSP90 complexes co-chaperone with HSP70 and other client proteins. It prevents apoptosis by activating nuclear factor- κB (NF-κB) and enhances cell proliferation by phosphorylation and inactivation of signalling molecules such as BAD and caspase-9. Breast cancer cells are found to be resistant to chemotherapy due to Akt

activated by HSP90/HSP70 complexes. Thus, HSP inhibitors such as ansamycins can downregulate Akt activity by inhibiting the Akt-dependent pathway (Sato *et al.,* 2000; Basso *et al.,* 2002).

1.2.3.3 *RAS/RAF (ERK) Pathway*

Evidence shows that the ERK pathway is important in signalling since it promotes cell proliferation, cell survival and metastasis. RAF kinases participate in the ERK pathway. A-Raf, B-Raf and C-Raf are members of RAF kinase family. This pathway is abnormally activated in cancer by upstream activation of epidermal growth factors and also leads to activation of mutated *B-Raf*. *A-Raf* and *C-Raf* are required for the stability of the HSP90 complex. Mutated *B-Raf* and *N-Ras* (components in ERK pathway) are observed in malignant melanoma. Inhibiting HSP90 disrupts the complex and reduces the level of ERK signals (Grbovic *et al.,* 2006).

1.2.3.4 *ErbB2/HER-2*

It is a type of Tyrosine kinase that is overexpressed in prostrate, gastric, ovarian and breast cancers. The human epidermal growth factor receptor-2 (HER-2) is a kinase receptor which acts as a client protein to HSP90. Therefore, it plays role in mainting stability of HSP90 mature complex and in cell regulation. Thus, Inhibiting the activity of HSP90 by ansamycin (HSP90 inhibitory compunds) causes degradation of the signalling molecules involved in cancer growth (Solit *et al.,* 2002).

Table 1.2: Client proteins and their interaction with heat shock proteins (Taken from Macias et al., 2011).

Chaperones	Cellular functions	Co-chaperone	Interaction proteins
HSP70	Signal transduction	BAG-1 BAG-1	Raf-1 Kinase Growth factor responses
	Hormone response	BAG-1 HIP	Hormone receptor Steroid receptor
	Cell death	BAG-1 Unknown	BCL-2 APAF-1
	Stress response	Unknown	HSF-1
	Complex assembly	HOP HDJ1	Chaperone complex Chaperone complex
HSP90	Signal transduction	CDC37	Kinases
	Hormone response	PP5 (TPR) Immunophilins (TPR) CyP40 FKBP52 FKBP51	Gluococorticoid receptor Hormone receptor Oestrogen receptor Steroid receptor Progestrone receptor
	Cell death	Unknown	APAF-1
	Stress response	Unknown	HSF-1
	Complex assembly	p23 HOP	Chaperone complex Chaperone complex

These are a few of client proteins that are responsible for cancer cell survival but many such associated client proteins can cause aberrant disease. These important client proteins play a role in chaperoning as HSP70 co-chaperones HSP90 which is a multi-chaperone complex. Moreover, the stabilization and activation of these chaperones requires client proteins that act as co-chaperones for protein folding and cellular activity.

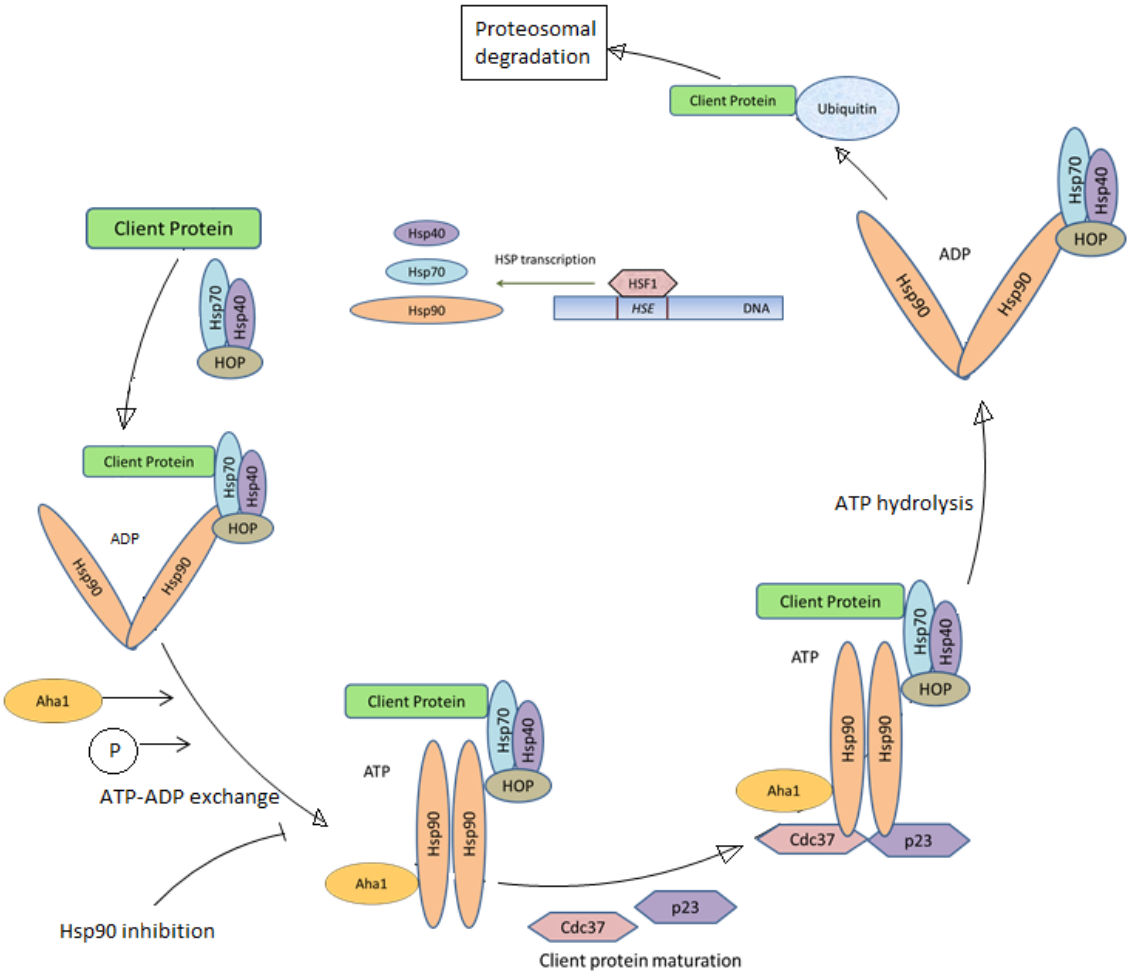

Figure 1.4: Diagram showing inhibition of HSP70/HSP90 machinery (Taken from Mahalingam *et al*., 2009).

HSP70 has been reported to play a key role in the HSP90 chaperone machinery. This HSP90 machinery maintains protein stability and activity of new synthesised proteins. During induction of stress, heat shock element (HSE) activates Heat shock factor-1 (HSF1) resulting I n the transcription of heat shock proteins. HSP90 complex comprised of co-chaperone HSP70 with other client proteins HOP and HSP40 forms 'open state' which results in possessing a higher affinity for client proteins and recruits client proteins such as Cyclin dependant kinase 4 (CDK4). The matured complex or 'Closed state' is formed due to phosphorylation by co-factors such as AHA1. On formation of the mature complex, recruited client proteins are activated resulting in cellular stress such as Akt phosphorylation, ERK activation, expression of oncogenes. Therefore, inhibiting phosphorylation or ATP binding may lead to proteosome degradation, thereby, preventing cell survival and cell proliferation (Figure 1.4) (Pearl *et al.,* 2006).

1.3 Heat shock protein inhibition as anticancer therapeutic target

HSP70 and HSP90 co-operate to maintain tumour cell survival (Zorzi *et al.,* 2011; Chatterjee *et al.,* 2012; Centenera *et al.,* 2013; Fawzy *et al.,* 2013). Targeting these proteins and their client proteins can be of therapeutic importance. Geldanamycin , a first generation of HSP90 inhibitor, is ansamycin-derivative benzoquinone compound that blocks the HSP90 activity by binding to ATP-binding site on the HSP90 N-terminal domain while Radicicol, another HSP90 inhibitor, targets the ATP binding site on the N-terminal domain of HSP90. Its hepatotoxicity prompted the discovery of its derivatives 17-AAG (Tanespimycin) and 17-DMAG, among which 17-AAG has lowest toxicity compared to other derivatives of Geldanamycin. Thus, has been successfully cleared Phase 1 clinical trials and is undergoing Phase 2 testing. Various studies have shown effectiveness of combinational treatment by targeting both HSP90 and HSP70. There are a few examples of HSP70 inhibitors categorised into three basic forms namely protein aptamers, small molecule inhibitors, and antibody treatments. Aptamers are designed to disrupt HSP70 function via NBD/SBD binding. In HeLa cells, combinational treatment using HSP70 aptamers A17 and 5-FU (5-fluorouracil) or Cisplatin reported enhanced cell survival (McConnell *et al.,* 2013). HSP70 can inhibit apoptosis by directly neutralizing the caspase-independent death effector, apoptosis inducing factor (AIF). Thus, peptide aptamers are developed with an ability to inhibit HSP70 function by acting as a substrate mimetic peptides such as ADD70 (AIF-Derived Decoy for HSP70) that has the ability to sequester inducible HSP70 by interacting with the peptide binding region of HSP70 and thereby avoiding binding AIF and other client proteins (Rerole *et al.,* 2011). There are small molecules which are target specific inhibitors, such as Pifithrin-μ (PFT-μ), MKT-007 and VER-155008. Previous studies have shown effect of PFT-μ in leukemic cell lines in combination with other chemotherapeutic agents such as 17-AAG (Kaiser *et al.,* 2011).

Recent study have demonstrated a synergistic effect of 17-AAG in combination with HSP70 inhibitor PFT-μ in bladder cancer and thus, suggest HSP70 as molecular target for HSP90 resistance (Ma *et al.,* 2014). MKT-007, a specific HSC70 inhibitor, also has an ability to bind actin. MKT-007 was identified as an anti-tumour agent during Phase 1 clinical trials but failed Phase 2 due to renal toxicity (McConnell *et al.,* 2013). Combinational treatment of VER-155008 with 17-AAG demonstrated to be effective in the treatment of multiple myeloma (MM) and also in human colon cancer (HCT-116) cells. RNA interference (RNAi) has emerged as new approach for cancer treatment. Reports have shown the regulation of HSPs using small interfering RNA (siRNA) to induce chemosensitivity in cancer (Cruickshanks *et al.,* 2010; Mehta *et al.,* 2013). However, this research will focus on targeting HSP70 using selective compounds namely 17-AAG & VER-155008 (Table 1.3) (Patel *et al.,* 2008; Thakkar *et al.,* 2011).

Table 1.3 Binding targets of heat shock protein compounds. (NBD: Nucleotide Binding Domain; SBD: Substrate Binding Domain) (Taken from Kaiser *et al.,* 2011; McConnell *et al.,* 2013).

Chaperones	Compounds	Binding targets
HSP70	A17-aptamer	NBD
	ADD70	SBD
	MKT-007	NBD
	Pifithrin-μ	NBD
	VER155008 (VER)	SBD
HSP90	17-AAG	NBD
	17-DMAG	NBD
	Geldanamycin	NBD
	Novobiocin	NBD/SBD
	Radicicol	NBD

1.3.1 17-AAG

Geldanamycin (GA) is a naturally occurring benzoquinone ansamycin antibiotic which blocks the nucleotide binding pocket by binding to the N-terminal of HSP90 with high specificity. It inhibits HSP90 ATPase activity by disrupting the stable complex, thereby preventing cell proliferation. In a similar manner, it also inhibits the cell survival process in normal cells (An *et al.,* 2000). The high concentration of HSP90 is responsible for the high accumulation of GA in tumour tissue (Graner *et al.,* 2005). One of the HSP90 inhibitors and analogues of GA, namely, 17-AAG (17-aminoallylgeldanamycin) (Figure 1.5) has been shown to down regulate HSP90 client proteins in animal xenograft models and has also been reported to be involved in cancer stabilisation, decreased cell proliferation and a reduction in apoptosis (Xiao *et al.,* 2006). 17-AAG has been found to be more effective than GA since it is less cytotoxic, though it binds with lower affinity but shows 100 times more affinity to HSP90 in cancer cells compared to normal cells (Soo *et al.,* 2008). 17-AAG was the first-in-class HSP90 inhibitor to enter clinical trials in both adult and paediatric patients and is presently in phase II/phase III clinical trials in adults (Gaspar *et al.,* 2009). Previous studies have shown that HSP90 was inhibited using 17-AAG and proteomic studies showed that on inhibition of HSP90, HSP70 was upregulated (Munje *et al.,* 2011). Thus, HSP70 is emerging as a molecular target for cancer treatment.

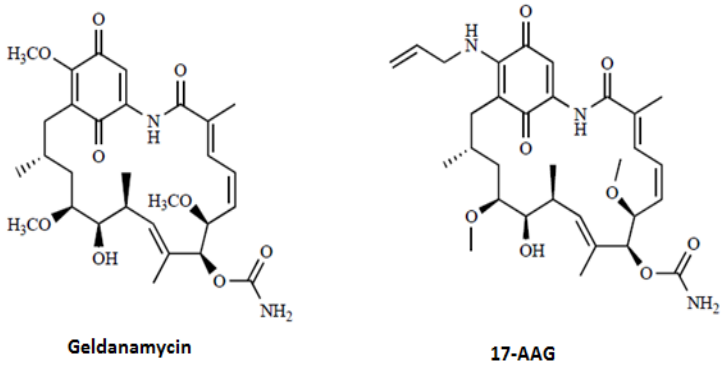

Figure 1.5: Chemical structures of geldanamyacin and its analogue, 17-AAG (Taken from Gava *et al*., 2009).

1.3.2 VER-155008 (VER)

VER-155008 (VER) (Figure 1.6) binds to HSP70 at very low concentrations and it also binds to other members of HSP70 family such as HSC70 and GRP78. It effectively binds HSP90β isoforms (Macias *et al.,* 2011). VER-155008 blocks HSP70 activity by binding to the ATPase pocket of HSC70/BAG-1 and the N-terminal domain, inhibiting cell proliferation. VER-155008 also induces apoptosis via both caspase 3/7 dependent and independent pathways (Massey *et al.,* 2010). It has also reported that VER-155008 targets HSP90 client protein degradation such as RAF-1 and HER2 in human colon carcinoma (HCT116 and BT474 cells). VER-155008 effectively arrests cells in G1-phase at low concentrations while at higher concentrations causes G2/M Phase arrest (Massey *et al.,* 2010). In myeloma cells, VER-155008 decreases cell viability and proved effective when treated in conjunction with HSP90 inhibitory compounds. When investigated *in vivo* (in tumour mice), it showed limited absorption, thus it is administered via the IV route (Massey *et al.,* 2010; McConnell *et al.,* 2013).

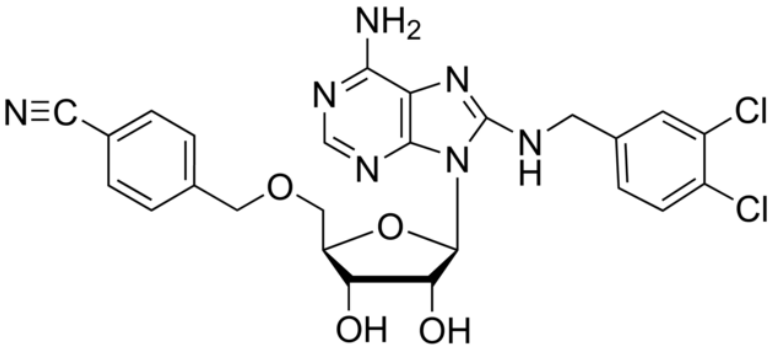

Figure 1.6: Chemical structure of VER-155008 (Taken from McConnell *et al*., 2013).

1.3.3 Temozolomide (TMZ)

The standard treatment of glioblastoma multiforme (GBM) involves chemotherapy, radiotherapy and surgical resection. Due to its aggressive nature, it is a challenge to eradicate glioblastoma. TMZ has emerged as an effective chemotherapeutic agent which is capable of increasing survival rates after diagnosis. TMZ, a 3-methyl derivative of mitozolomide, (Figure 1.7) is a second generation DNA methylating agent which is less toxic than derivatives of mitozolomide. It was first synthesized at Aston University in 1984 (Ohba *et al.,* 2010). Under physiological conditions, it undergoes spontaneous conversion to the active alkylating MTIC (5-(3-methyltriazen-1-yl) imidazole-4-carboximide). TMZ is used as a chemotherapeutic agent in the treatment of pancreatic cancer, melanomas and gliomas with fewer side effects compared to other anti-cancer reagents. It has the ability to cross the blood-brain barrier and has a 100% bioavailability when administered orally. The major disadvantage in the use of TMZ treatment is drug resistance developed as a result of DNA repair enzyme MGMT which transfers methyl group of O^6-methylguanine in DNA to Cysteine, thus rendering cells to TMZ resistance (Marchesi *et al.,* 2007; Gaspar *et al.,* 2010; Ohba *et al.,* 2010b; Pan *et al.,* 2012).

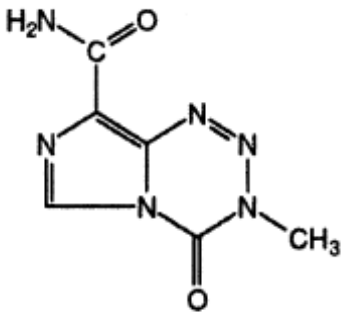

Temozolomide

Figure 1.7: Chemical structure of TMZ (Taken from Marchesi *et al*. 2007).

1.4 MicroRNA

miRNAs (19-22 nt) are conserved small non-coding RNA (Bartel *et al.,* 2009). They were first discovered in 1993 while studying small endogenous non-coding RNA *lin-4*, which regulates larval cell development in *Caenorhabditis elegans.* It has been reported that instead of coding for its protein, *lin-4* produces small RNA which further mediates repression of *lin-14* protein without affecting mRNA levels. Similar phenomena were reported in *let-4* which regulates transition cell development in larvae. Further studies reported miRNA genes in various species from flies, worms to humans. Due to the increasing number of identified miRNA, miRNA repository of published miRNA sequences was created and developed by Sam Griffith-Jones from the Wellcome Trust Sanger Institute known as miRBase. Today in miRBase online registry, there are more than 1900 mature human miRNA sequences (Bartel *et al.,* 2004; Bartel *et al.,* 2009; Kozomara *et al.,* 2014). According to the nomenclature guideline of miRBase databases 3 or 4 letters designate the species name, for instance hsa for Homo sapiens, followed by the sequence designation miR as mature sequence and the assigned unique identification number. In some cases, they are further followed with suffixes such as miR-146a or miR-146b which indicate the distinct sequences for same transcripts. 5p or 3p denotes the location of mature miRNA at 5'arm or 3'arm of the precursor miRNA.

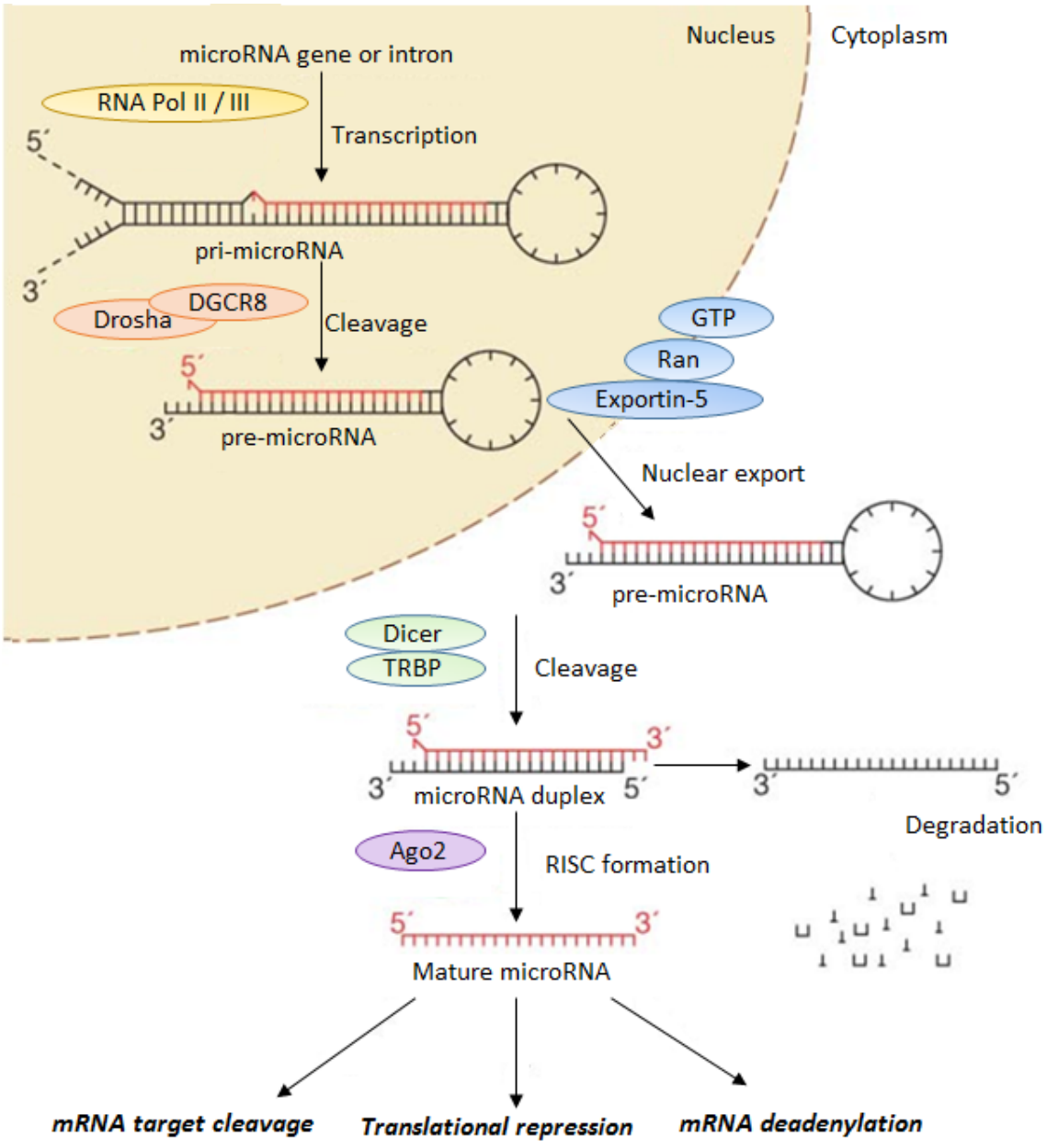

Figure 1.8: Biogenesis of miRNA The above figure shows canonical maturation of miRNA maturation which includes Primary miRNA transcript (Pri-miRNA) production by RNA polymerase II or III and formation of Pre-miRNA in the nucleus after cleavage of Pri-miRNA by microprocessor complex Drosha-DGCR8 (Pasha). Pri-miRNA are transported to cytoplasm by Exportin-5-Ran-GTP and cleaved by Dicer/TRBP to form mature miRNA duplex. Further, Functional strand is loaded into RNA-induced silencing complex (RISC) by Argonaute (Ago2), where it guides RISC to silence targeted mRNAs by either mRNA cleavage, translational repression or de-adenylation while passenger strand is degraded (Taken from Bartel *et al*., 2009).

1.4.1 Biogenesis of miRNA

Most of miRNAs can be encoded within an exon of a unique transcript, occurring as "Polycistronic" miRNAs, or can be found within the introns of protein coding or non-coding genes. About 40% of miRNA are encoded in the introns, while 10% in the exons (O'Carroll *et al.,* 2013). Irrespective of the genomic locations, miRNA biogenesis initiates with transcription using RNA polymerase II, processing a primary miRNA transcript (pri-miRNA) ranging from hundreds to thousands of nucleotides in length and folds to form imperfectly paired double stranded stem loop structure. Pri-miRNA is processed to mature miRNA by ribonuclease III (RNAse III). During the first step, DGCR8 (*Digeorge* syndrome *critical region* 8) identifies and binds to the stem region of the pri-miRNA, functions as a molecular ruler to determine the precise cleavage site. Then, Pri-miRNA recruits Drosha enzyme which cleaves 5' and 3' arm of the pri-miRNA hair pin structure to form Pre-miRNA (Pellegrino *et al.,* 2013). The nuclear export factor Exportin-5 binds the pre-miRNA and transports it to the cytoplasm and also protects pre-miRNAs against nuclear digestion. Exportin-5 recognises the pre-miRNA independently of its sequence or the loop structure, where the second RNase III, Dicer, processes the pre-miRNA into a 21 nt long miRNA/miRNA* duplex. The trans-activator RNA (tar)-binding protein (TRBP) enzyme also participates in the process of Pre-miRNA cleavage by forming a complex with the Dicer enzyme. The miRNA/miRNA* duplex is further processed or unwound by members of Argonaute (AGO) family which further loads into the RNA-induced silencing complex (RISC) participating in post-transcriptional regulation. Human genome encodes four AGO proteins (AGO 1-4) which forms part of RISC and are found to bind miRNAs with mRNA targets. Only one strand of the duplex will become the mature miRNA while strand (miRNA* or passenger strand) with less tightly paired 5' end is degraded (Figure 1.8) (O'Carroll *et al.,* 2013).

1.4.2 Gene Regulation

MicroRNA can direct the RISC to downregulate gene expression by either of two post-transcriptional mechanisms: mRNA cleavage or translational repression. Once the miRNA is incorporated in cytoplasmic RISC, further mechanism is carried out depending on complementarity of seed sequences. The full complementarity between miRNA and its mRNA targets will lead to mRNA cleavage and destruction by endonucleolytic activity of AGO2 protein or lead to translation repression in the absence of complementarity or insufficient group of complementarity. Both siRNA and miRNA cleave mRNA in a similar manner (Bartel *et al.,* 2009). The miRNA has the ability to regulate the cleavage of siRNA/mRNA duplexes with partial complementarity which prevents mRNA cleavage. These miRNAs have 2 – 7 bases which are complementary sequences, known as 'seed' sequence, responsible for target recognition. These bases must pair with the 3' untranslated region (3'UTR) complementary mRNA target bases which lead to translational inhibition and silencing of the targeted message (Su *et al.,* 2014).

1.4.3 Biological functions

Studies have shown that the miRNA exists not only in human cells (Zhu *et al.,* 2011), but also in serum, plasma, saliva, milk and tears (Zhu *et al.,* 2011; Zhang *et al.,* 2012) since they constitute an appropriate environment for circulating or transporting them to targeted sites for regulating physiological and pathological processes (Kosaka *et al.,* 2010; Zhang *et al.,* 2010). They are known to have the potential to transfer from plants via regular dietary consumption (Zhang *et al.,* 2012). Recently, proteomic studies reported the impact of a single miRNA on hundreds of mRNA targets. Referring to biogenesis of miRNA, its shows the potential to target hundreds of mRNA sequences simultaneously due to its efficient ability to regulate by binding to the 3'UTR region.

Thus, regulating thousands of mRNAs modulates gene expression by regulating cellular signalling pathways such as apoptosis, proliferation, cell cycle, differentiation, stem cell maintenance and metabolism.

Over the past few decades, investigations have highlighted the diversity of altered miRNAs that contribute to the pathogenesis of solid tumours and haematological malignancies. The miRNAs may act as potential 'oncogenes' by either targeting tumour suppressors or acting as 'tumour suppressors', on their functional damage such as genomic deletion, mutation, epigenetic silencing, and/or miRNA processing alteration; and thus play crucial roles in the development and progression of cancers (Griffiths-Jones *et al.,*2008). Some of the alterations are found in various cancers while others are type-specific. miRNAs can target various mRNAs but at the same time different miRNA's or its family may regulate one mRNA target. In A549 NSCLC (Non-Small Cell lung Cancer) cell lines, miR-29 acts as a tumour-suppressor but in breast cancer cells they play oncogenic functions (Fabbri *et al.,* 2007). In breast cancers, miR-155 acts as oncogene and is upregulated. The miR-373 and miR-520c regulate prognosis in breast cancer patients by inversely regulating CD44 isoform while miR-10b regulated tumour invasion by TWIST1 (Bartels *et al.,* 2009). Similarly, miR-26a down regulates in HCC (Hepatocellular Carcinoma) to induce apoptosis while it's up regulation and overexpression causes metastasis in glioma or NSCLC (Non-small Cell Lung Cancer) (Huse *et al.,* 2009; Kota *et al.,* 2009; Liu *et al.,* 2009). Thus, studying the role of miRNAs in cancers is complicated due to this functional diversity. This direction of research involving the identification of dysregulated miRNA profiles has been coined out on various cancers such as lung cancer (Takamizawa *et al.,* 2004), breast cancer (Iorio *et al.,* 2005), papillary thyroid carcinoma (He *et al.,* 2005), gastric carcinoma (Michael *et al.,* 2003) and colon cancer (Cummins *et al.,* 2006). For example, miR-155 is over-expressed

in various different cancers (Kluiver *et al.,* 2005; Volinia *et al.,* 2006; Li *et al.,* 2013; Rozovski *et al.,* 2013). Studies showed association of miRNAs with the hallmarks of cancer (see Figure 1.9) by interacting with development, invasion, differentiation, metabolism, metastasis and apoptosis (Chou *et al.,* 2013). miRNAs are reported to overlap with sets of genes by sharing similar seed sequences, known as families. The miR-34 family (miR-34a, miR-34b and miR-34c) is known to mediate tumour suppression by modifying p53 and inhibiting invasion and metastasis in various tumours (Yamazaki *et al.,* 2012; Javeri *et al.,* 2013). In addition, miR-17-92 clusters (miR-17-5p, miR-17-3p, miR-18a, miR-19a, miR-20a, miR-19-1, miR-92-1) that are overexpressed can be a biomarkers for multiple myeloma and B-cell lymphoma (He *et al.,* 2005; Gao *et al.,* 2012). However, in some miRNAs such as miR-26a, miR-129, miR-143 and miR-145 that are downregulated in cancer such as breast cancer, prostate cancer, cervical cancer, lymphocytic malignancy and colorectal cancer where they promote cancer stem cell or cell proliferation and migration (Michael *et al.,* 2003; Karaayvaz *et al.,* 2013; Su *et al.,* 2014). The reduced expression of miR-206 and 29b along with enhanced miR-126 and miR-335 expression, inhibits cancer development and inhibit metastasis in breast cancer cell lines (Negrini *et al.,* 2008; Pellegrino *et al.,* 2013).

1.4.4 miRNAs in glioma

Glioblastoma multiforme is grade IV brain tumour and accounts for approximately 70% of all diagnosed gliomas with approximately 3 % survival rate. Due to its highly invasive nature complete removal of the tumour is challenging. Research has shown that 50% of miRNAs are expressed in the mammalian brain (Lagos-Quintana *et al.,* 2002; Krichevsky *et al.,* 2003). Amongst 180 screened miRNAs, dysregulation of 8 miRNAs in glioblastoma has been reported using microarray (Chan *et al.,* 2005; Ciafre *et al.,* 2005). The miR-21 was the most common to be reported as an anti-apoptotic factor. miR-21 reported to

target p53 and the transforming growth factor-b (TGF-b) in GBM (Papagiannakopoulos *et al.,* 2008; Schramedei *et al.,* 2011; Samantarrai *et al.,* 2013). WHO classifies brain tumours according to their morphology and metastasis amongst which most malignant form is Grade IV glioblastoma (GBM). Approximately 16 miRNAs were reported to be altered in GBM. The overexpression of miR-196a and miR-196b was reported in GBM (Guan *et al.,* 2010). Various methods have been applied in order to determine miRNAs in malignant glioma, for example, 12 miRNAs were upregulated in glioma using stem-loop RT-PCR while 55 were upregulated and 29 downregulated miRNAs were identified by LNA (Locked nucleic array) microarray (Guan *et al.,* 2010; Malzkorn *et al.,* 2010; Rao *et al.,* 2010; Kim *et al.,* 2010). miRNA expression profiles are reported to be more precise than mRNA profiling (Lu *et al.,* 2005). Recently, the relationship between miRNA and mRNA was identified in glioblastoma (Srinivasan *et al.,* 2011) and similar to other cancers, miRNAs in glioma are also associated with the hallmarks of cancer.

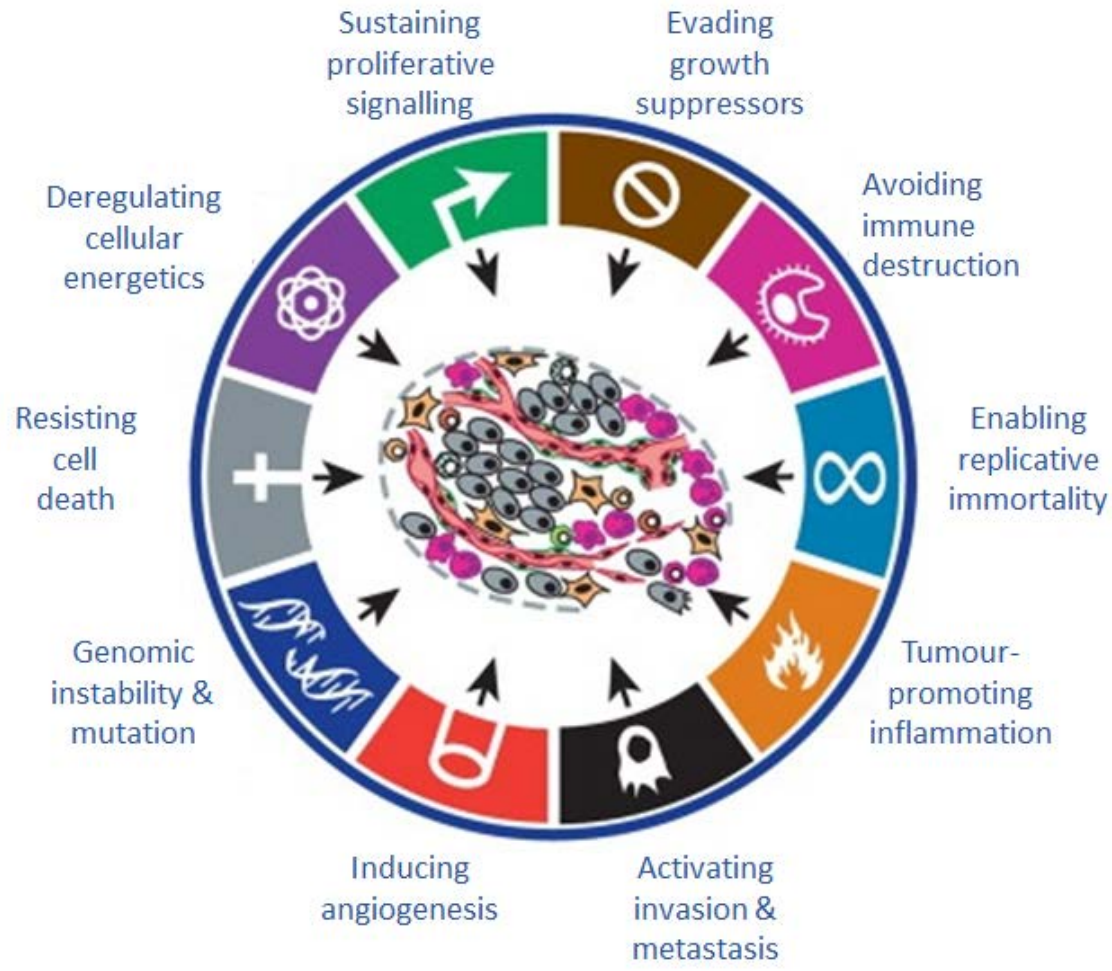

Figure 1.9: miRNAs interacting hallmarks of cancer miRNAs plays a crucial role in regulating cancer growth. They are known to interfere with the 10 hallmarks of cancer (Taken from Hanahan *et al*.,2011).

In glioma, cell proliferation is responsible for uncontrollable tumour growth which leads to disease progression. These involve cell cycle regulators such as CDK4 or CDKN2A that accelerate and promote glioma cell progression. For example, miR-137 stimulates cell proliferation by regulating CDK6 expression (Silber *et al.,* 2008). Also, miRNAs regulates anti-apoptotic and pro-apoptotic molecules such as miR-181 and miR-153 targets BCL-2 (b-cell lymphoma), an apoptotic protein in order to promote apoptosis and translation repression in glioma (Xu *et al.,* 2010). The miRNA regulating molecular mechanism involves cell migration and invasion such as miR-21 and miR-30. They are associated with glioma angiogenesis, playing a role in Akt, VGFR and NF-kB pathways. They also contribute to cell development and maintenance in cancer stem cells. Radiotherapy and chemoresistance have always been obstacle for anti-cancer treatment. The membrane transporters resist drug induced apoptosis contributing to multi-drug resistance (MDR). miRNAs can also interacts with drug resistance molecules such as ATP-binding cassette (ABC) transporters (ABCG2/BCRP1, ABCB1/MDR1 and ABCA3), COX-2, Ras, Cyclin-D1, BCL-2 and Survivin (Liu *et al.,*2009; Lopez-Chavez *et al.,*2009; Bardelli *et al.,* 2010). The miR-125b expression facilitates cancer cell resistance by blocking PI3K/Akt phosphorylation and caspase activation (Zhang *et al.,* 2011; Shiiba *et al.,* 2013).

1.4.5 miRNA Prediction tool

Bioinformatic algorithms tools are crucial for identification of miRNA targets. These algorithmic pipelines assist in predicting miRNA targets computational with precision and sensitivity. These databases provide details of the similar seed sequence targets of miRNA along with its conserved sites. Databases such as miR2Disease, MirnaMAP, MiRecords, miRSel, miRTarBase, miRWalk, StarBase, TarBase 5.0, Diana microT, miRDB, Target miner, TargetscanVert are miRNA-mRNA predicting databases (Griffiths-Jones *et*

al., 2006; Griffiths-Jones *et al.,* 2008) providing details of the miRNA validated or predicted target list accessed via these databases.

miRNAs are highly conserved small non-coding RNA which played a crucial role in regulating functions. Various diseases have reported deregulation of miRNA. Thus, it is significant as it could be a biochemical tool for identification of biomarker for a disease. miRNA expression research analysis had diverse technical tool including Northern blotting, dot blotting, primer extension analysis, RT-qPCR, next generation sequencing (NSGs) and microarray (Nelson *et al.,* 2006; Roy *et al.,* 2011 ; Streichert *et al.,* 2012). Among which, microarrays proved to be ideal for high throughput miRNA gene analysis as they were capable of simultaneously screening hundreds of target sequences within a single sample volume. They were appropriate for examining the relative expression between different biological samples. Thus, considering the advantages and cost-effectiveness compared to other technologies, miRNA microarray profiling was used for the present studies (Qavi *et al.,* 2010; Zhao *et al.,* 2012).

1.5 Glioma biology

Brain tumours which arise from different types of glial cells such as astrocytic, oligodendroglial and ependymal are collectively known as glioma (Appin et al., 2012, Wesseling et al., 2015). There are more than 130 types of brain tumours of which gliomas are most common primary brain tumours. The survival rate after diagnosis differs in age and gender. According to recent statistics in UK, 53% of diagnosed adults between ages of 15-39 have only five year survival time (Cancer Research UK, 2014). According to World Health Organisation (WHO), tumours are histologically characterized by their rate of proliferation, invasion, necrosis and angiogenesis. Grading of tumours are described below:

Grade I: This is least malignant form of tumour with low proliferative rate and thus associated with long-term survival. Cell morphology is almost similar to non-cancerous cells. Surgical resection is effective treatment for this grade (Louis *et al.,* 2007, Smoll *et al.,* 2012).

Grade II: Morphological appearance is slightly abnormal than non-cancerous cells. Despite of low proliferative rate they are known to recur as higher grade tumour after treatment indicating its infiltrative nature (Louis *et al.,* 2007, Smoll *et al.,* 2012).

Grade III: Level of malignancy can be validated by abnormal morphology. They have comparatively high proliferative rate continuously reproducing abnormal cells. They are invasive in nature and often recur as higher grade tumour (Louis *et al.,* 2007, Smoll *et al.,* 2012).

Grade IV: Most malignant form of tumour with high proliferation, invasive nature and mitotic activity. Due to its high proliferation rate, they tend to reproduce abnormal cells at higher rate and also cause high metastasis. Treating Grade IV is challenging due high

recurrence rate causing resistance to traditional treatment (Louis *et al.,* 2007, Smoll *et al.,* 2012).

Examples of different grading includes Pilocytic astrocytoma (Grade I), astrocytoma (Grade II) forms low-grade tumours with only increased cellularity, anaplastic astrocytoma (Grade III) and Glioblastoma (GBM) (Grade IV) have evidence of endothelial proliferation and/ or tumour necrosis (Buckner et al., 2007). Every year more than 2,200 cases are diagnosed with GBM which account for 55% of the malignant brain tumours (WHO grade I-IV) (Ohgaki & Kleihues, 2005, Cancer Research UK, 2014). GBM has extremely poor prognosis with median survival rate of 6 months (Cancer Research UK, 2014).

1.6 Rationale for research

1.6.1 Working hypothesis

Previous data have shown that HSP90α is highly expressed in glioma cell lines compared to normal astrocytes cells (Shervington *et al.,* 2008; Cruickshanks *et al.,* 2010). Thus, the HSP90 activity was targeted using 17-AAG, an HSP90 inhibitor. However, previous proteomics data showed that HSP70 was induced on inhibition of HSP90 (Munje *et al.,* 2011). Therefore, targeting HSP70 and HSP90 is imperative if glioma is to be tackled and overcome.

Although tumour cells are responsive to TMZ treatment, its chemoresistance has been proven to be rather poor. However, a number of studies have been reported that involve overcoming resistance to Temozolomide. In the present study, a novel approach is being investigated involving targeting both HSP70 and HSP90 using inhibitory compounds. In order to understand the causes of tumour initiation and growth, it is important to acquire a more in-depth analysis of the underlying mechanism. The miRNAs are aberrantly active in normal cells but are extensively involved in tumourigenesis. Due to their unique ability to target multiple mRNAs simultaneously, their expression and regulation can provide an insight on the efficacy of the cancer treatment. The miRNA microarray technology is utilised to obtain gene expression and identify therapeutic biomarkers for the treatment of glioma (Stupp *et al.,* 2005; Pearl *et al.,* 2006; Yoshino *et al.,* 2010).

1.6.2 Aim

The aim of our research was to identify potential targets to improve efficacy of HSP70 and HSP90 inhibitory drugs VER-155008 (VER) and 17-AAG, respectively comparing to Temozolomide (TMZ) as standard treatment.

1.6.3 Specific Aim

The main aim was to investigate HSP70 and HSP90 target in order to help treat glioma.

1. To develop the technique of tissue culture using 1321N1, GOS-3 and U87-MG cells and using them for further studies.

2. To undertake dose-dependent experiments to determine IC_{50} of TMZ, 17-AAG and VER-155008.

3. To assess the gene and protein expression in Hsp70 and Hsp90α in glioblastoma cell lines before and after treatment with inhibitory drugs using qRT-PCR and ELISA.

4. To determine the chemosensitivity using sequential and concurrent assay.

5. To prepare cells for miRNA microarray experiment.

6. Bioinformatic analysis of the miRNA microarray data.

7. Integrated miRNA-mRNA analysis to validate microarray data.

8. qRT-PCR validation using mRNA identified from integrated analysis.

9. To analyse the data and write up the thesis.

CHAPTER 2

MATERIALS AND METHODS

2.1 Materials

Table 2.1: Reagents used for cell culture in this study.

Reagents	Abbreviation and Storage temperature	Components	Volume (ml)	Suppliers
Eagle's minimum essential medium	EMEM, 2-8°C	2.0 g/l sodium bicarbonate, 4.5 g/l glucose, 10 mM hepes, 1.0 mM sodium pyruvate, 5.30×10^{-3} g/l phenol red	500	Lonza, UK
Dulbecco's modified eagle's medium	DMEM, 2-8°C	25 mM hepes, 1.0 g/l glucose, 1.0 mM sodium bicarbonate, 1.10×10^{-2} g/l phenol red	500	Lonza, UK
Foetal bovine serum	FBS, -20°C	Heat inactivated FBS (10%)	50	GIBCO,UK
L-glutamine	-20°C	200 mM L- glutamine	5	Sigma Aldrich, UK
Non-essential amino acids	2-8°C	100× non-essential amino acid	5	Sigma Aldrich, UK
Essential amino acids	2-8°C		5	
Phosphate buffer saline (PBS,1×)	PBS, 2-8°C	8 g/l NaCl, 0.2 g/l KCl, 1.44 g/l, Na_2HPO_4, 0.24 g/l KH_2PO_4, pH 7.4	2	Fischer Chemicals, UK
Trypan blue (0.4%)	Room temperature	0.81% sodium chloride, 0.06% potassium phosphate, dibasic	–	Sigma Aldrich, UK
Dimethyl sulfoxide	DMSO, Room temperature	99.5% dimethyl sulfoxide, 0.81% sodium chloride	–	Sigma Aldrich, UK
Sodium pyruvate (Na)	2-8°C	Pyruvic Acid Sodium Salt	5	Lonza, UK

Table 2.2: A list of reagents and solutions used for agarose gel electrophoresis.

Reagents	Suppliers	Preparation	Working Concentration
Ultrapure agarose	Gibco BRL, UK	0.6-2 g Agarose, 30-100 ml TAE (1×). Solubilised by boiling in a microwave for 3-4 min	2% weight/volume
10× TAE (Ultrapure 10× Tris Acetate EDTA electrophoresis buffer)	Sigma, UK	1 M Trizma base, 0.9 M Acetic acid (1×), 0.01 M EDTA Diluted to 1 x concentration with distilled water	1×
Gel loading dye	Sigma, UK	0.25% w/v Bromophenol blue, 0.25% w/v xylene cyanole, 40% w/v Sucrose. Supplied ready for use 4× concentration	1:4 Sample : dye
Ethidium bromide 10 mg/ tablet	Amresco, UK	10 mg Ethidium bromide in 10 ml distilled water. Diluted to 0.5 µg/ml with distilled water	1:20
100 base pair (bp) molecular marker	Sigma, UK	100 µg supplied ready for use	1 µg/ml

2.2 Methods

2.3 Cell Culture

2.3.1 Cell lines

The glioma cell lines U87-MG (Human glioblastoma astrocytoma grade IV), 1321N1 (Human brain astrocytoma Grade II) and GOS-3 (grade II/III astrocytoma/ oligodendroglioma) were purchased from the European Collection of Cell Cultures (ECACC) and Deutsche Sammlung von Mikroorganismen und Zellkulturen (DSMZ), respectively were of human origin. Normal cell line NHA (Normal Human Astrocytes) was purchased from ECACC. All Cell lines (Table 2.3) were supplied in frozen ampoules in 1 ml plastic cryotubes in an appropriate freezing medium and were present in an appropriate freezing medium with 10% foetal bovine serum (FBS), 2 mM L-glutamine and 10% (v/v) dimethyl sulphoxide (DMSO). According to company recommendation, cells were grown in 75 cm^2 or 25 cm^2 tissue culture sterile polystyrene flasks (Sigma, UK) and maintained by incubating at 37 °C in a humidified 5% CO_2 atmosphere. All cell lines were grown adherent as monolayer cultures.

Table 2.3: Cell line description and media formulation employed in this study.

Cell lines	Description	WHO grade	Culture Media	Suppliers
NHA	Normal human astrocytes	N/A	AGM™ BulletKit™	Lonza
U87-MG	Human brain glioblastoma-astrocytoma epithelial-like cell line	IV	EMEM, 10% (v/v) FBS, 2 mM L-glutamine, 1% (v/v) non-essential amino acid and, 1 M Sodium Pyruvate	ECACC, UK
1321N1	Astrocytoma	II	DMEM, 10% (v/v) FBS, 2 mM L-glutamine	ECACC, UK
GOS-3	Human brain mixed astrocytoma/ Oligodendroglioma	II/III	DMEM, 10% (v/v) FBS, 2 mM L-glutamine	DSMZ, Germany

2.3.2 Medium and reagents preparation

The cell culture medium was made according to ECACC/ATCC/DSMZ recommendations by adding required supplements with suggested concentrations in sterile conditions (Table 2.1). Media were stored at 4˚C for 2-3 weeks within the stability period. Concentrations for preparation of supplements were calculated using below formula:

$$V_1 C_1 = V_2 C_2$$

$$V_1 = \frac{V_1 C_2}{C_1}$$

V_1 =initial volume

C_1 = initial stock concentration

V_2 = final volume

C_2 = final concentration

The above formula had been used for all calculations to determine the volume and concentration of the reagents and chemicals used in this study.

2.3.3 Resuscitation of the cells

Each medium was pre-warmed at 37 °C in a water bath for approximately 30 min before thawing the frozen ampoules of cells. These ampoules were stored in liquid nitrogen and appropriate Personal Protective Equipment (PPE) was used. Following protocol of ECACC, ampoules of cell lines were partially opened in sterile conditions to release trapped nitrogen and then re-tightened. Cell lines were completely thawed at 37°C in a water bath for 1-2 min to minimise any damage to the cell membranes. Cells from cryotubes were resuspended in 2 ml of growth medium and centrifuged at 1000 rpm for 5 min. The supernatant was discarded and the pellet was resuspended in fresh medium. After determining the appropriate volume to attain seeding density, cells were resuspended in labelled 25 cm^2 flasks with the cell line name, passage number and date in a suitable volume of culture medium. Culture was mixed by shaking the flask backward and forward. These flasks were then incubated at 37°C with 5% CO_2 in filtered air and the medium was changed on alternate days. In order to maintain nutrient levels for slow growing cells, the medium was changed after every 48 h of incubation. Cells were observed under the light microscope with 10× magnification for monolayer growth of cells that were 70-80 % confluent after which they were sub-cultured.

2.3.4 Subculture and cell library maintenance

After obtaining appropriate confluence of cells, the cell culture medium was aspirated and the cells were washed using 2-3 ml of PBS. Thereafter, 1× trypsin was added to the cells by diluting in 2 ml of PBS and incubated at 37°C for approximately 3 min to remove cells that adhered to walls of flask. To ensure 95% cells detachment, the cells were observed under microscope. The medium with twice quantity of PBS (i.e. 4 ml) was added to flask to deactivate the effect of trypsin. Then, the media containing cells were transferred in a centrifuge tube and centrifuged at 1000 rpm for 5 min and cell pellet was obtained. Discarding supernatant media, cell pellet was resuspended in 1 ml of fresh media.

2.3.5 Quantification of cells using haemocytometer

Cell suspension (20 µl) was aliquoted and quantified using a moistened haemocytometer. The cover slip was attached by applying pressure to create Newton refraction rings to ensure that the cover slip has affixed. The cell suspension was diluted by adding 0.4% Trypan blue to stain the dead cells for determining the total number of live cells. Cell suspension mix was pipetted at the edge of the cover slip and was allowed to run under the cover slip. Stained cells were visualised under a light microscope in the haemocytometer grid using 20× magnification (Figure 2.1). Only cells from the middle square were counted and quantified. Cells count was recorded and calculations were carried out to determine the cell concentration per ml of cell suspension following formula mentioned below:

$$X = Y \times df \times 10^4 \text{cell/ml}$$

[*Y* is cell count in grid square, *df* is dilution factor; *df* = 20: *z* (*z*= total volume of Tryphan blue + total volume of cell suspension)]

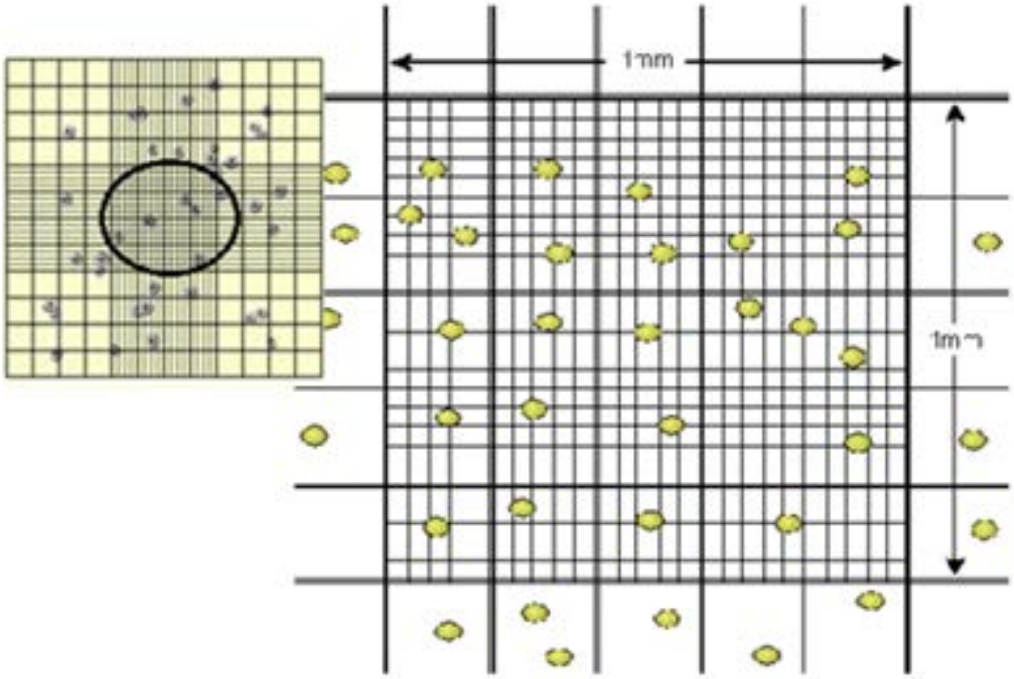

Figure 2.1: Diagram showing haemocytometer grid under light microscope (Taken from PHE, 2013)

2.4 Cell Treatment with 17-AAG, VER and TMZ

2.4.1 Cell viability assay

17-AAG (Invivogen, UK) and VER (Tocris Biosciences, UK) were dissolved in DMSO to provide a stock concentration of 2 mM. Temozolomide (TMZ) was dissolved in DMSO to make a stock concentration of 50 mM. To calculate the inhibitory concentration (IC_{50}) of the drugs, the stock concentrations were further diluted in culture medium to achieve varying concentration of drugs. These were added to untreated cells and incubated for 48 h in order to determine the IC_{50} and cell viability using all three cell lines. CellTiter-Glo® Luminescent Cell Viability Assay determines the number of viable cells by quantifying ATP signals from presence of metabolically active cells (Crouch *et al.,* 1993). Thus, cell viability was determined using CellTiter-Glo® Luminescent Cell Viability Assay (Promega, UK) according to the product protocol mentioned below:

In white flat clear bottom 96-well plate 1×10^3 cells were seeded and incubated for 24 h. The cells were treated with inhibitory concentration of the drugs (17-AAG, VER or TMZ) and further incubated for 48 h. Control well was prepared with only cell culture medium in order to obtain background luminescence value. A 96-well plate was equilibrated at room temperature for 30 min. Depending on the number of wells used, appropriate volumes of Cell Titer-Glo reagent was prepared by transferring the volume of Cell Titer-Glo buffer to the CellTiter-Glo substrate (1:1). The Content of the 96 well plates was emptied by pipetting. CellTiter-Glo reagent was diluted with the cell culture media and was added to appropriate wells. The 96-well plate was incubated on orbital shaker for 2 min in order to mix content and induce cell lysis. Thereafter, 96-well plate was then incubated at room temperature for 10 min, to stabilize luminescent signal. The

luminescent signal was detected using Tecan GENios Pro® (Tecan, Austria) at integration time of 0.25-1.00 second per well.

2.4.2 Chemosensitivity assay

Chemosensitivity assay was carried out using two different methods. The concurrent assay, cells were treated with IC_{50} concentrations of three drugs individually and in combinations, following protocol under cell viability mentioned earlier. Luminescence signal was analysed and the treatment was compared to the standard treatment using TMZ while in sequential assay, cells were treated with 17-AAG or VER individually, followed by treatment of TMZ after 48 h. Then following above protocol reading were taken after 48 h.

2.5 Gene transcription technique

2.5.1 mRNA isolation

Messenger RNA (mRNA) isolation was carried out using the mRNA isolation kit (Roche-Diagnostics, Germany). This kit helped to directly isolate mRNA from cultured cells without intermediate of total RNA. The poly $(A)^+$ tail of mRNA hybridized to a biotin-labelled oligo $(dT)_{20}$ probe. Using Streptavidin-coated magnetic particles biotinylated hybrids were captured and the magnetic particles were separated using a magnetic separator. The fluid was removed by washing with PBS buffer. Finally, the mRNA was isolated from the particles and incubated in redistilled water. Figure 2.2 below shows procedure for isolation of mRNA isolation and lists of the reagents and buffers used in this study (Table 2.4 and Table 2.5). This kit contains no aggressive reagent, thus it is safe and also has high purity.

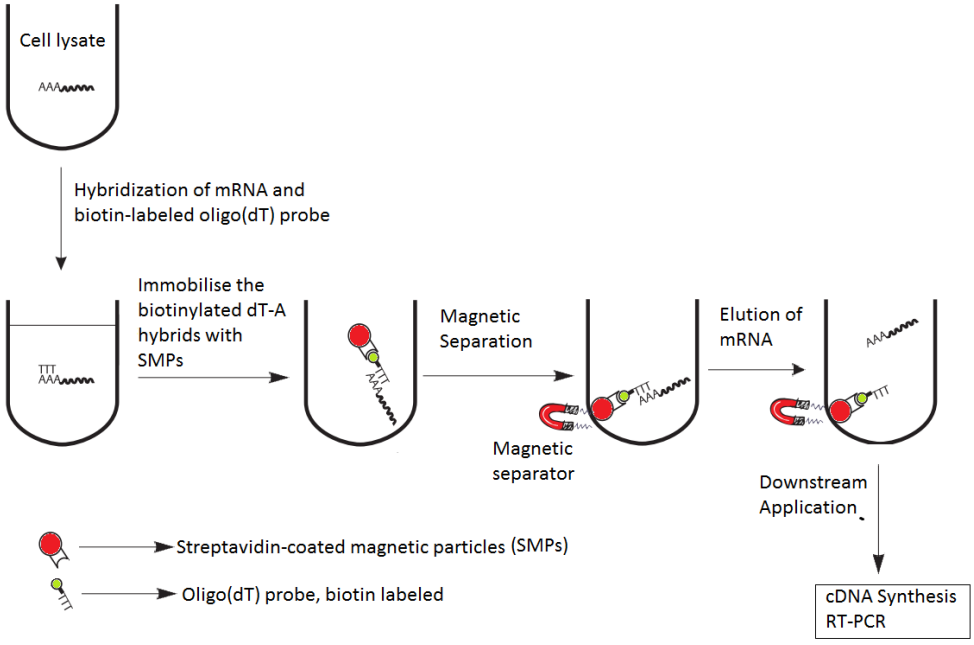

Figure 2.2: Experimental protocol for the mRNA isolation technique The poly $(A)^+$ tail of mRNA hybridized to a biotin-labelled oligo $(dT)_{20}$ probe and captured using streptavidin coated magnetic particles and these magnetic particles were removed using a magnetic separator. After the washes with PBS, mRNA was eluted and incubated in redistilled water. (Taken from mRNA isolation kit manual Roche Applied Sciences, UK 2014).

Table 2.4: Reagents and buffers used for mRNA isolation (Roche applied sciences, UK)

Reagents	Contents
PBS	Ice cold, pH 7.4
Lysis Buffer	0.1 M Tris buffer, 0.3M LiCl, 10 mM EDTA, 1% lithium dodecylsulfate, 5mM DTT (dithiothreitol), pH 7.5
Biotin-labelled Oligo(dT)$_{20}$ probe	100 pmol biotin-labeled Oligo(dT)$_{20}$ per µl of redistilled water
Streptavidin Magnetic Particles (SMPs)	Suspension of (10 mg/ml) in 50 nM Hepes, 0.1% bovine serum albumin, 0.1% chloracetamide, 0.01% methylisothiasolone, pH 7.4
Washing Buffer	10 mM Tris buffer, 0.2 M LiCl and 1 mM EDTA, pH 7.5
Redistilled Water (PCR Grade)	RNAse free
Storage buffer	10 mM Tris buffer, 0.1% chloracetamide, 0.01% methylisothiasolone, pH 7.5

Table 2.5: Volumes of reagents and buffer used for mRNA isolation of 2 × 10^6 cells.

Number of cells (2 × 10^6)	Volume (µl)
PBS	200
Lysis buffer	500
Biotin-labelled Oligo(dT)$_{20}$ probe	0.5
Volume of SMPs	50
Lysis buffer (preparation of SMPs)	70
Washing buffer	200 (× 3)
Redistilled water	10

Experimental procedure:

A total of 2×10^6 cells were pelleted to isolate mRNA. The Cells were washed twice using 200 µl of ice cold PBS to remove excess medium. At the same time, magnetic particles were prepared and streptavidin magnetic particles (SMP) were thoroughly mixed. A volume of 50 µl of streptavidin magnetic particles were aliquoted into a sterile eppendorf tube. The streptavidin magnetic particles were separated from the storage buffer using the magnetic separator. Storage buffer was discarded. The magnetic particles were washed in 70 µl of lysis buffer and separated to remove the buffer. After washes, Lysis buffer (500 µl) was added to the cells and mechanically sheared six times using 21-gauge needle (1 ml). On 6^{th} time of mechanical shearing with same needle. Sample was transferred to eppendorf tube containing magnetic particles in it. Biotin labelled oligo $(dT)_{20}$ (0.5 µl) was added to sample and mixed to form the hybridization mix. It was then incubated at 37˚C in water bath for 5 min for immobilisation of the hybridisation mix. This hybridisation mix was incubated at room temperature on magnetic particle separator and the lysate was discarded. SMPs were washed three times with a 200 µl washing buffer. The eppendorf was place on magnetic separator each time to discard washing buffer. It was centrifuged for 1 min in order to removing remaining wash buffer. mRNA was eluted in 10 µl redistilled water and incubated at 65˚C for 2 min. Using the magnetic separator, the eluted mRNA was separated from the magnetic particles and transferred to labelled eppendorf tube and then stored at -20˚C.

2.5.2 mRNA Quantification using NanoDrop spectrometer

The Thermo scientific NanoDrop 1000 Spectrophotometer was used as it is fast and efficient for determining quantity and the purity of mRNA. It measured 1 µl samples with high accuracy and reproducibility which are highly concentrated samples without dilution. The Instrument operated by a patented sample retention technology that utilizes surface tension to hold the sample in place. This instrument helped to eliminate the use of cuvettes and also limits contamination since it is easy to clean.

The instrument was controlled by a PC based software and the data were logged. After cleaning NanoDrop, application module settings were changed from Nucleic acid to RNA and a volume of 1 µl Distilled water was loaded on sampling arm with a fiber optic cable (the receiving fiber) and second fiber optic cable (the source fiber) was then brought into contact with the liquid sample causing the liquid to bridge the gap between the fiber optic ends. A spectrophotometer utilized linear CCD (Charged Coupled-Device) array to analyse light passing through the liquid sample and this was set as a blank. The mRNA sample was loaded to measure and 260:280 (nm) value and ng/µl was recorded to check purity of mRNA. mRNA purity between 260:280 values must be in the range of 1.5-2.00 which signified good purity.

2.5.3 Complimentary DNA (cDNA) synthesis

The First strand cDNA synthesis kit was used to reverse transcribe mRNA. This kit included AMV (Avian Myeloblastosis virus) enzymes isolated from Avian Myeloblastosis which synthesizes the new cDNA strand at the 3'-end of the poly (A)- mRNA where oligo dT was used as a primer. The quantity of mRNA sample used for cDNA synthesis varies according to purity of the mRNA obtained. From the concentration of mRNA obtained, the required concentration for 100 ng was determined. The quantity of 100 ng was to maintain as a constant quantity for preparation of all samples.

The Protocol of Roche applied sciences was followed to synthesis first strand cDNA. All reagents and samples were thawed at room temperature while the RNase inhibitor and AMV reverse transcriptase were thawed on ice and vortexed. In order to avoid contamination, all equipments used were autoclaved. The master mix of 11.8 µl was prepared using reagents provided in first cDNA synthesis kit (Roche applied sciences, UK) (Table 2.6). The quantified amount of mRNA (100 ng) was added, followed by the addition of sterile water to attain a final volume of 20 µl in each sample and the mixture was briefly vortexed and centrifuged.

Mastermix was first incubated at 25°C for 10 min for the primer to anneal to the mRNA template. During the second incubation at 42°C for 60 min, mRNA was reverse transcribed to cDNA and following incubation at 99°C for 5 min, AMV Reverse Transcriptase denatured on incubation. Sample was then cooled to 4°C for 5 min and stored at −20°C.

Table 2.6: Reagents used in first strand cDNA synthesis for one sample.

Reagents	Volume of reagents (µl)	Final concentration
10× Reaction buffer	2.0	1×
25 mM Magnesium chloride ($MgCl_2$)	4.0	5 mM
Primer Oligo-p$(dT)_{15}$	2.0	0.04 A_{260} units (0.06 µg)
RNAse inhibitor	1.0	50 units
AMV-Reverse Transcriptase	0.8	≥20 units
Deoxynucleotide mix	2.0	1 mM
Total volume	11.8	

2.5.4 Gene sequence and Primer design

GAPDH (glyceraldehyde-3-phosphate dehydrogenase) is used as housekeeping gene while *Hsp70* (*Hspa8* from Heat shock protein 70 kDa family also known as HSC70) and *Hsp90a* (Heat shock protein 90 kDa) are targeted genes which are constitutively expressed. Using GeneCards database, gene locations were determined. The mRNA sequence of each gene was obtained using NCBI database. In order to carry out a study of genes using polymerase chain reaction (PCR), requires a primer to amplify the gene. This primer was designed using Primer3Plus software analysing obtained mRNA sequence. As described in Figure 2.3 -Figure 2.11.

2.5.4.1 *GAPDH*

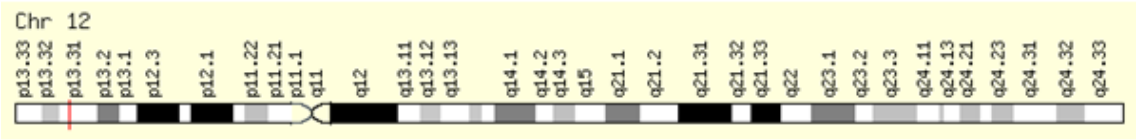

Figure 2.3: Gene location of *GAPDH*, a housekeeping gene using GeneCards database. Red bar represents location of *GAPDH* gene.

```
1       ggctgggact  ggctgagcct  ggcgggaggc  ggggtccgag  tcaccgcctg
51      ccgccgcgcc  cccggtttct  ataaattgag  cccgcagcct  cccgcttcgc
101     tctctgctcc  tcctgttcga  cagtcagccg  catcttcttt  tgcgtcgcca
151     gccgagccac  atcgctcaga  caccatgggg  aaggtgaagg  tcggagtcaa
201     cggatttggt  cgtattgggc  gcctggtcac  cagggctgct  tttaactctg
251     gtaaagtgga  tattgttgcc  atcaatgacc  ccttcattga  cctcaactac
301     atggtttaca  tgttccaata  tgattccacc  catggcaaat  tccatggcac
351     cgtcaaggct  gagaacggga  agcttgtcat  caatggaaat  cccatcacca
401     tcttccagga  gcgagatccc  tccaaaatca  agtggggcga  tgctggcgct
451     gagtacgtcg  tggagtccac  tggcgtcttc  accaccatgg  agaaggctgg
501     ggctcatttg  cagggggggag ccaaaagggt  catcatctct  gccccctctg
551     ctgatgcccc  catgttcgtc  atgggtgtga  accatgagaa  gtatgacaac
601     agcctcaaga  tcatcagcaa  tgcctcctgc  accaccaact  gcttagcacc
651     cctggccaag  gtcatccatg  acaactttgg  tatcgtggaa  ggactcatga
701     ccacagtcca  tgccatcact  gccacccaga  agactgtgga  tggcccctcc
751     gggaaactgt  ggcgtgatgg  ccgcggggct  ctccagaaca  tcatccctgc
801     ctctactggc  gctgccaagg  ctgtgggcaa  ggtcatccct  gagctgaacg
851     ggaagctcac  tggcatggcc  ttccgtgtcc  ccactgccaa  cgtgtcagtg
901     gtggacctga  cctgccgtct  agaaaaacct  gccaaatatg  atgacatcaa
951     gaaggtggtg  aagcaggcgt  cggagggccc  cctcaagggc  atcctgggct
1001    acactgagca  ccaggtggtc  tcctctgact  tcaacagcga  cacccactcc
1051    tccacctttg  acgctggggc  tggcattgcc  ctcaacgacc  actttgtcaa
1101    gctcatttcc  tggtatgaca  acgaatttgg  ctacagcaac  agggtggtgg
1151    acctcatggc  ccacatggcc  tccaaggagt  aagacccctg  gaccaccagc
1201    cccagcaaga  gcacaagagg  aagagagaga  ccctcactgc  tggggagtcc
1251    ctgccacact  cagtccccca  ccacactgaa  tctcccctcc  tcacagttgc
1301    catgtagacc  ccttgaagag  gggaggggcc  tagggagccg  caccttgtca
1351    tgtaccatca  ataaagtacc  ctgtgctcaa  ccaaaaaaaa  aaaaaaaaaa
1401    a
```

Figure 2.4: mRNA sequence of *GAPDH* gene & the locations of the primers using NCBI database. Primer locations have been highlighted in blues and yellow indicating sense and antisense primers, respectively.

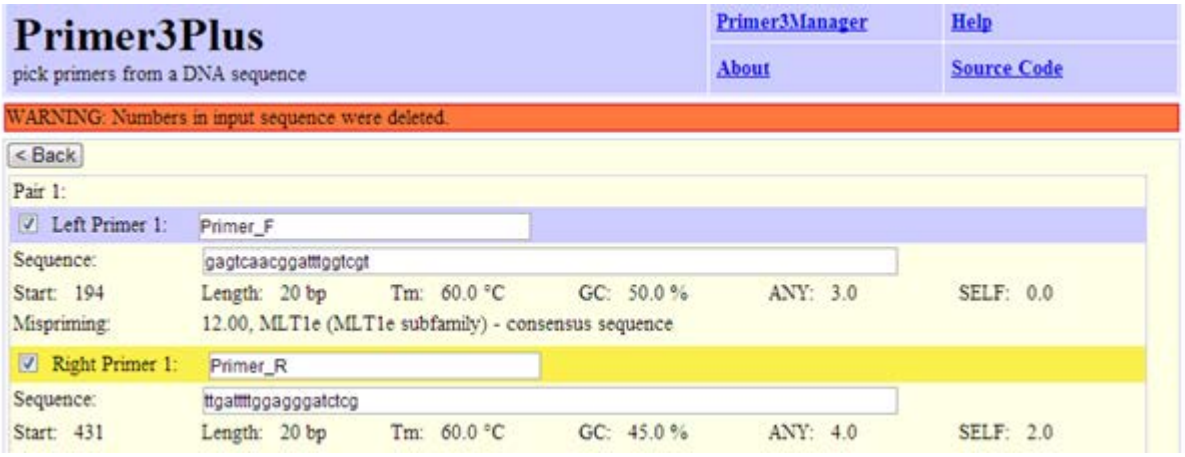

Figure 2.5: Primer design of *GAPDH* gene using Primer3Plus. The output page of Primer3 provides the right and the left primers.

2.5.4.2 *Hsp70*

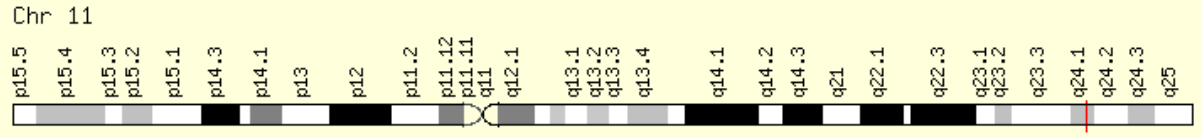

Figure 2.6: Gene location of *Hspa8 (Hsp70)* using GeneCards. Red bar represents location of *Hsp70* gene.

```
1       ccttctggaa  ggttctaaga  tagggtataa  gaggcagggt  ggcgggcgga
51      aaccggtctc  attgaactcg  cctgcagctc  ttgggttttt  tgtggcttcc
101     ttcgttattg  gagccaggcc  tacaccccag  caaccatgtc  caagggacct
151     gcagttggta  ttgatcttgg  caccacctac  tcttgtgtgg  gtgttttcca
201     gcacggaaaa  gtcgagataa  ttgccaatga  tcagggaaac  cgaaccactc
251     caagctatgt  cgcctttacg  gacactgaac  ggttgatcgg  tgatgccgca
301     aagaatcaag  ttgcaatgaa  ccccaccaac  acagtttttg  atgccaaacg
351     tctgattgga  cgcagatttg  atgatgctgt  tgtccagtct  gatatgaaac
401     attggccctt  tatggtggtg  aatgatgctg  gcaggcccaa  ggtccaagta
451     gaatacaagg  gagagaccaa  aagcttctat  ccagaggagg  tgtcttctat
501     ggttctgaca  aagatgaagg  aaattgcaga  agcctacctt  gggaagactg
551     ttaccaatgc  tgtggtcaca  gtgccagctt  actttaatga  ctctcagcgt
601     caggctacca  aagatgctgg  aactattgct  ggtctcaatg  tacttagaat
651     tattaatgag  ccaactgctg  ctgctattgc  ttacggctta  gacaaaaagg
701     ttggagcaga  aagaaacgtg  ctcatctttg  acctgggagg  tggcactttt
751     gatgtgtcaa  tcctcactat  tgaggatgga  atctttgagg  tcaagtctac
801     agctggagac  acccacttgg  gtggagaaga  ttttgacaac  cgaatggtca
851     accattttat  tgctgagttt  aagcgcaagc  ataagaagga  catcagtgag
901     aacaagagag  ctgtaagacg  cctccgtact  gcttgtgaac  gtgctaagcg
951     taccctctct  tccagcaccc  aggccagtat  tgagatcgat  tctctctatg
1001    aaggaatcga  cttctatacc  tccattaccc  gtgcccgatt  tgaagaactg
1051    aatgctgacc  tgttccgtgg  caccctggac  ccagtagaga  aagcccttcg
1101    agatgccaaa  ctagacaagt  cacagattca  tgatattgtc  ctggttggtg
1151    gttctactcg  tatccccaag  attcagaagc  ttctccaaga  cttcttcaat
1201    ggaaaagaac  tgaataagag  catcaaccct  gatgaagctg  ttgcttatgg
1251    tgcagctgtc  caggcagcca  tcttgtctgg  agacaagtct  gagaatgttc
1301    aagatttgct  gctcttggat  gtcactcctc  tttcccttgg  tattgaaact
1351    gctggtggag  tcatgactgt  cctcatcaag  cgtaatacca  ccattcctac
1401    caagcagaca  cagaccttca  ctacctattc  tgacaaccag  cctggtgtgc
1451    ttattcaggt  ttatgaaggc  gagcgtgcca  tgacaaagga  taacaacctg
1501    cttggcaagt  ttgaactcac  aggcatacct  cctgcacccc  gaggtgttcc
1551    tcagattgaa  gtcacttttg  acattgatgc  caatggtata  ctcaatgtct
1601    ctgctgtgga  caagagtacg  ggaaaagaga  acaagattac  tatcactaat
1651    gacaagggcc  gtttgagcaa  ggaagacatt  gaacgtatgg  tccaggaagc
1701    tgagaagtac  aaagctgaag  atgagaagca  gagggacaag  gtgtcatcca
1751    agaattcact  tgagtcctat  gccttcaaca  tgaaagcaac  tgttgaagat
1801    gagaaacttc  aaggcaagat  taacgatgag  gacaaacaga  agattctgga
1851    caagtgtaat  gaaattatca  actggcttga  taagaatcag  actgctgaga
1901    aggaagaatt  tgaacatcaa  cagaaagagc  tggagaaagt  ttgcaacccc
1951    atcatcacca  agctgtacca  gagtgcagga  ggcatgccag  gaggaatgcc
2001    tgggggattt  cctggtggtg  gagctcctcc  ctctggtggt  gcttcctcag
2051    ggcccaccat  tgaagaggtt  gattaagcca  accaagtgta  gatgtagcat
2101    tgttccacac  atttaaaaca  tttgaaggac  ctaaattcgt  agcaaattct
2151    gtggcagttt  taaaaagtta  agctgctata  gtaagttact  gggcattctc
2201    aatacttgaa  tatggaacat  atgcacaggg  gaaggaaata  acattgcact
2251    ttataaacac  tgtattgtaa  gtggaaaatg  caatgtctta  aataaaacta
2301    tttaaaattg  gcaccataaa  aaaaaaaaaa  a
```

Figure 2.7: mRNA sequence of *Hspa8 (Hsp70)* & the locations of the primers using NCBI database. Primer locations have been highlighted in blues and yellow indicating sense and antisense primers, respectively.

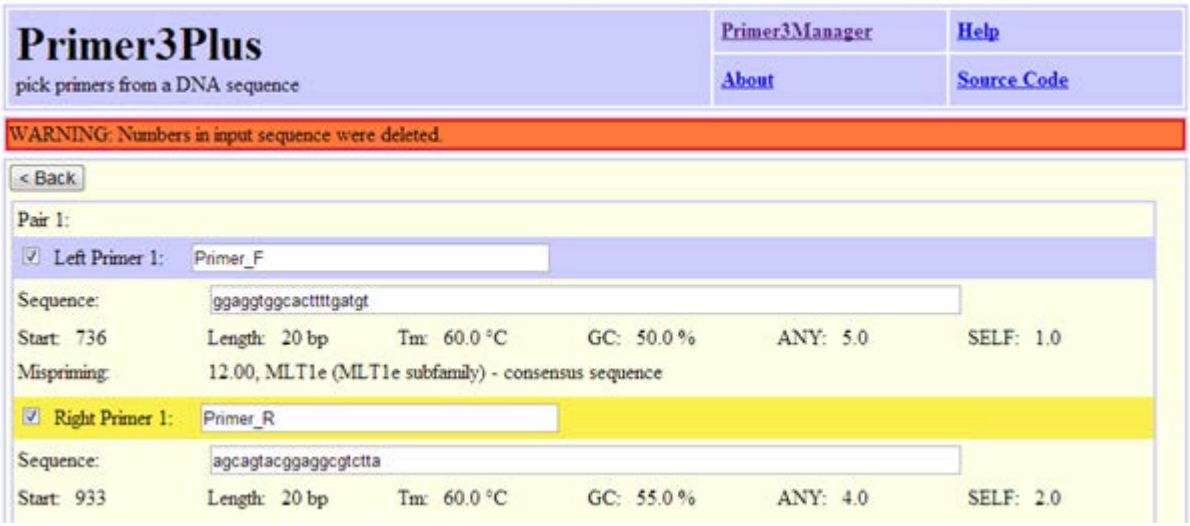

Figure 2.8: Primer design of *Hspa8 (Hsp70)* using Primer3Plus. The output page of Primer3 provides the right and the left primers.

2.5.4.3 *Hsp90*

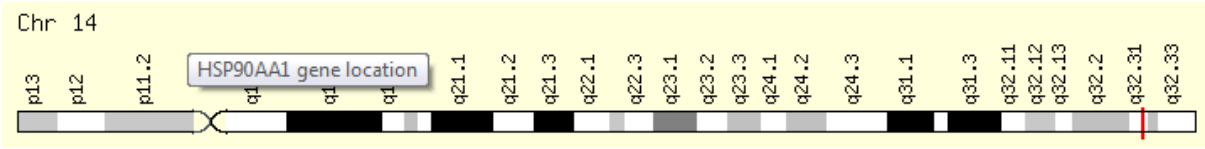

Figure 2.9: Gene location of *Hsp90a (Hsp90)* gene using GeneCards database. Red bar represents location of *Hsp90* gene.

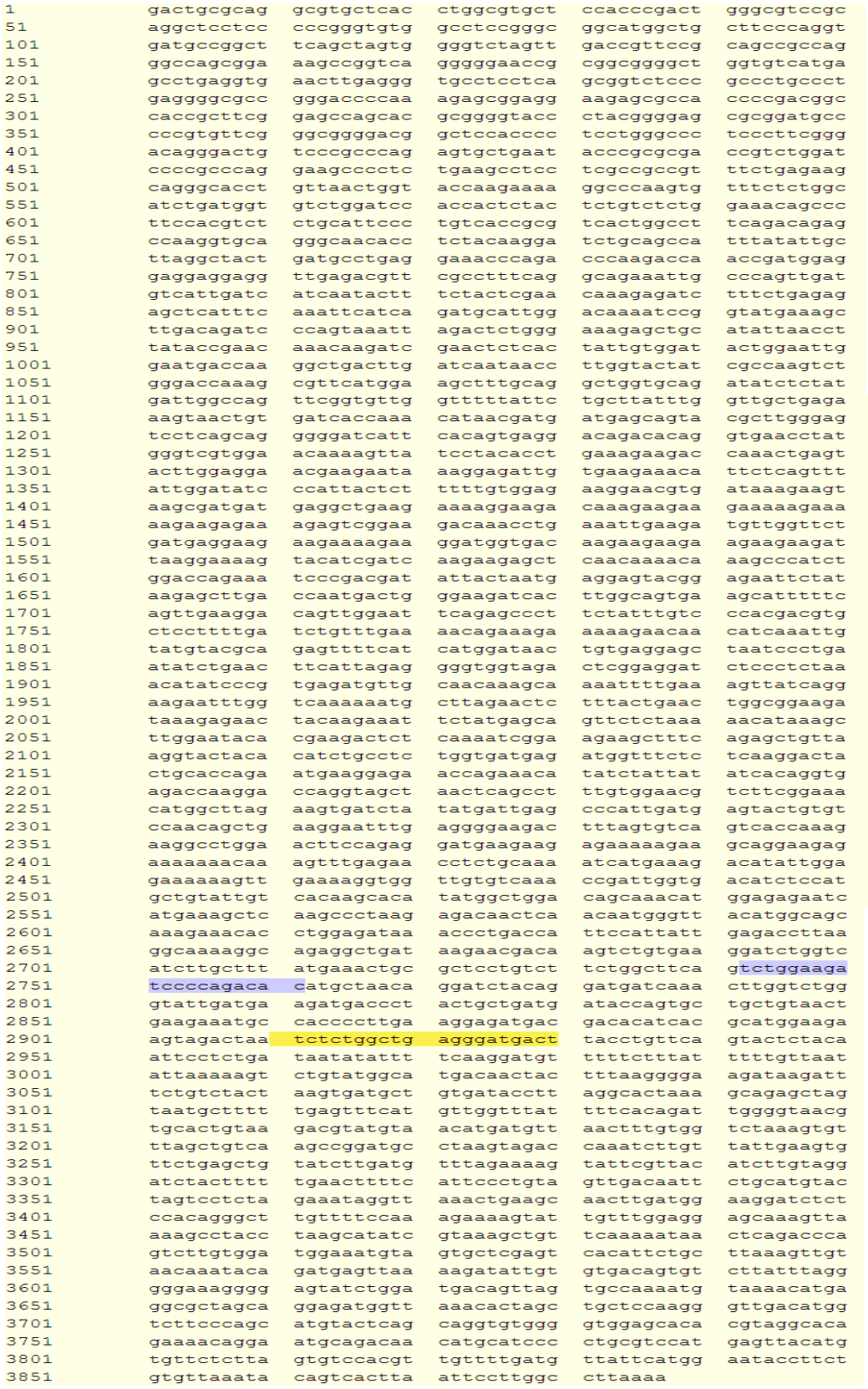

Figure 2.10: Gene location of *Hsp90a (Hsp90)* gene & the locations of the primers using GeneCards database. Primer locations have been highlighted in blues and yellow indicating sense and antisense primers, respectively.

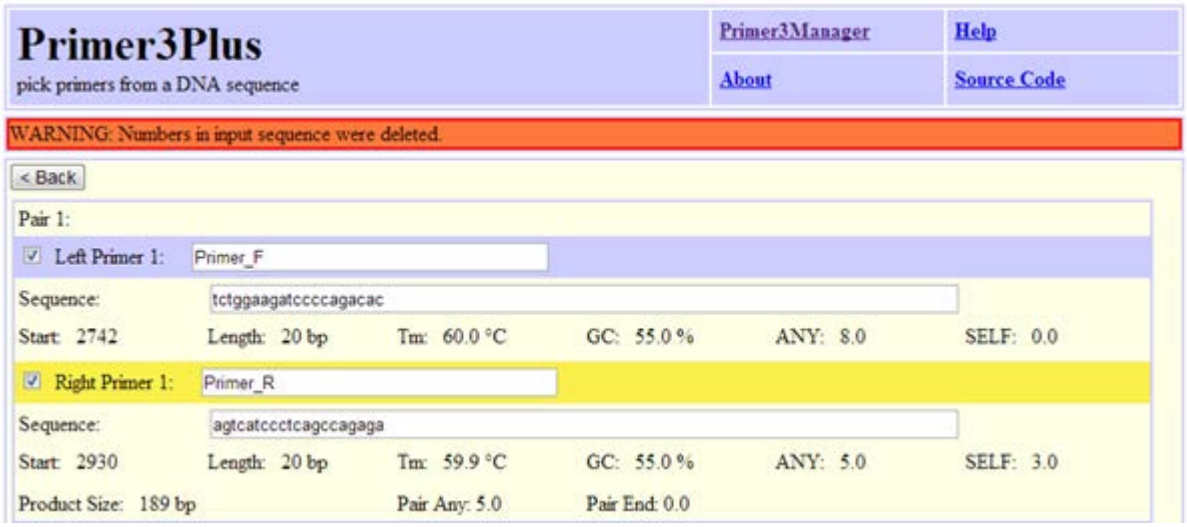

Figure 2.11: Primer design of *Hsp90a (Hsp90)* using Primer3Plus. The output page of Primer3 provides the right and the left primers.

2.5.4.4 *Primer preparation*

Primers were synthesised by TIB MOLBIOL (Berlin, Germany). Each primer (right/sense and left/antisense) was dissolved in 250 µl of molecular biology grade water to obtain 20 µM stock solutions and stored at -20°C as recommended by the manufacturer. Annealing temperature of Primers were used using manufacturers recommendations as mentioned in Table 2.7.

Table 2.7: Primer sequence, annealing temperatures and amplicon size *for GAPDH, Hsp90α and Hsp70* primers used in qRT-PCR.

Gene	Primer sequence	Annealing Temperature (°C)	Amplicon size (base pair (bp))
GAPDH	Sense: 5' – gagtcaacggatttggtcgt – 3' Antisense: 5' – ttgattttggagggatctcg – 3'	56	238
Hsp70	Sense: 5' – ggaggtggcacttttgatgt – 3' Antisense: 5' – agcagtacggaggcgtctta – 3'	60	198
Hsp90α	Sense: 5' – tctggaagatccccagacac – 3' Antisense: 5' – agtcatccctcagccagaga – 3'	63	189

2.5.5 Quantitative real time polymerase chain reaction (qRT-PCR)

qRT-PCR is a technique enabling consistent detection and quantification of products generated during each cycle of the PCR process. It logarithmically amplified short DNA sequences (usually 100-600 bases) within a longer double stranded DNA molecule. Thus, it enabled detection of very low copies of the target-specific product amplification (Roche Applied Science, UK). *Hsp90a, Hsp70* and *GAPDH* were amplified by performing qRT-PCR on the LightCycler 2.0 system (Roche Diagnostics, Germany). The experiments were carried out using LightCycler® FastStart DNA Master PLUS SYBR Green I kit following the manufacturer's instructions. LightCycler reaction Master Mix was prepared by using the reagents from the kit provided that includes 1a (white cap) Lightcycler FastStart Enzyme and 1b (Green Cap) Lightcycler FastStart DNA Master^{PLUS} Reaction Mix. A volume of 14 µl of 1a was pipetted into 1b. The 1b was re-labelled as 1 which represents the Mastermix. Mastermix was stored at 4°C and protected from light.

The reagents and samples were thawed and kept on ice throughout the experiment. PCR enzyme mastermix was made from components of the LightCycler® FastStart DNA Master PLUS SYBR Green I kit (Table 2.8) with the recommended volume for each sample. PCR mastermix was briefly centrifuged. Capillaries were placed on the capillary adapter and 2µl PCR grade H_2O was loaded as a negative control and 2 µl cDNA sample in the other capillaries. Capillaries were centrifuged for a minute and then transferred to LightCycler sample carousel and then into the LightCycler instrument.

Table 2.8: Components required for LightCycler® FastStart DNA Master PLUS SYBR Green I kit sample preparation for qRT-PCR primer mastermix.

Components	Volume (µl)
Molecular biology H_2O, PCR grade	12
PCR Primer mix (Left + Right Primer)	2 (1 µl + 1µl)
PCR enzyme master mix	4
cDNA template	2

Following the settings found in Table 2.9, qRT-PCR run was carried out. This protocol involved several steps which played an important role. Pre-incubation, FastStart DNA polymerase was activated and DNA was denatured. This also increased PCR specificity and sensitivity by preventing non-specific elongations. Target DNA was amplified and melting provides melting curves for analysis of the PCR product. The final step involved cooling of the rotor and the thermal chamber where PCR product is placed.

Table 2.9: LightCycler program for qRT-PCR utilizing Fast Start DNA MasterPLUS SYBR Green Kit.

Analysis mode	Cycles	Segments	Target temperature (°C)	Hold time (sec)
Pre-incubation	1		95	
Amplification	35	Denaturation	95	15
		Annealing	Variable to (refer table primers)	15
		Extension	72	9
Melting	1	Denaturation	95	0
		Annealing	10 higher than amplification	15
		Extension	95	0
Cooling	1		40	30

2.5.6 Analysis of RT-PCR amplicons using agarose gel electrophoresis

Gene expression was determined by running PCR products of cDNA samples on 2% agarose gel electrophoresis (AGE). Agarose (0.8 g) was dissolved in 40 ml of 1× TAE buffer to obtain 2% agarose gel. This solution was heated in a domestic microwave at 700 W power for 2 min until agarose particles were thoroughly dissolved. The solution was then poured into casting tray set with comb and cooled for 45 min to set gel. The comb was removed after solidified of the agarose gel and was placed into electrophoresis gel tank. 1× TAE running buffer (300 ml) was poured into gel tank until the level to cover the gel (Table 2.2). The loading sample contained 2 µl of loading dye and 5 µl of PCR products sample amplicons. A volume of 5 µl of 100 bp molecular marker was loaded along with samples to determine the molecular weight as standard at 50 V for approximately 1 h. The gel was stained with 0.5 µg/ml of Ethidium bromide (EtBr) for 30 min, followed by destaining in water for 20 min. The bandings patterns were observed using a GENE GENIUS Bioimaging system, UK and Gensnap software (Syngene, UK).

2.5.7 Copy Number Quantification

Copy number standard curve (Figure 2.12) was generated to calculate the copy numbers of the unknown samples (*Hsp70, Hsp90a and GAPDH*) by plotting the crossing point or Ct value against copy numbers. This standard curve was previously established in our laboratory (Shervington *et al.,* 2007).

The external standard of known concentration or copy number was used to accurately determine amount of target amplicon. Previous experiments have established the quantification of copy numbers from the crossing point by using genomic DNA as a template (Shervington *et al.,* 2007). A standard curve was plotted for the quantitative method established on the Light Cycler® 2.0 Real-Time PCR (Mohammed *et al.,* 2008). A standard genomic DNA (QIAGEN, UK) with known concentration of 1 µg equivalent of 3.4×10^5 copies of a single gene was prepared using five concentrations (5 pg, 50 pg, 500 pg, 5 ng and 50 ng, Table 2.10). Further amplification was achieved by the LightCycler® using *GAPDH* reference gene with its threshold cycle (Ct) numbers in order to plot the standard curve. The equation generated (y = -1.3124Ln(x) + 32.058) from the standard graph was rearranged to (=EXP {Ct value-32.058)/-1.3124}) to determine the copy numbers of the mRNA expression of all the genes used throughout the study.

Table 2.10: Genomic DNA correspondence to its average Ct values and equivalent copy number.

Genomic DNA concentration (ng)	Dilution factor	Average Crossing point (Ct)
50	17000	18.3
5	1700	22.6
0.5	170	26.42
0.05	17	29.12
0.005	1.7	30.15

(a)

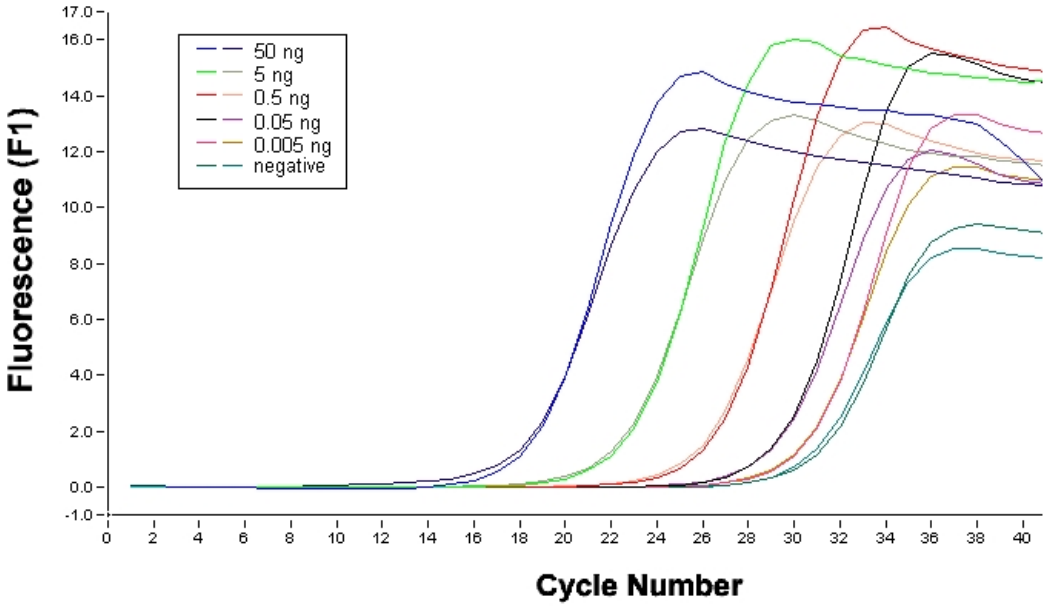

(b)

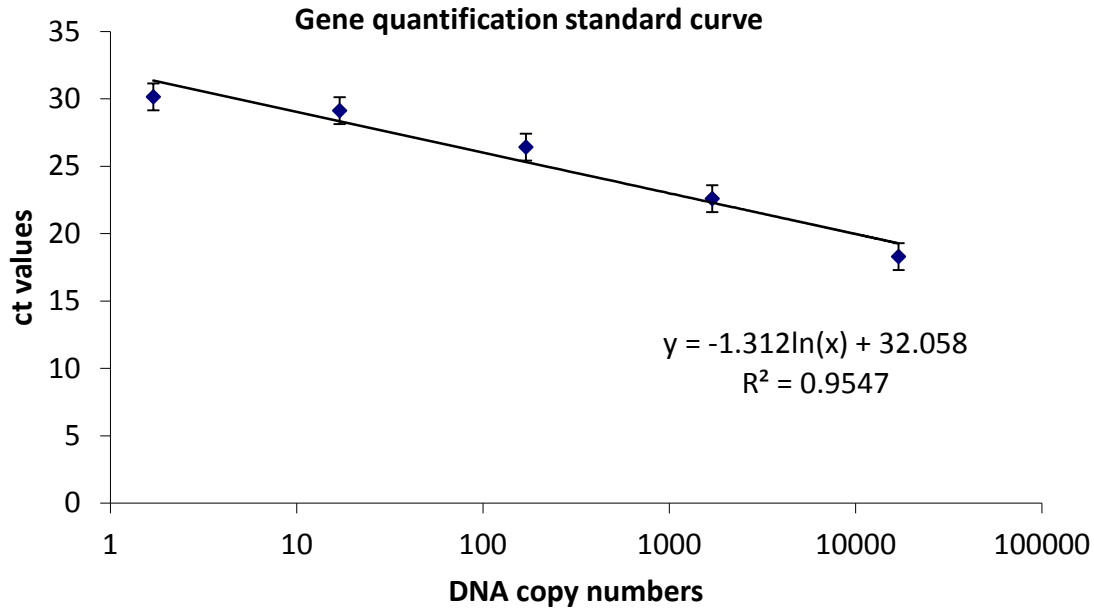

Figure 2.12: Standard to calculate the copy number of the targeted gene. (a) Light Cycler quantification curve generated with known concentration of genomic DNA amplified, showing that the higher the concentration of DNA the lower the Ct values. The negative control (Primer alone) shows no fluorescence acquisition until after 30 Ct (straight line). (b) The standard generated from the crossing points showing the relationship between Ct values and the copy numbers of the amplified genomic DNA using *GAPDH* as a reference gene (n=3) (Taken from Mohammed et al., 2008).

2.5.8 Protein extraction and quantitation

Bradford reagent is quick, efficient and sensitive which utilises Coomassie blue dye. This dye appeared to be red-brown in an acidic solution but when binds to protein due to a shift in dissociation constant, it changes to blue colour. This dye was measured at 595 nm. Thus, the absorbance reading obtained was directly proportional to amount of dye bound to protein enabling the determination of the concentration of protein in the sample. In order to determine unknown concentrations of protein in samples, a standard curve was plotted with increasing concentration of bovine serum albumin (BSA) ranging from 1-8 µg/µl prepared in PBS (1×). BSA was used and recommended since it shows negligible interference in absorbance readings.

Protocol was carried out as follows:

Cell Pellets were thawed and centrifuged at 1200 rpm for 5 min at 4°C to obtain the cell pellet and the supernatant was discarded. Cells were washed with 500 µl of ice cold PBS. According to the amount of cell pellet, cells were resuspended in Celytic M cell lysis reagent (Sigma, UK). For 1×10^6 Cells, a volume of 50 µl of Cell lysis reagent was added while for less than 1×10^6 Cells, 30 µl of cell lysis reagent was added. On cell lysis, the release of proteases could lead to degradation of protein. Thus, 1 µl of protease inhibitor was added to prevent degradation. Further, samples were incubated at room temperature on a shaker for 15 min. Followed by centrifugation at 13000 rpm for 5 min at 4°C. The supernatant was collected in a fresh tube (supernatant contains protein). The protein concentration was measured using the Bradford protein assay method. The protein quantitation was carried out using Coomassie blue reagent (1 ml CBR + 9 ml distilled H_2O) at 595 nm. CBR and sample (1:1000) was aliquoted into cuvettes and incubated for 2 mins. The absorbance was measured at 595 nm using gamma thermo

Helios spectrophotometer (Thermospectronics, UK). A standard curve was plotted and the concentration of the unknown protein was extrapolated Figure 2.13. Each protein was assayed at least 2 times and the mean values taken.

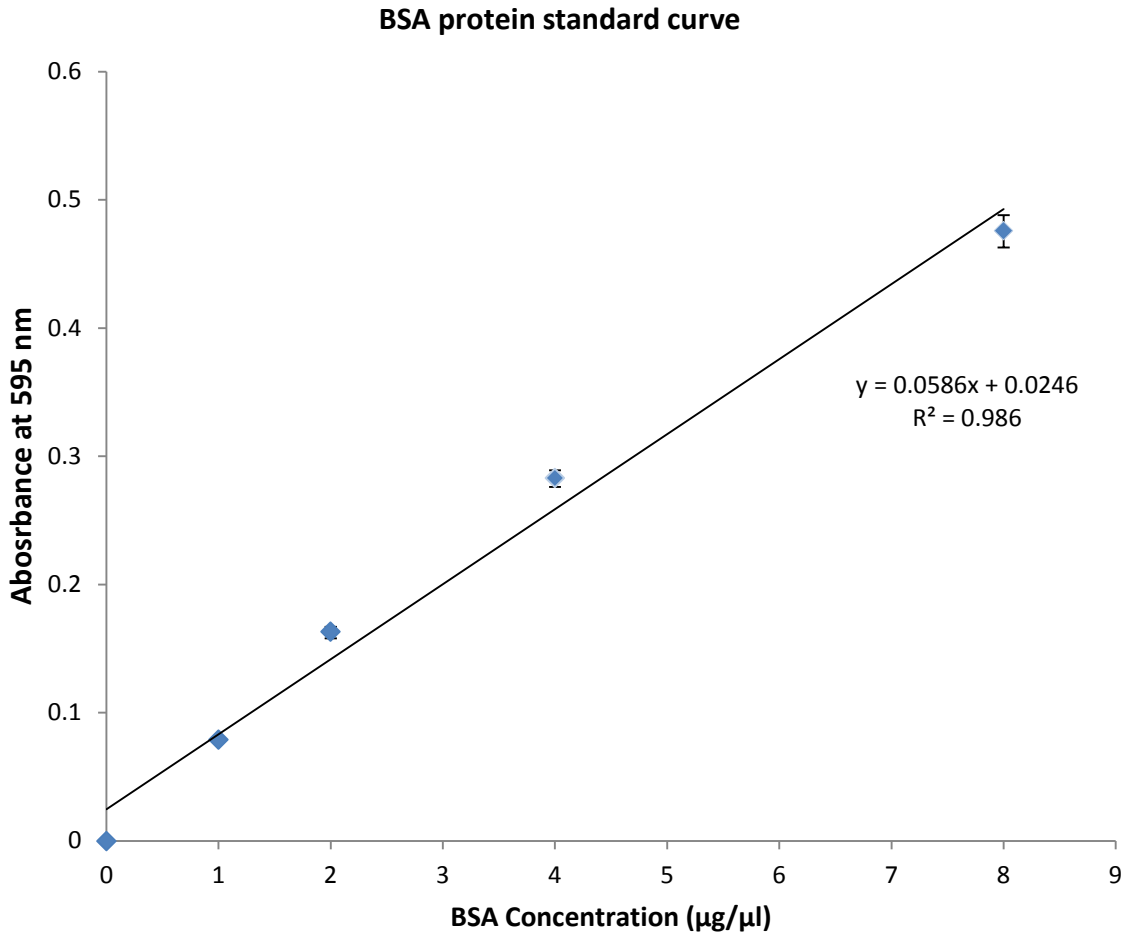

Figure 2.13: Protein quantitation standard curve. The equation was used to calculate the concentration of protein in test samples. The values shown are mean ± SD, n = 3.

2.5.8.1 *Akt/PKB kinase assay*

Akt/PKB kinase activity kit was designed for analysis of PKB (Protein Kinase B) activity in the solution; based on solid phase enzyme linked immune-absorbent assay (ELISA). It utilised a synthetic peptide as substrate for PKB accompanied by a polyclonal antibody to recognise phosphorylated forms of substrate. The Akt Kinase activity kit is a safe, rapid and a reliable technique.

The components of kit that included PKB substrate microtitre plate, Antibody dilution buffer, Kinase assay dilution buffer, TMB substrate and Stop solution 2 were equilibrated at room temperature before use and the reagents were prepared according to manufacturer's instructions. Required number of wells from the PKB substrate microtitre plate was soaked with 50 µl of Kinase assay dilution buffer at room temperature for 10 min. After aspirating the liquid from each well, varying concentration of active PKB (2.5, 5, 10, 20 and 40 ng) were added to the appropriate wells in microtitre plate. Except for the blank, 10 µl of diluted ATP was added to each well in order to initiate the reaction. The plate was then incubated at 30°C in an orbital shaker at 60 rpm for 60 min. The reaction was stopped by emptying the content of the well. Except for the blank, 40 µl of phosphospecific substrate antibody was added to each well and then incubated for 60 min. at room temperature. All the wells were washed four times with 100 µl of 1× wash buffer considering 2 min interval for each wash. Except for the blank, 40 µl of diluted Anti-Rabbit IgG: HRP Conjugate was added to each well. After incubating the plate at room temperature for 30 min, the wells were washed four times with 100 µl 1× wash buffer. Each well was then treated with 60 µl of TMB substrate. The plates were incubated at room temperature. According to the development of the colour, incubation time was determined between 10-15 min. In a similar order to that of the TMB substrate, 20 µl of the stop solution 2 was added. The absorbance was then

measured at 450 nm using a microtitre plate reader. A standard curve was then plotted (Figure 2.14).

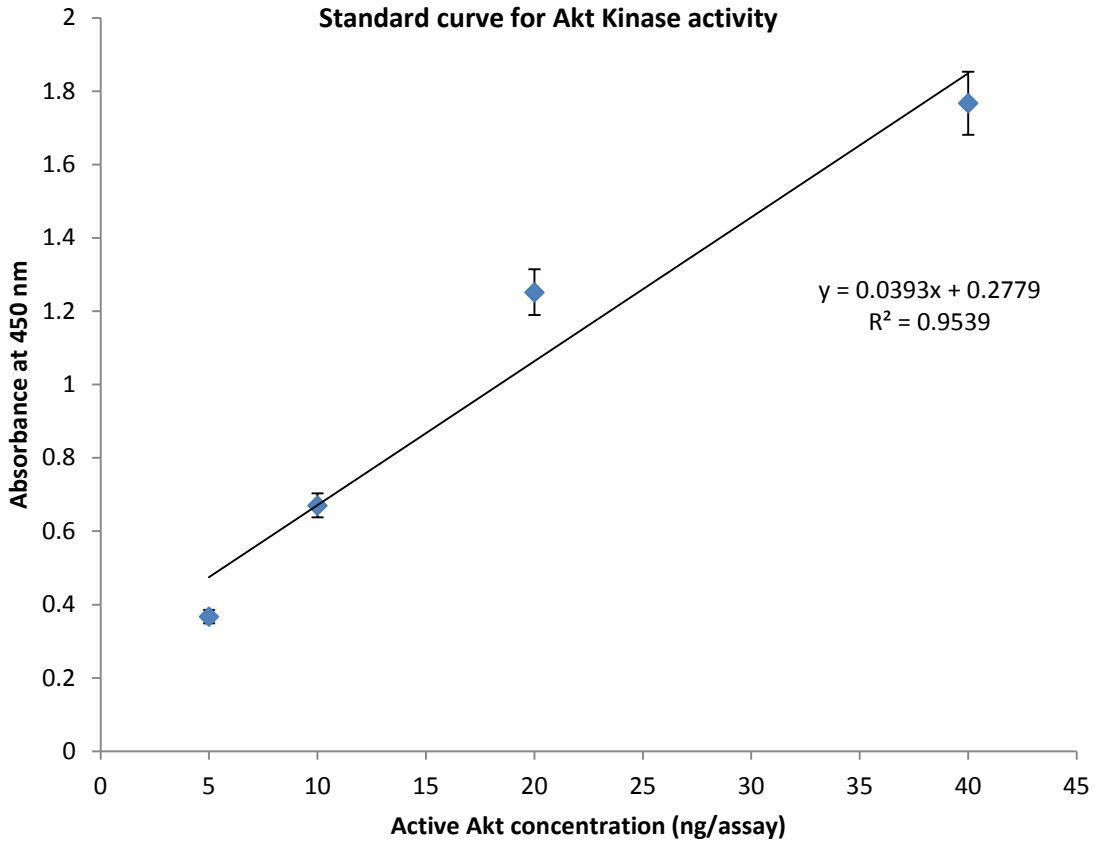

Figure 2.14: Standard curve for Akt kinase activity assay obtained using purified recombinant active Akt The provided recombinant active Akt was diluted in Kinase Assay Dilution Buffer to give final concentration from 5-40 ng/assay. The equation derived from the curve was then used to calculate the Akt activity in treated and untreated samples based on the absorbance readings. This graph is typical of three independent experiments. Data values are mean ± SD, n = 3.

2.5.8.2 *Assay Procedure*

Protein sample (1 µg) was calculated using protein standard curve and diluted in kinase buffer to obtain volume of 30 µl. The assay procedure performed was similar to the standard curve procedure but with a few modifications. At step 3, after aspirating the liquid from each well, the sample volume was added to the appropriate wells in the microtitre plate. After reading absorbance at 450 nm. Values were further analysed and the kinase activity was determined by using the standard curve of PKB kinase. A similar protocol was followed for both the untreated and drug-treated cells. The working principle is explained in Figure 2.15.

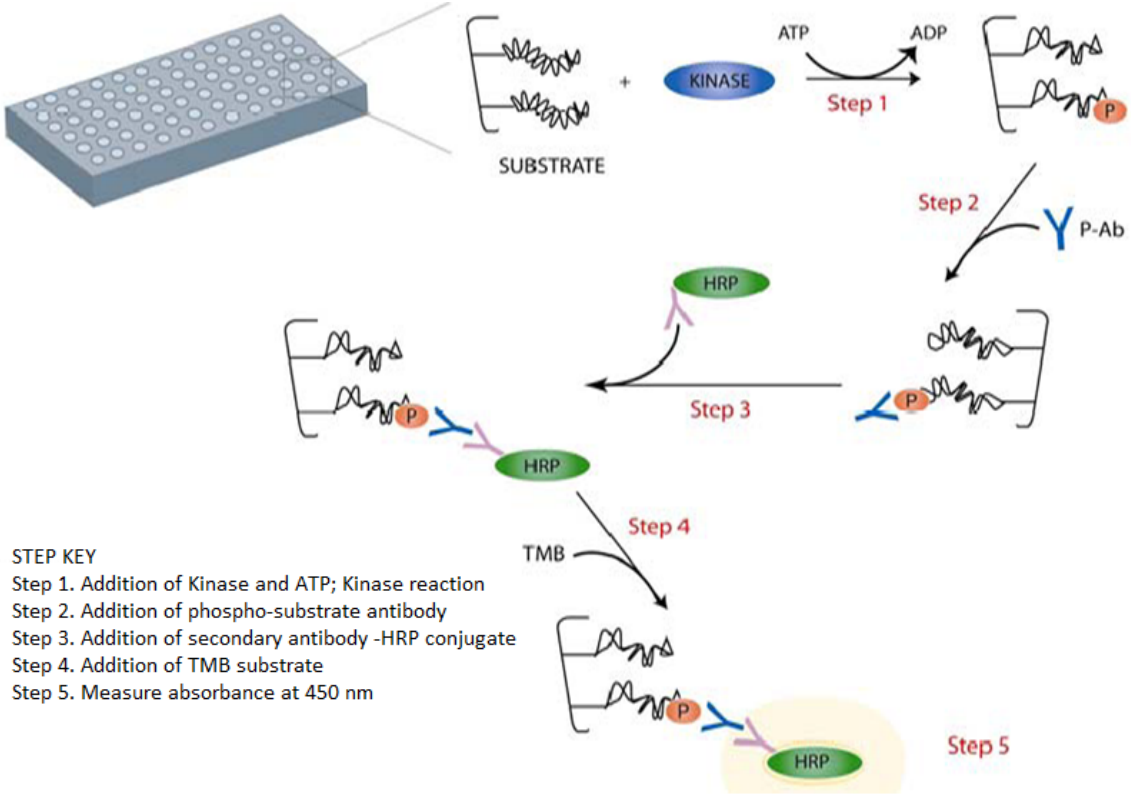

Figure 2.15: Schematic representation of Akt/PKB kinase activity kit mechanism Adapted from instruction manual (adapted from Enzo life sciences, UK).

2.6 miRNA microarray profiling

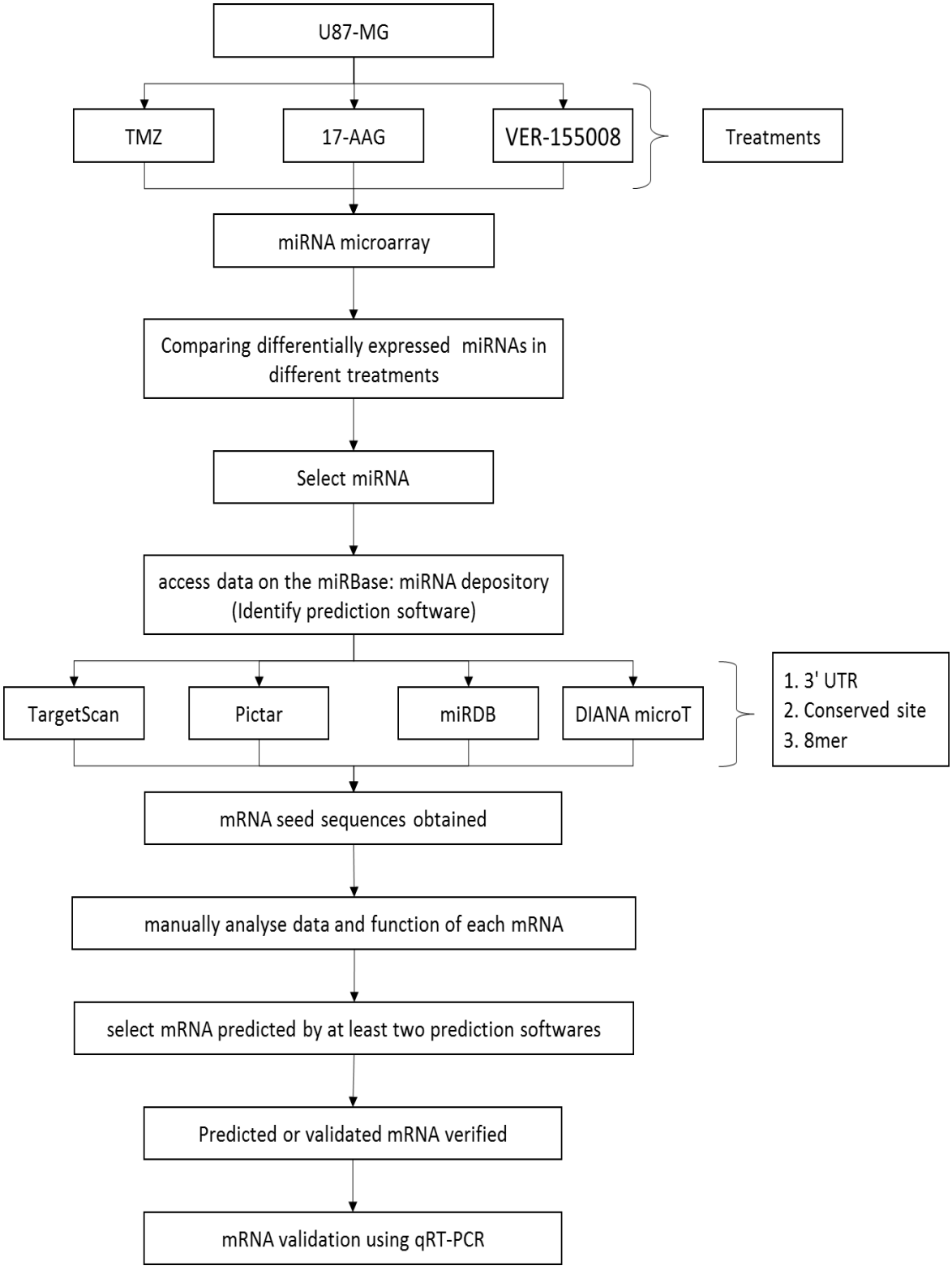

Figure 2.16: Schematic diagram representing workflow for miRNA microarray experiment.

2.6.1 Drug treatment for miRNA microarray analysis

U87-MG cells were seeded in 75 cm^2 flasks 48 h prior to treatment. Cells were treated with IC_{50} of drugs (TMZ, 17-AAG or VER). After 48 h, cells were harvested for miRNA microarray analysis and stored in RNA protect Cell reagent (Qiagen, UK) at -80°C. The cells samples were shipped on dry ice for analysis. miRNA microarray analysis was carried out by IMGM laboratories.

2.6.2 miRNA microarray analysis

2.6.2.1 *Isolation of total RNA including small RNAs*

miRNeasy Mini kit utilised phenol/guanidine for sample lysis and silica membrane–based technique of purification of total RNA. QIAzol lysis reagent provided in the kit had monophasic solution, Phenol/guanidine thiocyanate which lysis cell/tissue by inhibiting RNases and helped in extracting Total RNA without traces of cellular DNA and proteins from the extracted lysate. In order to isolate Total RNA, Cell sample pellets were collected by centrifugation at 5,000×g for 20 min. in order to remove supernatant RNAprotect Cell Reagent and total RNA including the small RNA fractions was isolated using the miRNeasy Mini Kit (Qiagen) mentioned below (Figure 2.17).

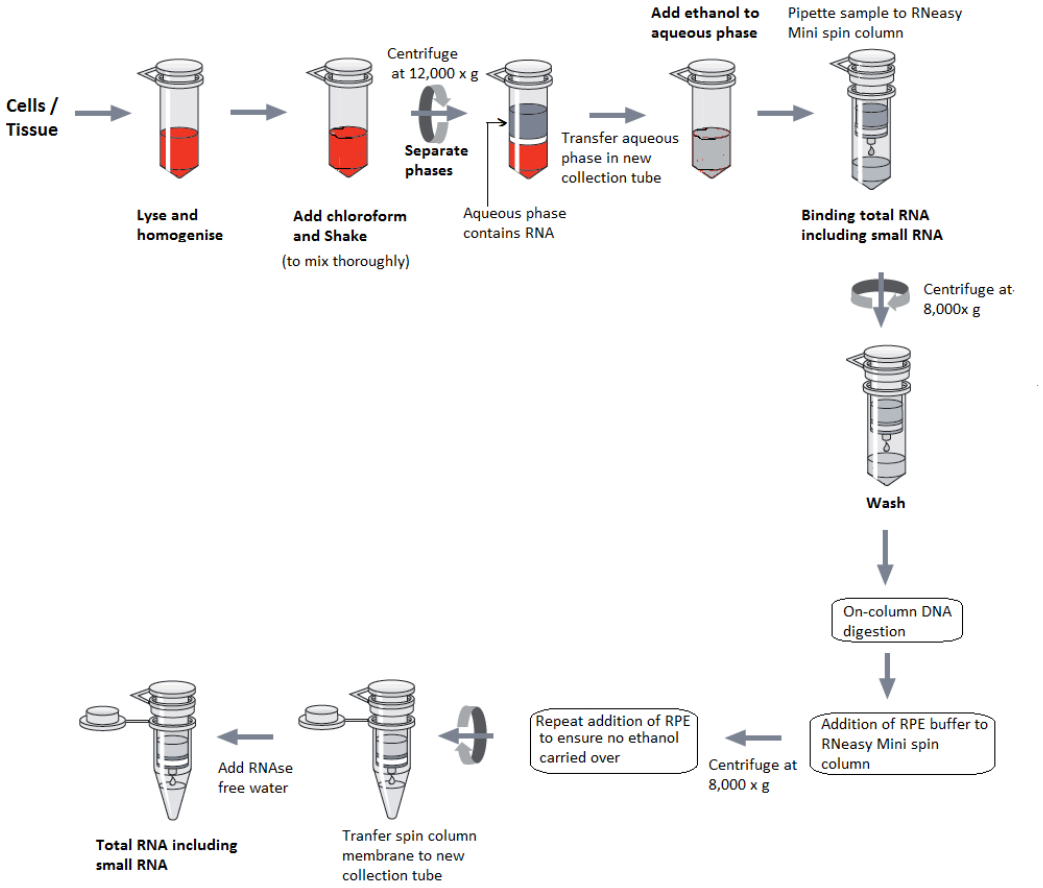

Figure 2.17: Schematic representation of isolation of total RNA (Adapted from Qiagen miRNeasy protocol).

QIAzol lysis Reagent (700 µl) was added to the cell pellet and pellet was loosen by flicking and then vortexing for 1 min. in order to avoid inefficient lysis of cells and homogenising. (for ≤ 3 × 10^6 cells). The sample was placed at RT for 2-3 min. in order to promote dissociation of nucleoprotein complexes. This homogenate containing tube was vigorously shaken after addition of Chloroform (140 µl) to ensure thorough mixing followed by incubation at RT for 2-3 mins. The sample was centrifuged for 15 min. at 12,000× *g* at 4°C which separated samples into 3 phases: upper colourless phase containing RNA, whiter Phase and lower red organic phase. The upper aqueous phase was transferred to new collection tube provided in the kit. Followed by addition of 1.5 volumes of 100% ethanol and thorough mixing. (Followed next step immediately without any delay as addition of ethanol may form precipitate). A volume of 700 µl of the sample was pipetted including any formed precipitate into an RNeasy Mini spin column in a 2 ml collection tube. Samples were centrifuges at 8,000× *g* (10,000 rpm) for 15 s at RT (15-25 °C). Flow through containing QIAzol lysis reagent was discarded. Repeat above step using remainder sample and discarded the flow through.

Followed by On-column DNA digestion for >1 µg total RNA approximately as described. A volume of 350 µl of Buffer RWT was pipetted into the RNeasy Mini Spin column and centrifuge 15s at 8,000× *g* (10,000 rpm) to wash and discard flow through. DNAse I stock solution 10 µl was added to 70 µl Buffer RDD and mixed gently by inverting. DNase I incubation mix (80 µl) was pipetted directly onto the RNeasy Mini spin column membrane and incubated for 15 min at RT (20-30°C). Complete DNase mix was loaded on membrane by avoiding residue sticking to walls or o-ring of the RNeasy mini spin column. A volume of 350 µl Buffer RWT was pipetted into the RNeasy Mini Spin column and centrifuge 15s at 8,000× *g* (10,000 rpm) to wash and discard flow through. A volume of 350 µl buffer RPE was pipetted onto RNeasy Mini spin column and centrifuged 15s at

8,000× *g* (10,000 rpm) to wash and discard flow through. This was followed by addition of 500 µl Buffer RPE to the RNeasy Mini spin column and centrifuged 15s at 8,000× *g* (10,000 rpm) drying spin column membrane ensuring no ethanol carried over. RNeasy spin column was transferred onto new 1.5 ml collection tube and RNase-free water (30 µl) added directly on the spin column membrane. The lid was closed gently and centrifuged for 1 min at 8,000× *g* (10,000 rpm) and total RNA was eluted.

2.6.2.2 *Determination of RNA concentration and purity*

The concentration and Purity of RNA was determined by using NanoDrop ND-1000 spectral-photometer (peqLab). The working of spectrometer was mentioned earlier in section mRNA quantification. Total RNA samples with A260/A280 ratio of > 1.6 indicated absence of contaminating proteins while A260/A230 ratio of > 1.0 indicated the absence of other organic compounds such as guanidinium isothiocynate, alcohol and phenol also other cellular contaminants.

2.6.2.3 *RNA integrity control*

The Agilent 2100 bioanalyzer is a device utilised to monitor total RNA samples quality using capillary electrophoresis prior to performing labelling reaction for microarray analysis. The Bioanalyzer is a microfluidic electrophoretic device that separated RNA according to fragment size and produces an electropherogram used to assess RNA degradation and RNA quantity. It calculated RNA integrity number (RIN) allowed user to easily assess the quality of their RNA samples. RIN scale ranges from 1 to 10, where 1 denoted massive RNA degradation and 10 denoted excellent RNA quality. RIN measured sample integrity and this was determined by ribosomal-RNA ratio 28s /18s r-RNA along with entire electrophoretic profile including the presence or absence of degradation products (Figure 2.18). According to recommendations of Agilent technologies, All

samples were analysed using RNA Nano LabChip Kit and also, only Total RNA samples with RIN values ≥ 7.5 were used for labelling reaction in order to achieve high quality cRNA and evaluable microarray results.

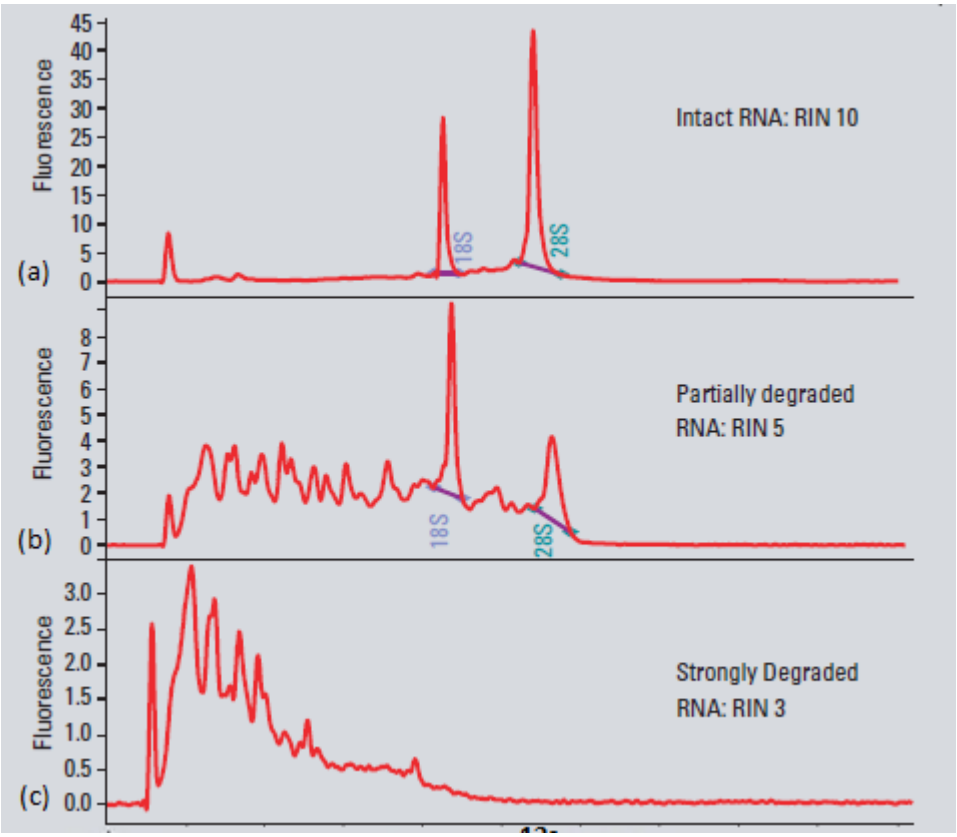

Figure 2.18: Typical electropherograms representing eukaryotic total RNA degradation analysed on 2100 Bioanalyzer (a) intact RNA (b) Partially degraded RNA (c) Degraded RNA (Adapted from Schroeder *et al.,* 2006).

2.6.2.4 *Preparation of Cyanine-3 labeled miRNA*

The Total RNA samples were spiked using microRNA Spike-In kit (Product no.: 5188-5282), Agilent Technologies to serve as an internal labelling control to measure labelling and hybridisation efficiency. 100 ng Total RNA samples were then introduced to ligation-based reaction where samples were treated with Calf Intestinal Alkaline Phosphatase (CIP) and the dephosphorylated RNA were labelled using T4 RNA Ligase which involved ligation of one Cynanine 3-pCp molecule to the 3' end of a RNA molecule (miRNA Complete Labelling and Hyb kit, Agilent Technologies).

2.6.2.5 *Microarray hybridization*

This procedure was followed by preparation of One-Color based hybridisation of the Cyanine 1-pCp-labelled miRNA sample. Samples were hybridised at 55°C for 20 h. on separate Agilent Human miRNA Microarrays Release 19.0 in 8×60K format (AMADID 046064). Microarrays were washed with increasing stringency using Triton X-102 supplemented Gene Expression Wash Buffers (Agilent Technologies) followed by drying with acetonitrile (SIGMA). Fluorescent signal intensities were detected with Scan Control A.8.4.1. Software (Agilent Technologies) on the Agilent DNA microarray scanner and extracted from the images using Feature Extraction 10.7.3.1 software (Agilent Technologies) and the design file *046064_D_F_20121223.xml.* This part of the work was carried out by IMGM laboratories in Germany.

2.6.3 Bioinformatics data analysis

This study used software tools Feature Extraction 10.7.3.1, GeneSPring GX 12.5 (Agilent Technologies) and Sportfire Decision Site 9.1.2 (TIBCO) for quality control, statistical data analysis, miRNA annotation and visualization.

Quantile data normalization was applied to the data set in order to impose the same distribution of probe signal intensities for each array. It maintained median values and intensity distribution of all arrays by shifting all intensities at uniform levels enabling comparison of microarray for downstream analysis. The data was visualised as $\log_2$ transformed manner (after normalization) or as raw data (before normalization).

The similarity between the samples were detected using correlation analysis. Pearson's correlation coefficients (r) were calculated for all biological replicates within the groups and for all pairwise comparisons of the samples in the experiment and correlation coefficient heat map were produced.

Further, raw data was produced by calculating average with replicated sample $\log_2$ transformed data. Three pairwise sample comparisons were analysed. U87-MG untreated cells were used as reference group and gene expression of U87-MG TMZ-treated, U87-MG 17-AAG-treated and U87-MG VER-treated, respectively, was compared to the reference group (U87-MG untreated Control).

2.6.4 Statistical analysis of microarray data

Welch's approximate Student's t-test was applied to the comparison of these different groups which produces a *p*-value (*p*). Benjamini and Hochberg False Discovery Rate (FDR) adjustment algorithm was applied to avoid multiple testing errors which could usually occur when there is more number of standard probes compared to analysed samples and corrected *p* value was determined. Sample groups were then compared in

pair-wise manner in order to achieve differential expression between the groups by calculating fold change (FC). The ratio of raw values between the groups was calculated.

Using Feature Extraction 10.7.3.1 software robust differentially expressed probes were detected which screens only probes which are reliably detectable in at least one out of all samples of the two compared groups. Following these statistical analyses, data sets was further filtered by applying different stringency levels:

a) Stringent filtering in which a probe was only classified as induced or repressed if its corrected p-value (corrected) is ≤ 0.05 and its Fold change (FC) is ≤ (+/-) 2

b) Non-stringent filtering in which a probe is only classifies as induced or repressed if its non-corrected p-value (non-corrected) is ≤ 0.05 and its Fold change (FC) is ≤ (+/-) 2. The multiple testing errors were not taken into consideration while applying Non-stringent filtering.

2.6.5 miRNA Target prediction

The experimental identification and validation of miRNAs regulatory site was a challenge due to its multi targeting ability of miRNA. Thus, various different pipelines or algorithms were developed in order to predict its mRNA targets. Moreover, they had specific working principle. The main method of prediction of miRNA targets implied identification by perfect or imperfect complementarity by Watson-Crick base pairing between miRNA and possible mRNA target. Some utilised perfect pairing in the seed sequence while other also considers evolutionary conservation of the miRNA target. Also, the prediction of target was done by identifying binding energies between imperfect base pairing. There were few other factors by which is utilised by algorithms for prediction of miRNA targets. Currently, an online repository for miRNA is maintained by University of Manchester (www.mirbase.org) developed by Sanger Institute. This

database provided details of miRNAs along with validated and predicted algorithm links which mainly included Target Scan Human 6.2, DIANA-microT and miRBD miRBase V18. As mentioned earlier, each algorithm predicted miRNA target utilising different method. Thus, in order to reduce false target, this study considered miRNA targets with high conserved sites and miRNA target which were validated or co-predicted by two or more algorithms. Further, Intersection analysis was carried out by overlapping with down regulated and up regulated data set (Park *et al.,* 2013). Further, Predicted mRNA targets were validated using qRT-PCR. Following the primer design (Table 2.11), qRT-PCR and statistical analysis procedure carried out as mention earlier in this chapter.

Table 2.11: Primer sequence, annealing temperatures and amplicon size for selected primers used in qRT-PCR.

Gene	Primer sequence	Annealing temperature (°C)	Amplicon size (base pair)
Dnmt3a	Sense 5'–ccggaacattgaggacatct–3', Antisense 5'–cagcagatggtgcagtagga–3'	56	162
Alcam	Sense: 5'–cgtctgctcttctgcctctt–3' Antisense: 5'–taaatactggggagccatcg–3'	56	175
Cdk4	Sense 5'–gaaactctgaagccgaccag–3', Antisense 5'– aggcagagattcgcttgtgt–3'	56	213
Dnajc16 (Hsp40)	Sense 5'– ctcccaaagtgctgggatta–3', Antisense: 5'–agagcttttgggctgaaaca–3'	54	196
R-Ras2	Sense 5'–agcacggcagcttaaggtaa–3', Antisense: 5'–tggcagcctttcttgtcttt–3'	54	165

2.7 Preparation of cell lysate

The cells were treated with respective drugs and approximately 1 × 10^6 cells were harvested for measuring activity of HSP70 and HSP90. Cell pellets were thawed and centrifuged at 1200 rpm for 5 min at 4°C to obtain the cell pellet and the supernatant was discarded. Cells were washed with 500 µl of ice cold PBS. According to the amount cell pellet, cells were resuspended in 1× Extraction reagent was added (For 1 × 10^6 Cells 1 × 10^7 Cells = 1 ml Extraction reagent). Extraction regent helped homogenisation of cells. Also, in order to avoid protein degradation, a volume of 1 µl Protease inhibitor cocktail was added to 1× Extraction reagent. Suspension was incubated on ice for 30 min with occasional mixing. This was followed by centrifuge at 21,000× *g* for 10 min at 4°C. The supernatant (Cell lysate) was transferred into new labelled polypropylene tubes without disturbing pellet.

2.7.1 HSP90α ELISA kit

HSP90α ELISA kit is a quantitative sandwich immunoassay used to determine HSP90α concentration in cell lysates of human origin. It utilised HSP90α specific mouse monoclonal antibody pre-coated on the wells to capture HSP90α in the sample or standard which was detected using an HSP90α antibody conjugated with horseradish peroxidase (HRP). Quantity of HSP90α was detected by measuring colour using microtitre plate reader at 450nm developed by TMB substrate and acidic stop solution which developed endpoint colour.

According to manufacturer's protocol, the reagents of the kit was thawed and brought to room temperature (Anti-HSP90α immunoassay plate, 20× wash buffer, sample diluent, HRP conjugate diluent, TMB substrate and Stop Solution 2). The recombinant HSP90α standard (0.0625 – 4 ng ml) and samples (500 ng/mL total protein) were prepared in sample diluent making up total volume 250 µl. Thereafter, standards and samples (100 µl) were added to the wells of Anti-HSP90α immunoassay plate and incubated at room temperature for 60 min. Zero standard (sample diluent only) was added as blank or reference. This was followed by washes (6 times) with 1× wash buffer and pat dry each time. Then, diluted HRP conjugate (100 µl) was added to the wells except blank and incubated for 60 min. Again repeating washes (6 times) with 1× wash buffer. Followed by addition of TMB substrate to each well and further incubate for 20 min at room temperature. Followed by addition of Stop Solution 2 to each well following same order as TMB substrate was added. Absorbance was measured at 450 nm. Standard curve was plotted and concentration of HSP90α in each samples was determined using the standard plot equation (Figure 2.19).

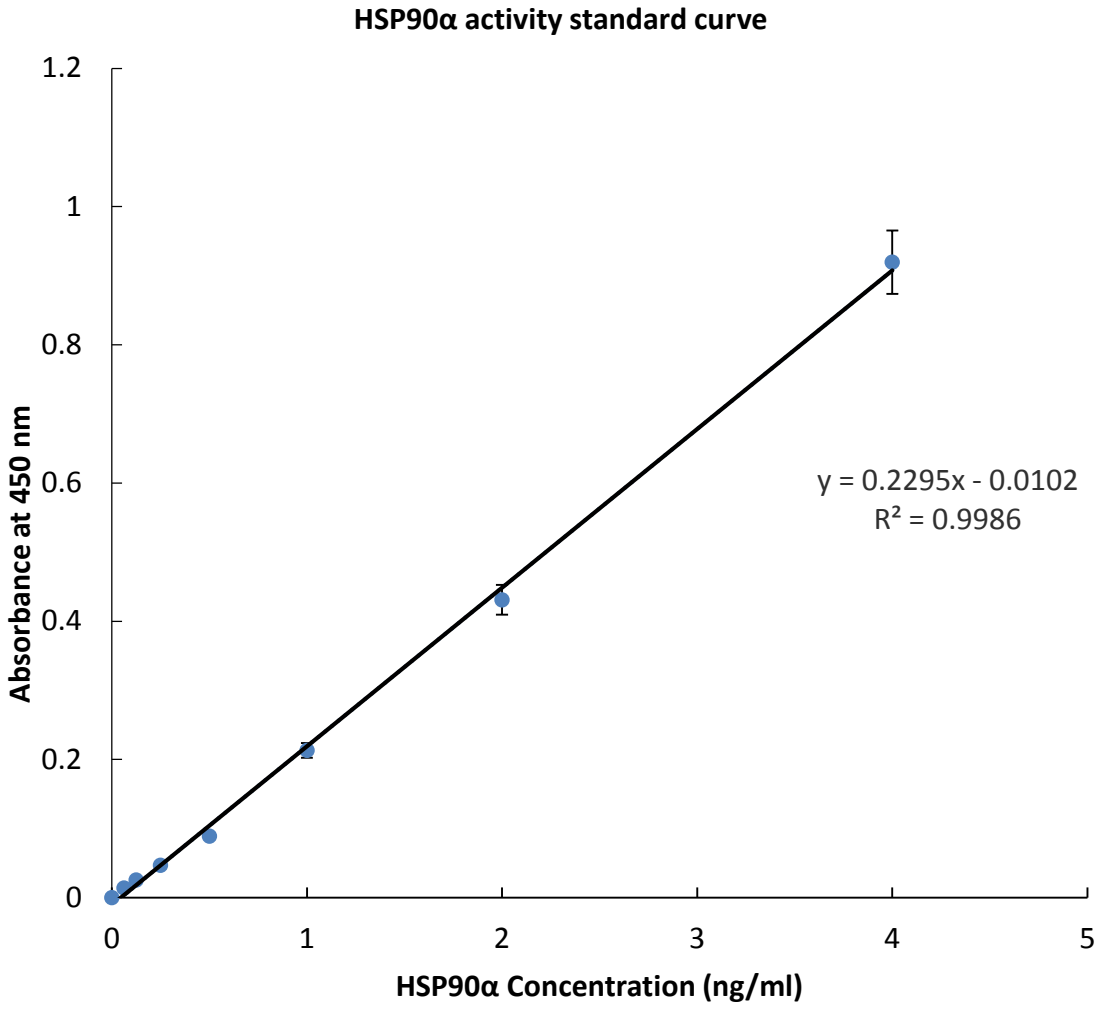

Figure 2.19: HSP90α activity standard curve Active recombinant HSP90α standard was diluted in Kinase Assay Dilution Buffer to give final concentration from 0.0625 - 4 ng/assay. The equation derived from the curve was then used to calculate the HSP90α activity in treated and untreated samples based on the absorbance readings. This graph is typical of two independent experiments. Data values are mean ± SD, n = 4.

2.7.2 HSP70 ELISA kit

HSP70 ELISA kit is a quantitative sandwich immunoassay. Immunoassay plate was pre-coated with HSP70 specific mouse monoclonal antibody which was detected by the HSP70 specific rabbit polyclonal antibody. These HSP70 specific antibody were further bound by a horseradish peroxidase conjugated anti-rabbit IgG secondary antibody. The concentration of HSP70 was measured by measuring intensity produced by TMB substrate at endpoint after adding Stop solution 2. The intensity of colour developed was directly proportional to concentration of HSP70 present in the standards and samples.

According to manufacturer's protocol, the following reagents were brought to room temperature: Anti-HSP70 Immunoassay Plate (required number of wells), Sample Diluent 2, Wash Buffer, HSP70 Antibody HSP70 Conjugate, TMB Substrate, and Stop Solution 2. Recombinant HSP70 Standards and samples were prepared using Sample diluent. Standards and Samples (100 µl each) were added in duplicates to the wells of Anti-HSP70 Immunoassay Plate. Zero standard (0 ng/mL) with sample diluent was added. Plate was covered and incubated at room temperature for 2 h. Wells were washed 4 times using 1× wash buffer and Pat dried each time. Plate was covered and incubated for 1 h at room temperature after addition of HSP70 Antibody (100 µl) except blank. Followed by washes (4 times) using 1× wash buffer and Pat dried each time. Except Blank, HSP70 Conjugated 100 µl was added to all the wells and incubated at room temperature for 1 h. Repeating wash procedure (4 times). Wells were pat dried. TMB substrate (100 µl) was added to each well and incubated at room temperature for 30 min. Stop solution (100 µl) was added to each well after 30 min to stop reaction and absorbance was measured using Tecan Microplate reader at 450nm. Standard curve of

HSP70 concentration was plotted and HSP70 concentration of Samples was calculated using the equation obtained by HSP70 standard curve (Figure 2.20).

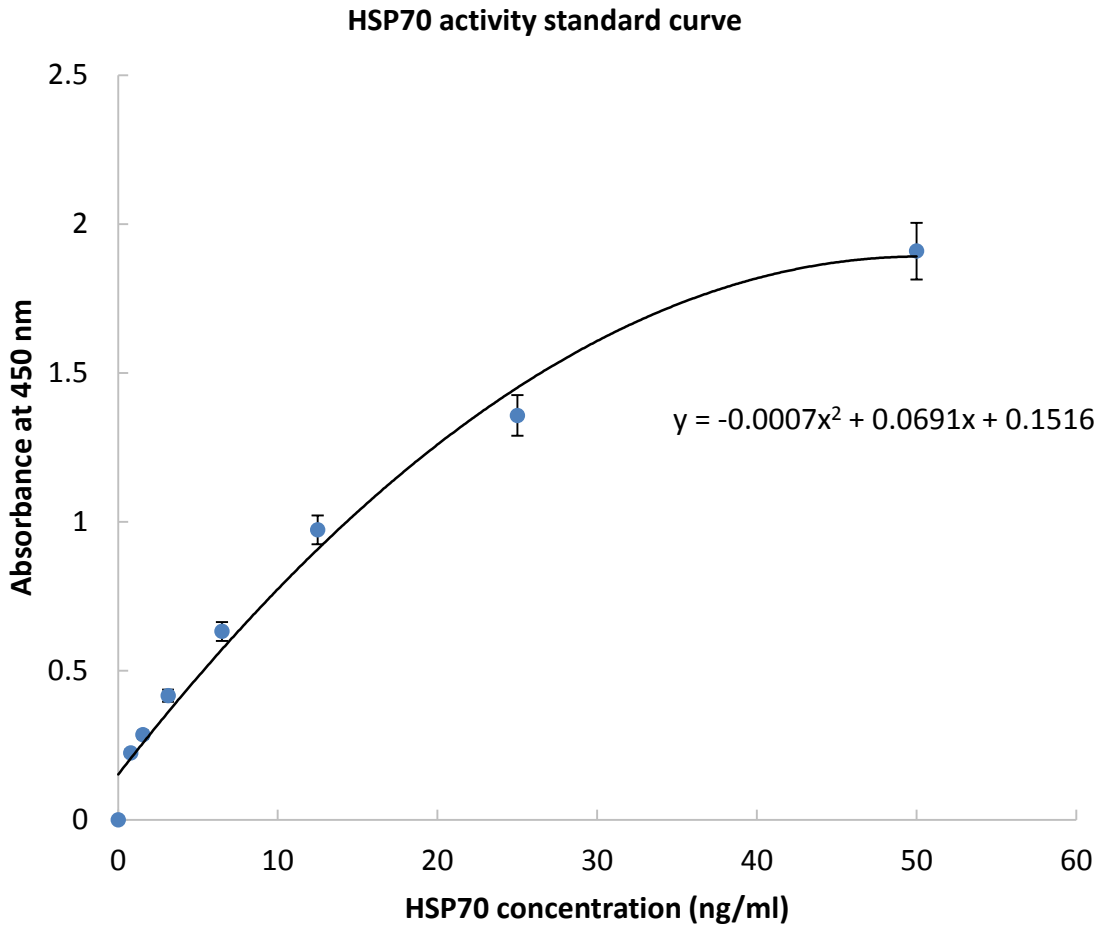

Figure 2.20: HSP70 activity standard curve The active recombinant HSP70 standard was diluted in Kinase Assay Dilution Buffer to give final concentration from 0.78-50 ng/assay. The equation derived from the curve was then used to calculate the HSP70 activity in treated and untreated samples based on the absorbance readings. This graph is typical of two independent experiments. Data values are mean ± SD, n = 4.

2.8 Statistical analysis

The data were analysed using SPSS package and Graph pad Prism for One-Sample Student's T-test and Paired-Sample T-test. A value of *$p < 0.05$ and **$p < 0.001$ was taken as significant.

CHAPTER 3

RESULTS

3.1 Cell culture growth curves

Error! Reference source not found. shows time course of growth curves for 1321N1, GOS-3 and U87-MG glioma cell lines. The results show that all three cell lines grow in similar manner over the period of six days. However, U87-MG were used for further analysis involving drug treatments. Cells were used after four days of culture.

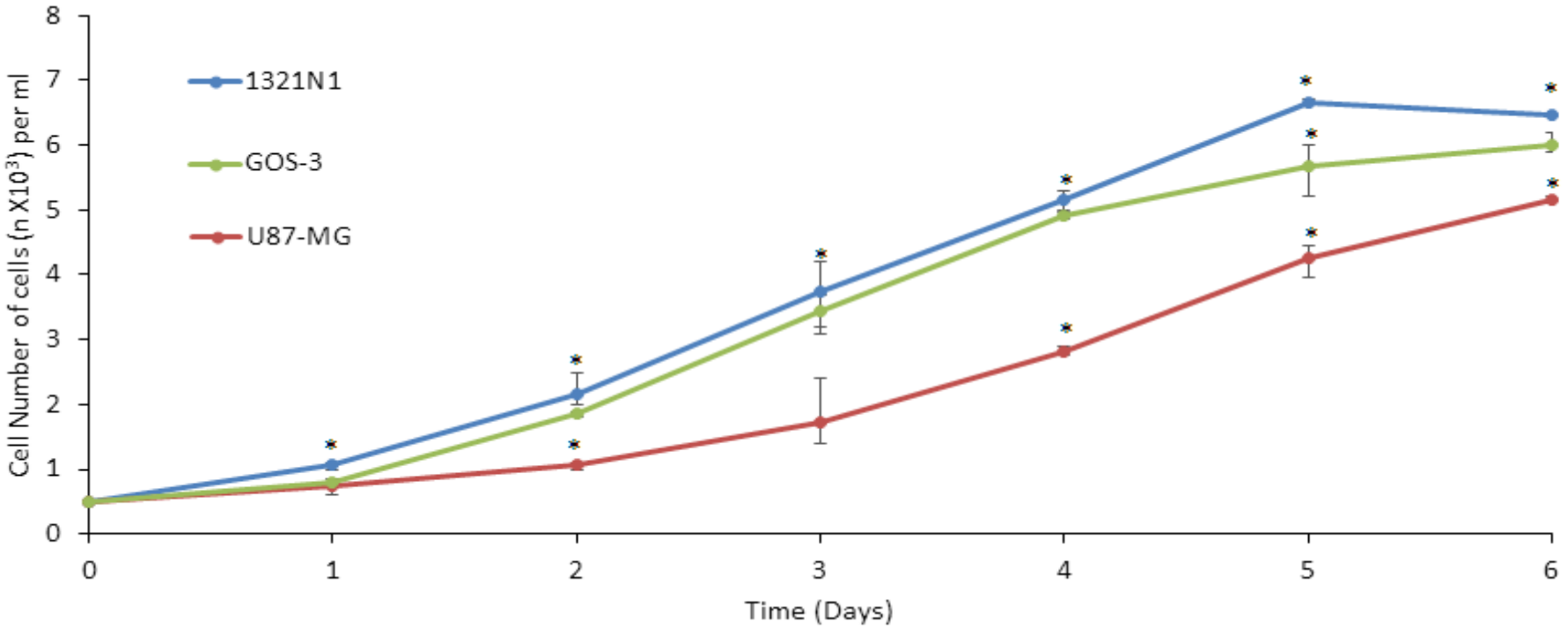

Figure 3.1: Growth curves of glioma cell lines used in this study The values shown are mean ±SD, n = 3 (*p=0.05).

3.2 mRNA isolation and qRT-PCR

mRNA purity was determined by analysing the absorbance ratio at 260: 280 on mRNA isolation using NanoDrop spectrophotometer. mRNA concentrations used for cDNA synthesis are in Table 3.1.

Table 3.1: mRNA purity using Nanodrop spectrometer and mRNA concentration used for cDNA synthesis. Data are mean ±SD, n = 3.

Cell Lines	Ratio (A_{260}/A_{280})	mRNA concentrations (ng/µl)
1321N1	1.89 ± 0.03	35.5 ± 3.2
GOS-3	1.92 ± 0.02	62.5 ± 5.4
U87-MG	2.05 ±0.02	60.3 ± 4.3
NHA	1.99 ± 0.1	52.3 ± 3.6

The volume of mRNA (100 ng) was calculated for cDNA synthesis. *GAPDH*, *Hsp70* and *Hsp90α* gene transcription was measured using Real time PCR. The data shows that *Hsp70* and *Hsp90α* levels were significantly induced in glioma cell lines (*$p < 0.05$), while *Hsp70* was absent. Similarly, *Hsp90α* was transcribed at basal levels in the normal cell line. Thus, there was no reason to use normal astrocyte cell line for further study.

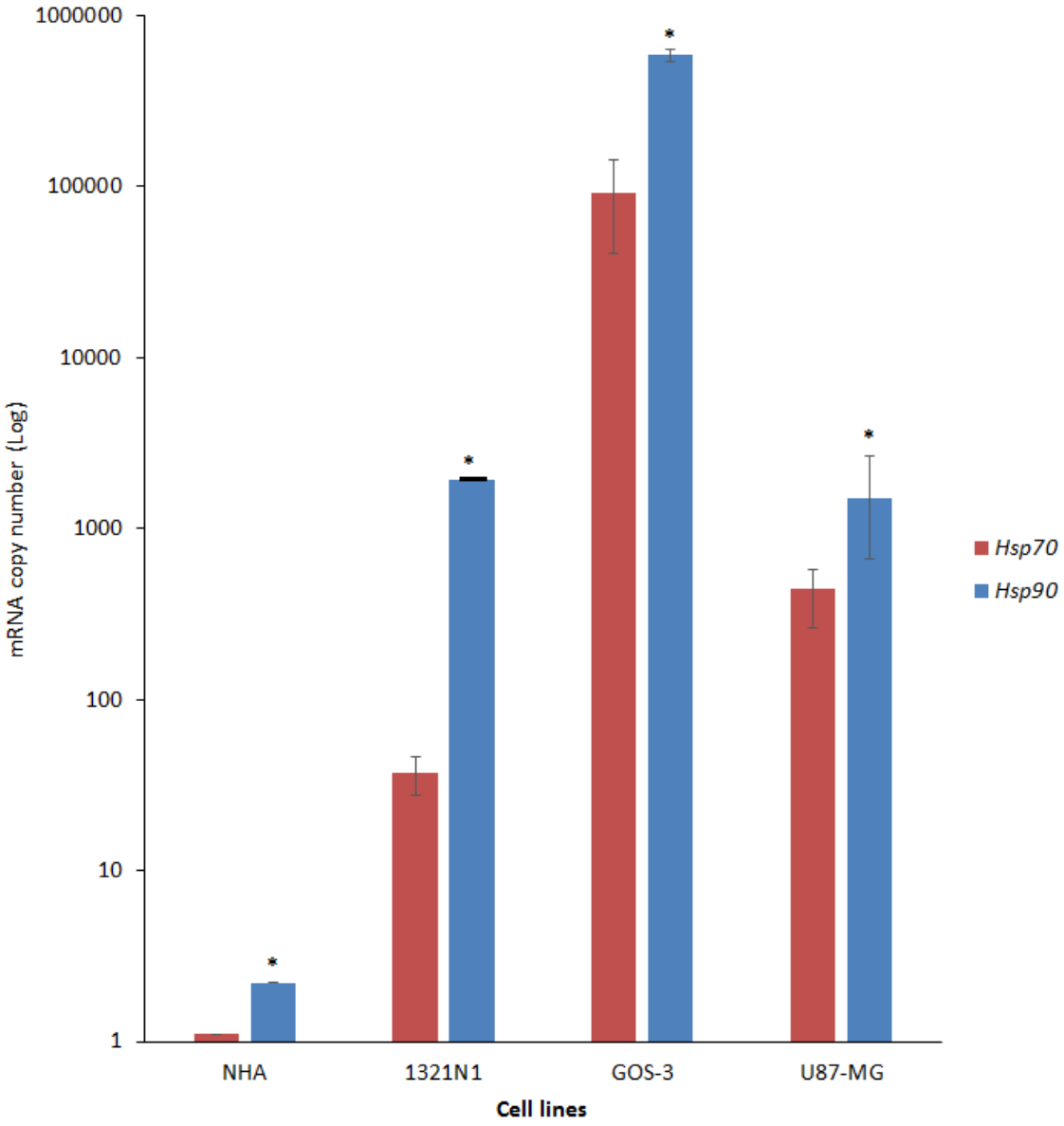

Figure 3.2: Bar chart showing the gene expressions of *Hsp70* and *Hsp90α* in glioma cell lines mRNA copy number of *Hsp70* and *Hsp90α* in glioma cell line and normal cell lines has been shown. *p < 0.05 was considered statistically significant. Data values are mean ± SD, n = 3. The data show graphical representation of elevation of Hsp70 and Hsp90 in glioma cell lines compared to control cell line (NHA).

3.3 Inhibitory concentration (IC_{50}) of TMZ, 17-AAG and VER in glioma cell lines

The 50% Inhibitory concentrations of Temozolomide, 17-AAG and VER for 48 h were determined on each of the three glioma cell lines. The cells were treated with increasing concentrations of the inhibitory compounds and the cell viability was analysed using *CellTiter-Glo*® Luminescent cell viability assay. Previously, cell viability using non-cancerous glioma cell line was established using HSP inhibitory drug (Mehta *et al.,* 2011). Thereby, NHA was excluded for this experiment. Figure 3.3-Figure 3.5 below show decreased glioma cell viability with increases in the drugs dose. The 50% inhibition concentrations (IC_{50}) for glioma cell lines are listed in Table 3.2.

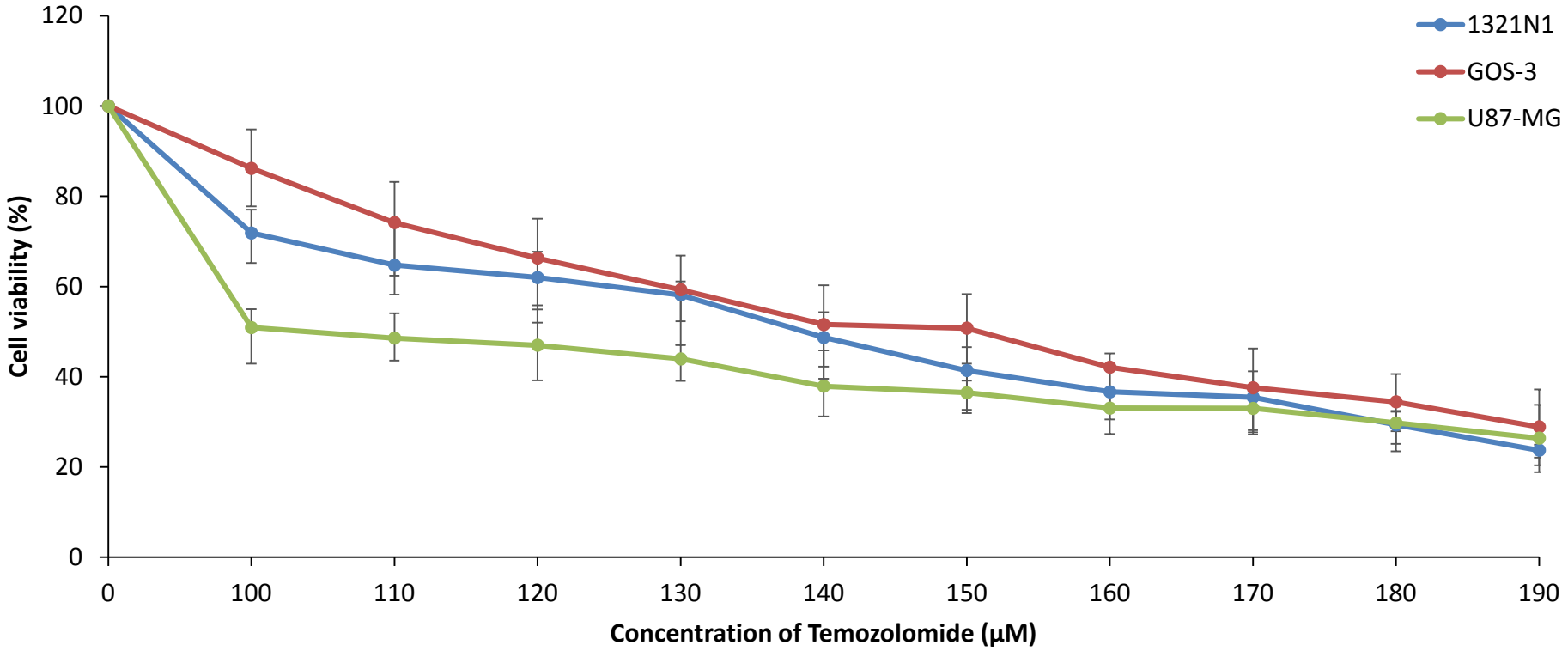

Figure 3.3: Dose-dependent inhibitory effects on cell viability employing different concentrations (µM) of Temozolomide. The drug was assessed by increasing concentrations of TMZ on 1321N1, GOS-3 cell line, U87-MG cell line.The data values are mean ± SD, n = 3.

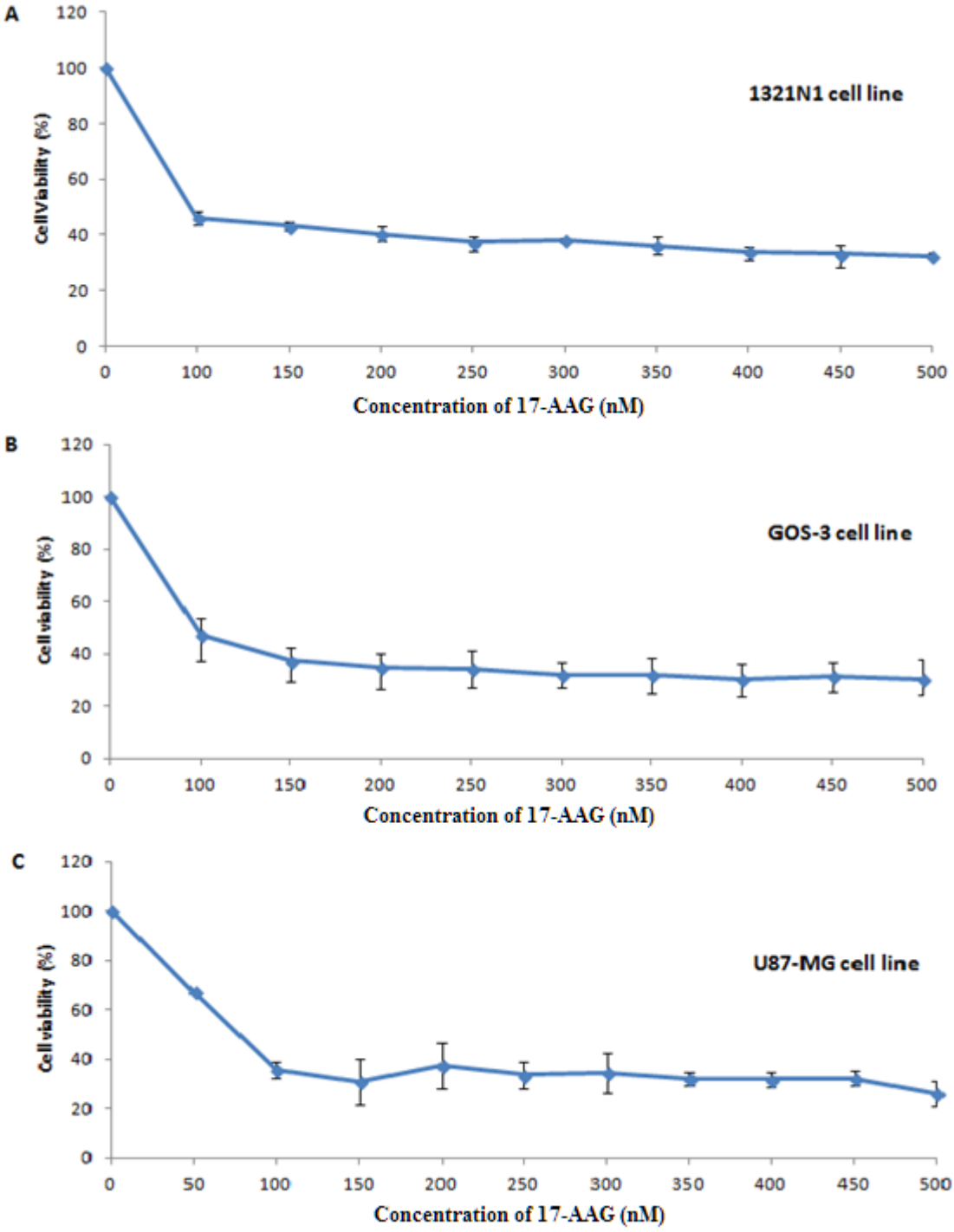

Figure 3.4: Dose-dependent inhibitory effects on cell viability employing different concentrations (0 – 500 nM) of 17-AAG. The Hsp90 inhibitor was assessed by increasing concentrations of 17-AAG on (A) 1321N1, (B) GOS-3 and (C) U87-MG. The data values are mean ± SD, n = 3.

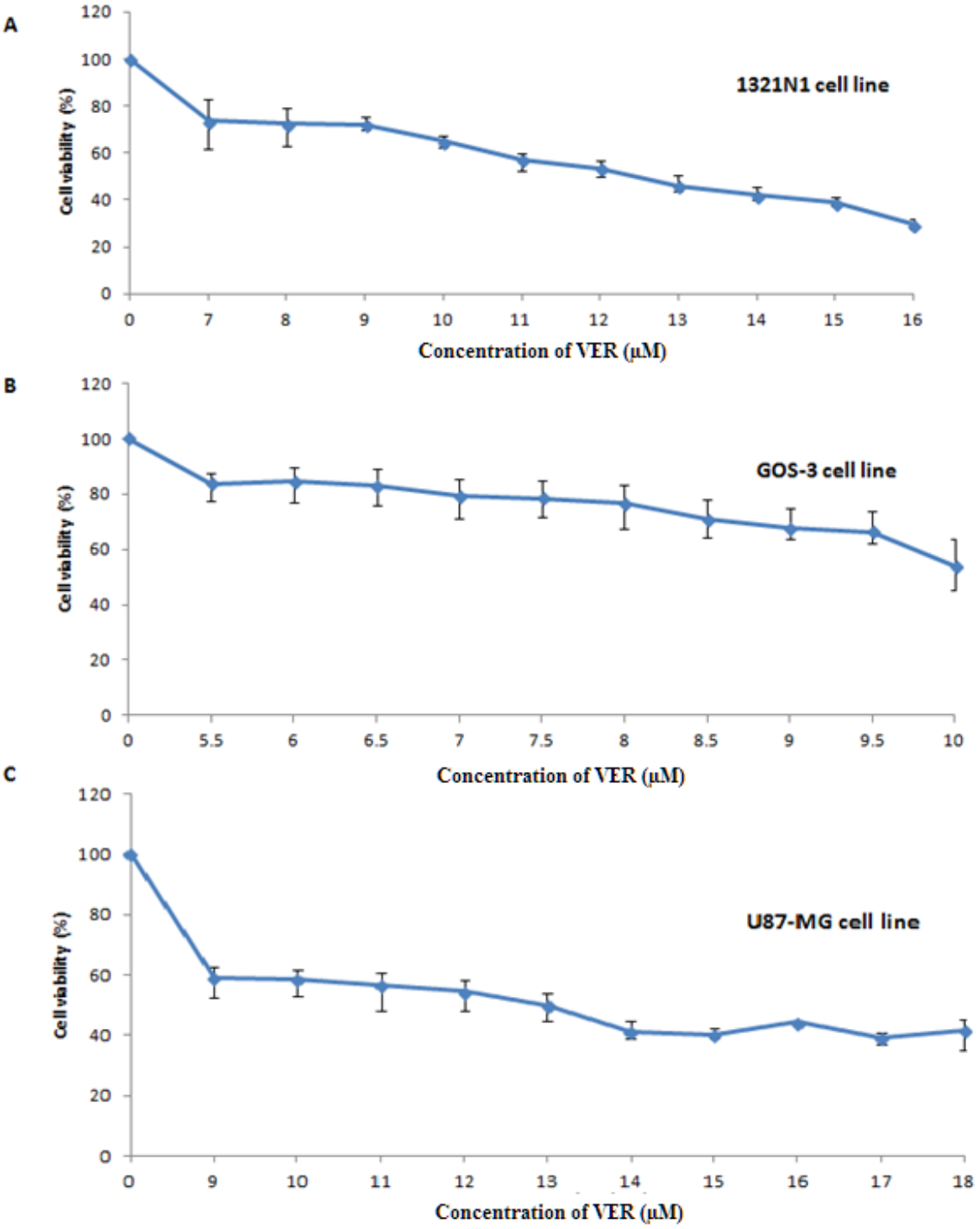

Figure 3.5: Dose-dependent inhibitory effects on cell viability employing different concentrations (µM) of VER. The Hsp70 inhibitor was assessed by increasing concentrations of VER on (A) 1321N1 cell line (0.0-16.0 µM), (B) GOS-3 cell line (5.5-10.0 µM) and (C) U87-MG cell line (9.0-18.0 µM). The data values are mean ± SD, n = 3.

Table 3.2: The IC_{50} concentrations of chemotherapeutic drug TMZ and *Hsp* inhibitory drugs 17-AAG & VER on the three different cancer cell line. The values are mean, n = 3.

Cell lines	17-AAG (nM)	VER (µM)	Temozolomide (µM)
1321N1	100	12.3	135
GOS-3	100	12	147
U87-MG	80	13	180

3.4 Akt activity in glioma cell lines

Akt kinase plays a major biochemical role as a client protein to HSP70-HSP90 complex. Akt stabilises HSP90 and activates HSP70/90 complex through phosphorylation which leads to activation of signalling proteins involved in cell survival. Thus, the presence of HSP70 and HSP90 can be determined by increased levels of Akt/PKB levels. The Akt/PKB levels in glioma cell lines were measured using established method. The Akt activity in glioma cell lines treated with TMZ, 17-AAG and VER was assessed in order to examine the effect of each inhibitory drug on the Akt/PKB kinase activity levels.

The protein was extracted from drug-treated and untreated samples of 1321N1, GOS-3 and U87-MG and quantified using a standard curve (Figure 2.13). The determined quantity of protein was used to measure protein Akt levels. Akt activity level was obtained (Table 3.3) by extrapolating experimental absorbance values on standard curve equation obtained from standard curve graph (Figure 2.14). These data showed correlation with the gene expression data of *Hsp70* and *Hsp90α.*

Table 3.3: Determination of Akt kinase activity (ng/assay). *p < 0.05 was considered statistically significant. Data values are mean ± SD, n=3.

Cell lines	Treatment	Kinase activity for ng/assay
NHA	Untreated	43 ± 2
1321N1	Untreated	84 ± 37
	TMZ	22 ± 3*
	17-AAG	7 ± 3*
	VER	52 ± 4*
GOS-3	Untreated	201 ± 7
	TMZ	69 ± 4*
	17-AAG	82 ± 6*
	VER	156 ± 5*
U87-MG	Untreated	121 ±15
	TMZ	17 ± 3*
	17-AAG	32 ± 5*
	VER	20 ± 2*

3.5 Chemosensitivity assay with 17-AAG and VER in the glioma cell lines

Chemosensitivity assay was carried out on the three glioma cell lines in two different ways, using both Concurrent assay and Sequential assay. In the concurrent assays, cells were exposed to 17-AAG, VER and TMZ in different combination or alone followed by incubation for 48 h (Figure 3.6). In sequential assays, cells were exposed to 17-AAG, VER and TMZ alone for 24 h followed by treatment with TMZ. The cells were further incubated for 48 h (Figure 3.7).

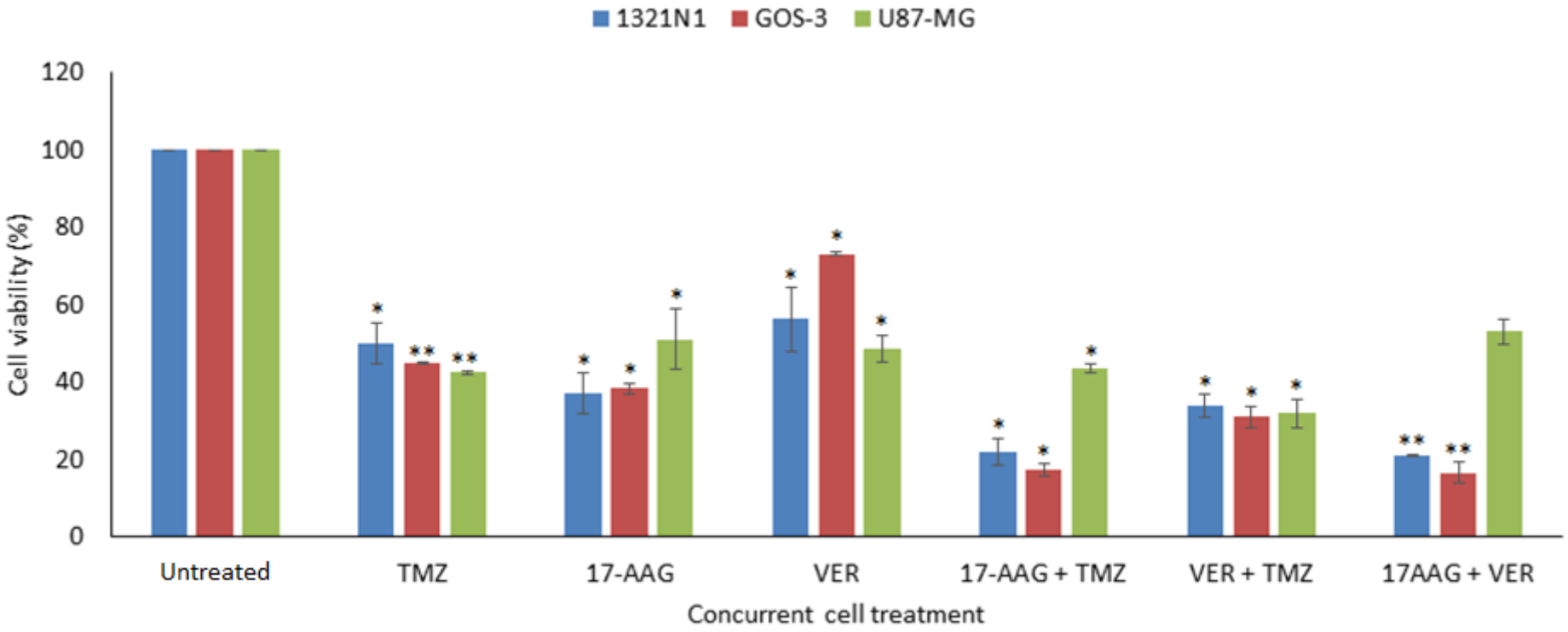

Figure 3.6: Bar charts showing concurrent chemosensitivity assay using glioma cell lines. The data showed that cell viability was significantly reduced in combinational treatment for 48 h where three cell lines were examined for treatment along with TMZ. *$p < 0.05$ and **$p < 0.001$ were considered statistically significant (Data values are mean ± SD, n = 3).

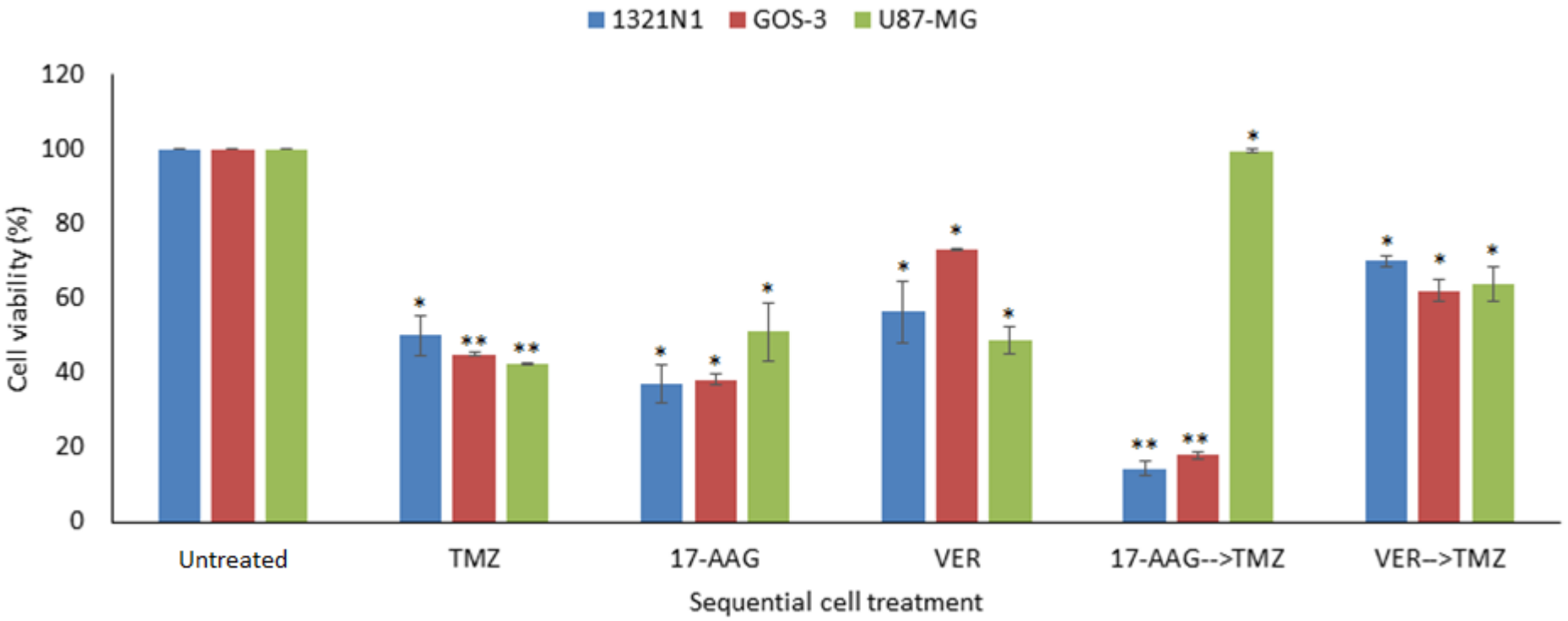

Figure 3.7: Bar charts showing sequential chemosensitivity assay using glioma cell lines. The data showed that cell viability was significantly reduced in combinational treatment where three cell lines were treated with TMZ, 17-AAG and VER. After 24 h, 17-AAG and VER treated cells was exposed to TMZ followed by incubation of 48 h. *$p < 0.05$ and **$p < 0.001$ were considered statistically significant (Data values are n = 3, mean ± SD).

3.6 Analysis of miRNA regulation

Earlier data have confirmed elevated HSP70 and HSP90α activity in glioma cells as mRNA expression profiles and Akt kinase activity in the three glioma cell lines. These initial data have established importance of Heat shock proteins based on chemosensitivity assay results. Thus, U87-MG cell line was used for further analysis. miRNAs are commonly dysregulated in human malignancies and they possess the ability regulate thousands of mRNA simultaneously (Lu *et al.,* 2005). Thus, in order to understand therapeutic effects of drug at molecular level and to further determine potential molecular targets, miRNA microarray was carried out. Further in the research, U87-MG cells were treated with IC_{50} of TMZ (Standard treatment) and heat shock protein inhibitory compounds, 17-AAG and VER, respectively for 48 h (Table 3.2). miRNA expression profiling was performed on 8 samples (includes 3 treated samples and a untreated as control). Samples were analysed on Agilent Human miRNA Microarrays Release 19.0 (8×60K format). All the procedures were carried out according to manufacturer's protocol.

3.6.1 Total RNA concentration, purity and integrity

Total RNA was extracted from the samples and concentrations and A269/A280 ratios of each sample was determined by spectral photometry on the NanoDrop ND-1000 instrument. RNA integrity was assessed on the Agilent 2100 Bioanalyzer. The results are shown in Table 3.4. The results show that RNA concentrations of all samples were found to be sufficient for microarray analysis and their purity (as indicated by the A260/A280 and A260/A230 ratios) was found to be very good. All total RNA samples were found to have RIN (RNA Integrity Number) values above 9.4, indicating excellent RNA quality. The electropherogram of all analysed samples along with electrophoretic gels are also shown in Figure 3.8 and Figure 3.9**.** All samples were used for miRNA microarray analysis.

Table 3.4: Table showing quality control results for the total RNA samples using U87-MG. (Data values are mean ±SEM, n=2)

Treatment	Sample	Concentration (ng/µl)	A260/A280 ratio	A260/A230 ratio	RIN
U87-MG Untreated	**Control 1**	560.8	2.04	1.76	9.7
	Control 2	513.9	2.06	1.53	9.8
U87-MG Treated	**TMZ 1**	568.6	2.06	2.25	9.7
	TMZ 2	540.3	2.08	2.25	9.8
	17-AAG 1	658.8	2.08	2.24	9.7
	17-AAG 2	695.5	2.07	1.94	9.6
	VER 1	126.8	2.04	1.97	9.4
	VER 2	106.4	2.07	2.18	9.6

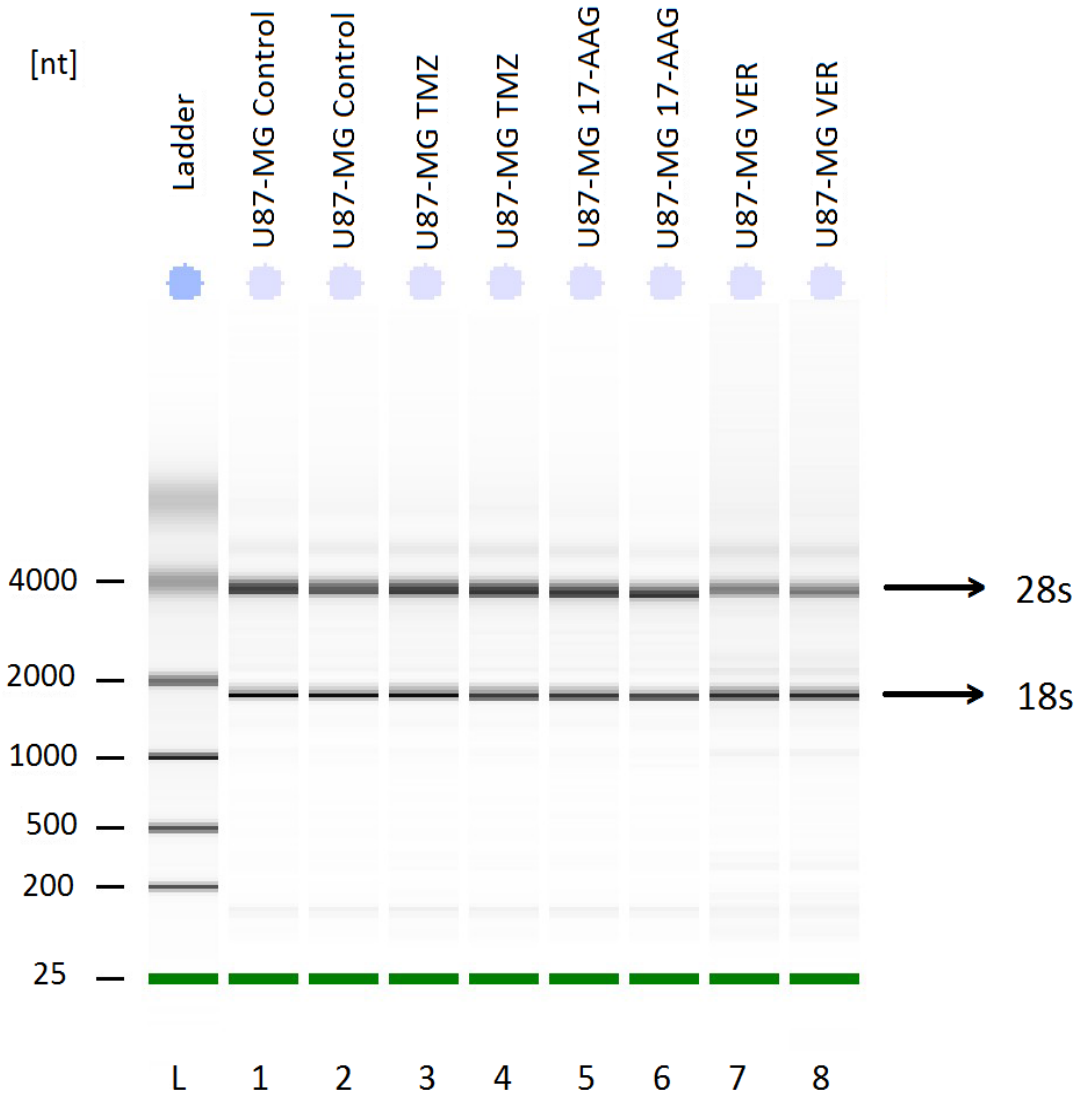

Figure 3.8: Original electrophoresis gel for assessing RNA integrity. L represents marker ladder and lane 1-8 represents total RNA samples used for miRNA microarray (1) U87-MG Control-Set 1 (2) U87-MG Control-Set 2 (3) U87-MG TMZ-Set 1 (4) U87-MG TMZ-Set 2 (5) U87-MG 17-AAG-Set 1 (6) U87-MG 17-AAG-Set 2 (7) U87-MG VER-Set 1 (8) U87-MG VER-Set 2. (A) 18s (B) 24s. (Correlating with Figure 3.9).

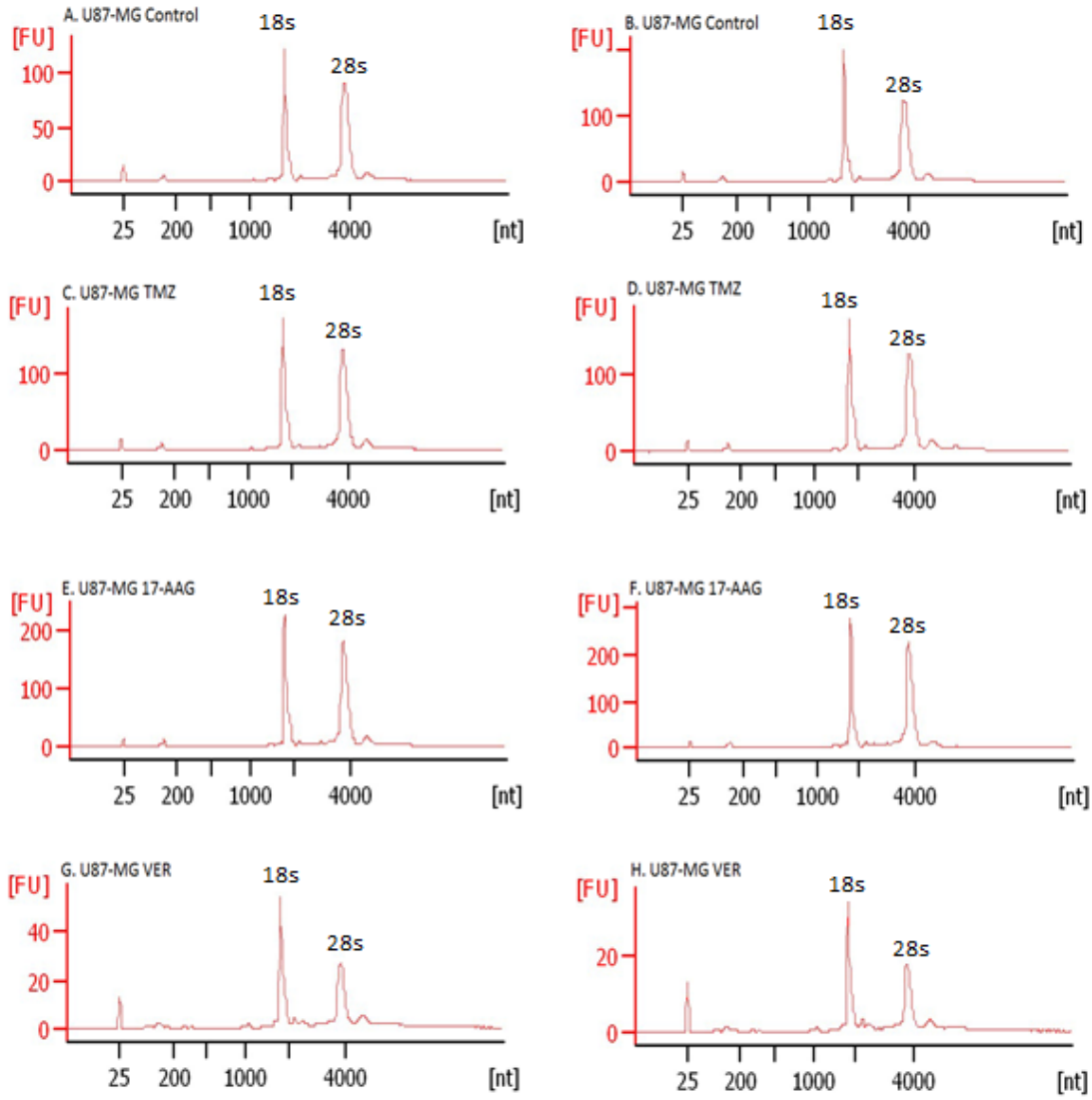

Figure 3.9: Original chart recordings showing electropherogram for RNA integrity. Each graph recording produced by Bioanalyzer represents total RNA samples used for miRNA microarray (A) U87-MG Control-Set 1 (B) U87-MG Control-Set 2 (C) U87-MG TMZ-Set 1 (D) U87-MG TMZ-Set 2 (E) U87-MG 17-AAG-Set 1 (F) U87-MG 17-AAG-Set 2 (G) U87-MG VER-Set 1 (H) U87-MG VER-Set 2.

3.6.2 Microarray analysis

Each array was analysed using Feature extraction software. All criteria of Feature extraction quality analysis was fulfilled. The Additive Errors was in below 12 for each array as recommended by one-Color-based hybridization (Agilent). Analysis of Spike-In signals demonstrated equal and good performance of each single labelling and hybridisation experiment. Hyb Spike-in Signal obtained in between range of 4.49 – 4.57 which is above recommended threshold of 2.50 for all arrays.

3.6.3 Quantile normalization of microarray data

Quantile normalization is commonly used for nonlinear normalization which adjusts all microarray samples to similar data distribution. It helps to eliminate intensity differences within microarrays and ensure that differential data obtained. The box plot in Figure 3.10 demonstrates the effects of quantile normalization for all analysed samples (Bolstad *et al.,* 2003). Box plots are usually representation of normalised distribution of data. In Figure 3.10, 50% of the data are within boxes and blue horizontal line represents median of the data. The red part above the box plot whiskers represents outliners. Box plot obtained in the study is different than the standard plot. This may be due to low overall signal intensities and low or weakly expressed miRNA data sets within each samples.

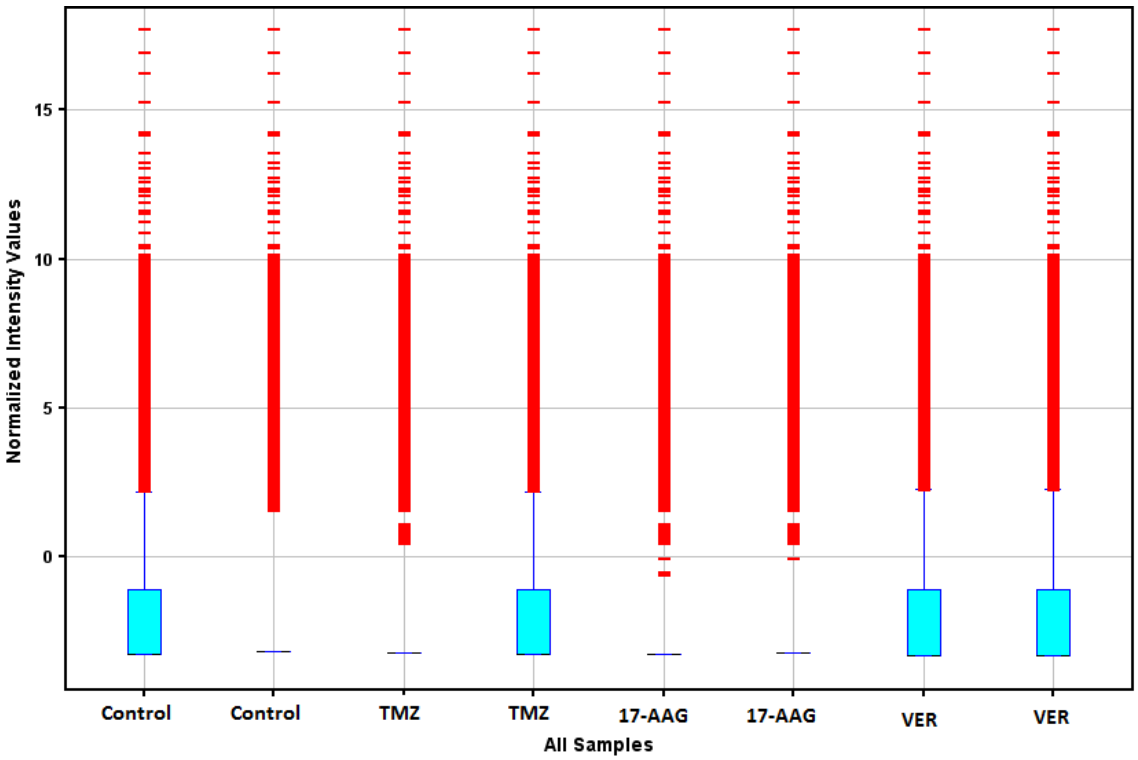

Figure 3.10: BoxWhisker plot after quantile normalization. (Data values are mean ±SEM, n=2)

3.6.4 Correlation analysis

In order to determine degree of relationship within and between the samples, Pearson's correlation coefficient was analysed. The heat map of correlation coefficient shown in Figure 3.11 represents the correlation coefficient from obtained values within biological samples and also, between the different experimental groups. The data shows that **r** within biological samples shows high level of correlation ranging from 0.982 to 0.995 and **r** between experimental group such as control and TMZ, control and 17-AAG, control and VER shows average correlation ranging from 0.954 to 0.975.

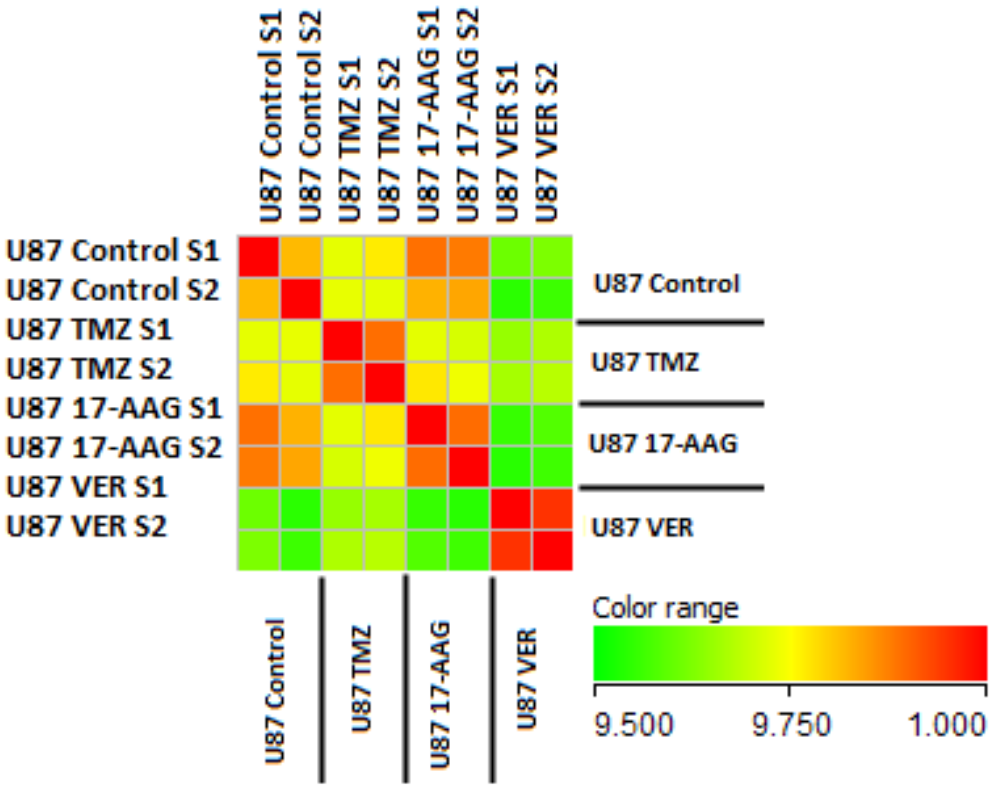

Figure 3.11: Heat-Map plot for correlation coefficients (r). Demonstrating correlation between and within the experimental samples. The colour range start at a low level of r=0.950 (green) and ends at the highest level of r= 1.000 (red). Red represents high correlation. Data values are mean ±SEM, n=2.

Each microarray was analysed for quality control using standardised set of QC metrics to ensure samples can be accounted for bioinformatic analysis. The filtered flag information was applied on each array to obtain 'Detected' (D) and 'Not Detected' (ND) data. In Table 3.5, % Detected is mentioned for each sample array. 2,027 systemic names were found to be 'Detected' in each sample.

Table 3.5: Data showing detected systemic names on application of filtered flag information. Data values are mean ±SEM, n=2**.**

Samples	% Detected
U87_Control S1	25.4
U87_Control S2	22.9
U87_TMZ S1	24.5
U87_TMZ S1	25.4
U87_17-AAG S1	24.9
U87_17-AAG S2	24.6
U87_VER S1	28.0
U87_VER S2	27.8

3.6.5 Differential miRNA expression

Following % detected samples, the data were filtered to obtain quantile normalisation and $\log_2$ transformed data were averaged within biological replicates. The pair-wise comparison was carried out using U87-MG-Control as reference group and gene expression of U87-TMZ, U87-17-AAG and U87-VER were compared to the reference group. Different filtering approaches were carried out for identification of differentially expressed miRNAs in the pair-wise comparisons. Statistical analysis included application of both FDR (False Discovery Rate)-corrected p-value (*p (Corr)* and the non-corrected p-value (*p*), respectively, in combination with a Fold change ≥ |2|. Initially, 2074 systemic names in each sample and on applying stringent approach on pair-wise comparison, 13 differentially expressed miRNAs were obtained which are expressed in VER Vs control (See Table 3.6). There are no miRNAs expressed on stringent filter on comparison with TMZ and 17-AAG. Table 3.6 also shows non-stringent filtering data which have high a number of miRNAs, but these miRNAs have less reliability as they are not FDR-corrected p-value-based filtering.

Table 3.6: Table showing the summary of differentially expressed miRNAs.

Comparison	p(Corr) ≤ 0.05 |FC| ≥ 2		p ≤ 0.05 |FC| ≥ 2	
	Up	Down	Up	Down
TMZ Vs Control	0	0	19	7
17-AAG Vs Control	0	0	4	1
VER Vs Control	9	4	61	62

3.6.6 Analysis of significantly regulated miRNAs

Differentially expressed miRNAs were further evaluated for determining overlapping of expressed miRNAs in different groups from both stringent and non-stringent data sets (Table 3.7). A total of 12 upregulated miRNA was present in both TMZ Vs control and VER Vs control. Among the upregulated miRNAs, hsa-miR-194-5p, hsa-miR-215, hsa-miR-449a, hsa-miR-744-5p and has-miR-3161 showed higher fold change difference while there was only one downregulated hsa-miR-4636 with lower fold difference.

Table 3.7: Significantly regulated miRNAs with overlapping of expressed miRNAs. (FC-Fold change, ✓ represents p(corrected) miRNAs). Data values are mean ±SEM, n=2

TMZ Vs Control				17-AAG Vs Control				VER Vs Control			
Up	FC	Down	FC	Up	FC	Down	FC	Up	FC	Down	FC
hsa-miR-215	164.61	hsa-miR-3654	-72.55	hsa-miR-3161	29.29	hsa-miR-345-5p	-2.03	hsa-let-7e-5p	2.03	hsa-miR-10b-3p	-31.15
hsa-miR-194-5p	138.93	hsa-miR-335-3p	-70.32	hsa-miR-557	18.90			hsa-let-7g-5p	2.26	hsa-miR-1225-5p	-2.59
hsa-miR-550a-3p	64.87	hsa-miR-3620-5p	-49.68	hsa-miR-3692-5p	17.71			hsa-miR-103a-3p	2.62	hsa-miR-1227-5p	-2.94
hsa-miR-769-5p	63.60	hsa-miR-431-3p	-41.62	hsa-miR-664b-5p	17.18			hsa-miR-107	2.21	hsa-miR-1234-3p	-2.53
hsa-miR-744-5p	63.11	hsa-miR-4636	-32.06					hsa-miR-1180	23.93	hsa-miR-1234-5p	-2.15
hsa-miR-449a	61.97	hsa-miR-193a-5p	-2.20					hsa-miR-125a-5p	2.62	hsa-miR-135a-3p	-5.36
hsa-miR-101-3p	49.19	hsa-miR-4697-5p	-2.06					hsa-miR-128	2.55	hsa-miR-138-2-3p	-3.19
hsa-miR-200c-3p	33.26							hsa-miR-1285-3p	2.26	hsa-miR-139-3p	-3.60
hsa-miR-652-3p	29.38							hsa-miR-1306-3p	2.15	hsa-miR-1469 ✓	-10.14
hsa-miR-7-1-3p	23.49							hsa-miR-148b-3p	2.32	hsa-miR-1587	-2.24
hsa-miR-4521	23.13							hsa-miR-152	2.84	hsa-miR-1915-3p	-2.59
hsa-miR-500a-3p	19.00							hsa-miR-185-5p	2.22	hsa-miR-197-5p	-2.33
hsa-miR-4758-3p	18.65							hsa-miR-194-5p	62.83	hsa-miR-2861	-2.90
hsa-miR-557	17.92							hsa-miR-1972	2.03	hsa-miR-3137	-2.11
hsa-miR-382-5p	16.00							hsa-miR-204-5p	2.02	hsa-miR-3188	-2.25
hsa-miR-192-5p	4.94							hsa-miR-215 ✓	60.74	hsa-miR-3196	-3.11
hsa-miR-324-5p	2.10							hsa-miR-23b-3p	2.18	hsa-miR-3663-3p	-2.02
hsa-miR-331-3p	2.08							hsa-miR-26a-5p	2.20	hsa-miR-371b-5p	-3.13
hsa-miR-148b-3p	2.03							hsa-miR-30c-2-3p	2.19	hsa-miR-3940-5p	-2.01
								hsa-miR-30d-5p	2.03	hsa-miR-4428	-3.08
								hsa-miR-30e-3p	2.05	hsa-miR-4430	-3.13
								hsa-miR-3152-3p	2.39	hsa-miR-4446-3p	-2.63
								hsa-miR-3158-5p	2.16	hsa-miR-4462	-2.58
								hsa-miR-3161	2.18	hsa-miR-4478	-2.23
								hsa-miR-324-5p	2.12	hsa-miR-4505	-2.48
								hsa-miR-342-3p	2.71	hsa-miR-4507	-2.08
								hsa-miR-3617-5p ✓	61.40	hsa-miR-4515	-2.30
								hsa-miR-374b-5p	2.11	hsa-miR-4530	-2.89
								hsa-miR-379-5p ✓	54.30	hsa-miR-4532	-2.02
								hsa-miR-382-5p	57.71	hsa-miR-4538	-2.04
								hsa-miR-432-5p	2.15	hsa-miR-4634	-3.26
								hsa-miR-4443	3.03	hsa-miR-4636	-33.24
								hsa-miR-4458	92.84	hsa-miR-4647	-26.47
								hsa-miR-4484	3.37	hsa-miR-4656	-2.26
								hsa-miR-449a	76.65	hsa-miR-4665-5p	-2.81
								hsa-miR-449c-5p	43.48	hsa-miR-4721	-2.10
								hsa-miR-4506	42.65	hsa-miR-4728-5p	-2.03
								hsa-miR-4521	55.63	hsa-miR-4739	-2.04
								hsa-miR-4710	39.07	hsa-miR-4741	-2.47
								hsa-miR-4726-5p	2.16	hsa-miR-4767	-42.21
								hsa-miR-486-5p	23.39	hsa-miR-4787-3p ✓	-36.67
								hsa-miR-493-5p	18.18	hsa-miR-4787-5p	-2.66
								hsa-miR-497-5p	2.01	hsa-miR-5001-5p	-2.42
								hsa-miR-498	2.11	hsa-miR-5006-5p	-2.07
								hsa-miR-500a-3p ✓	17.46	hsa-miR-503-5p	-51.76
								hsa-miR-5010-5p ✓	17.79	hsa-miR-513a-5p ✓	-3.22
								hsa-miR-502-3p ✓	32.91	hsa-miR-513b	-3.27
								hsa-miR-5196-5p	37.43	hsa-miR-513c-5p	-3.49
								hsa-miR-520c-3p	2.24	hsa-miR-548q	-126.10
								hsa-miR-532-3p	2.71	hsa-miR-5585-3p	-95.73
								hsa-miR-550a-3p	81.24	hsa-miR-575	-3.96
								hsa-miR-6134	2.23	hsa-miR-6068	-3.95
								hsa-miR-652-3p	40.79	hsa-miR-6089	-2.57
								hsa-miR-7-1-3p	61.35	hsa-miR-6090	-2.01
								hsa-miR-744-5p ✓	43.32	hsa-miR-6125	-3.06
								hsa-miR-758-5p	3.04	hsa-miR-638	-2.83
								hsa-miR-769-5p	48.11	hsa-miR-650	-15.32
								hsa-miR-885-5p ✓	28.68	hsa-miR-6722-3p	-2.22
								hsa-miR-9-5p	2.38	hsa-miR-718	-8.71
								hsa-miR-98-5p	2.63	hsa-miR-921	-5.53
										hsa-miR-940	-3.82

3.6.7 miRNA target genes

Further details about each miRNA was obtained using the miRBase: The miRNA database (http://www.mirbase.org). Each miRNA description was filtered for cancer relevant miRNAs. These database also provide details of validated experiments on predicted targets. Based on the differentially expressed miRNAs Table 3.7, further targets were determined using different target predicting algorithm such as Target Scan Human 6.2, DIANA-microT and miRBD miRBase V18. These algorithms predict mRNA targets according to the complementarity of the miRNA seed. As each algorithm utilises different method for determination, therefore, in order to avoid false targeting, mRNA targets which are confirmed by two or more algorithms were taken into account. According to functions, publication or novel gene relevant for this study, was determined. miRNA related to cancer progression was used for quantification of expression (Table 3.8).

Table 3.8: Table showing the predicted gene using gene target algorithms

miRNA	Treatment	Regulation	Predicted gene target
hsa-miR-194-5p	TMZ & VER	Upregulated	*Dnmt3a*
hsa-miR-215	TMZ & VER	Upregulated	*Alcam*
hsa-miR-449a	TMZ & VER	Upregulated	*Cdk4*
hsa-miR-744-5p	TMZ & VER	Upregulated	*Dnajc16 (hsp40)*
hsa-miR-3161	17-AAG & VER	Upregulated	*R-Ras2*

3.6.8 Validation of selective gene expression

In Table 3.9 and Figure 3.12, gene expression levels of selected gene were monitored to examine treatment efficiency in U87-MG cell lines.

Table 3.9: **Table showing the validation of gene expression analysis of selected genes.** (Data values are mean ±SEM, n=3, *P<0.05 compared to control).

	Control	TMZ	17-AAG	VER
Dnmt3a	2 ± 0	2 ± 0	2 ± 0	25 ± 6
Alcam	33 ± 5	4253 ± 603	477 ± 100	84 ± 1*
Dnajc16 (hsp40)	293 ± 41	30976 ± 281	5102 ± 370	1455 ± 119
Cdk4	160 ± 15	1359 ± 203	482 ± 21*	561 ± 31*
R-Ras2	51 ± 6	214 ± 41*	357 ± 28*	441 ± 77*
Hsp70	442 ± 129	129 ± 16*	192 ± 8*	43334 ± 847
Hsp90	829 ± 145	373 ± 71*	1484 ± 362	91863 ± 877

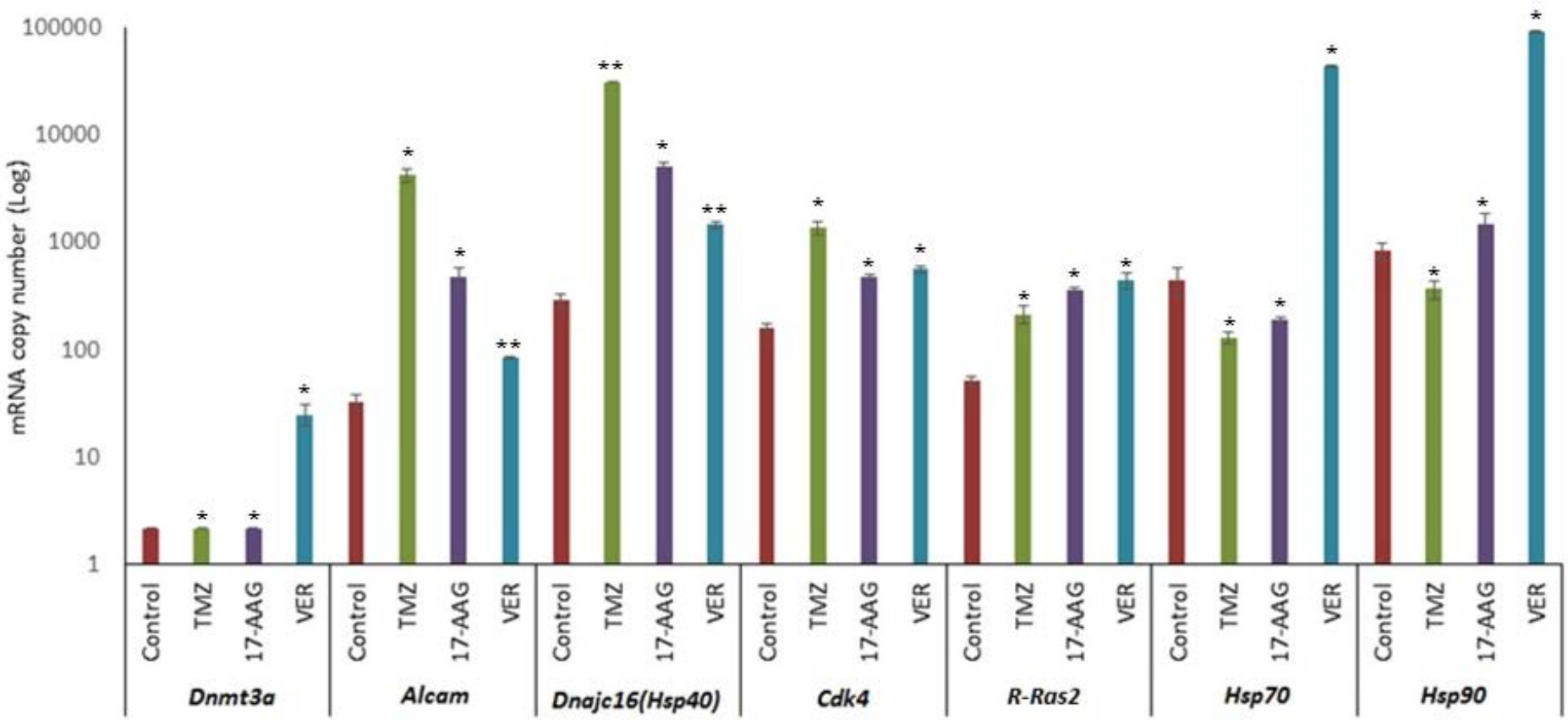

Figure 3.12: Bar charts showing Gene transcription levels of selected genes. (Data values are mean ±SEM, n=3; *p<0.05for test compared to control for each set)

3.7 HSP70 and HSP90 activity

HSP70 and HSP90 are predominantly expressed heat shock proteins and they found to be elevated in glioma (See Table 3.10 and Table 3.11). In this study, VER and 17-AAG have been used as HSP70 and HSP90 inhibitory drugs, respectively. Therefore, validated variation is confirmed in protein expression after treatment of inhibitory compounds using HSP70 and HSP90 activity ELISA kit.

Standard curves were plotted to determine HSP70 and HSP90 activities in treated and untreated samples using recombinant HSP70 and HSP90. The equation in each graph was utilised to calculate the HSP70 and HSP90 activity levels in the samples (Figure 2.19 and Figure 2.20). In order to determine effects of Hsp-specific inhibitory treatment and validate gene transcription data investigation was carried out using U87-MG cell lysate of total protein 0.5 μg.

Table 3.10: Table showing HSP70 activity in U87-MG cell lines. (Data values are mean ± SD, n=3, *p<0.05 compared to untreated)

Samples	HSP70 activity for 0.5 µg protein
U87-MG Untreated	77 ± 11
U87-MG TMZ	67 ± 17*
U87-MG 17-AAG	81 ± 9*
U87-MG VER	62 ± 6*

Table 3.11: Table showing HSP90 activity in U87-MG cell lines. (Data values are mean ± SD, n=3, *p<0.05 compared to untreated)

Samples	HSP90 activity for 0.5 µg protein
U87-MG Untreated	558 ± 62
U87-MG TMZ	92 ± 12*
U87-MG 17-AAG	322 ± 36*
U87-MG VER	198 ± 16*

CHAPTER 4

DISCUSSION

Heat shock proteins are molecular chaperones that function to facilitate protein folding and they regulate cellular activity in both normal and diseased conditions (Sreedhar *et al.,* 2004). Particularly, in cancers, heat shock proteins are key mediators in regulating cell survival and, they are known to interfere in pathways leading to apoptosis. In this way, they encourage cell division and cell proliferation. HSP70 and HSP90 together with client proteins form a mature complex in order to maintain proliferation, progression of cell cycle and apoptosis. Heat shock proteins are also involved in invasion, angiogenesis and metastasis.

Therefore, targeting both HSP90 and HSP70 can be an effective approach in the treatment of cancer. The expression of both HSP70 and HSP90 have been reported in malignant tumours such as breast cancer, prostate cancer and cervical cancer (Fawzy *et al*., 2013). Both HSP70 and HSP90 families have different isoforms which play major roles in various locations in the cellular environment, of which HSP70 and HSP90α are known to be the most inducible forms (Bisht *et al*., 2003). Therefore, this research focuses on the expressions HSP70 and HSP90α in glioma cells.

Glioma cell lines (1321N1, GOS-3 and U87-MG) were cultured in the lab using appropriate and safe techniques. Cell growth curve data shows that under normal conditions, 1321N1 and GOS-3 cell lines attain doubling time after 48hrs while U87-MG doubling time was after 72hrs. Cell growth curves validated cell viability or density at a given time, the subculture frequency and the phase of cell growth. Therefore, cell growth was restricted to 70-80 % confluence to avoid external stress (Assanga *et al.,* 2013). The results obtained after studying the expression of heat shock proteins have clearly demonstrated the presence of *Hsp70* and *Hsp90α* in glioma cell lines and their relative absence in normal cell lines. Previous studies in our laboratory have reported

the expression of *Hsp90α* gene and protein in glioma cell lines (Shervington *et al*., 2008; Mehta *et al*., 2011). Quantitative analysis of transcription levels of *Hsp90α* and *Hsp70* gene was assessed using qRT-PCR. *GAPDH* (Glyceraldehyde 3-phosphate dehydrogenase) was used as housekeeping gene since it is stable and constitutively expressed at high levels. The mRNA copy number has shown an overexpression of HSP90α and HSP70 in glioma cell lines compared to NHA (normal human cell lines). HSP70 belongs to the heat shock protein 70 family which plays key roles in stabilising HSP90 by acting as major co-chaperone to HSP90. Together, they maintain a stable cellular environment and carry out the main function of chaperoning misfolded proteins.

Similar to HSP90, HSP70 is also present at minimal levels in unstressed cells but under stress like conditions, the number of misfolded proteins rises, therefore increasing the need for heat shock proteins. In stress-like conditions, this leads to the overexpression of HSP70 and HSP90α. HSC70 (Heat shock cognate protein 70) is expressed at basal levels while HSP70, which is the more inducible form, is overexpressed in cancers. Heat shock Factor-1 (HSF-1), is known as a transcription factor which binds to both HSP70 and HSP90 in the inactive state. HSP70 and HSP90 dissociate from HSF-1 and subsequently, they are phosphorylated by regulatory protein kinases, bound to heat shock element (HSE) on the promoter region of *Hsp90* leading to the over expression of *Hsp* gene. Even though HSP90 inhibition is a highly efficient cellular mechanism, its effect is overcome by triggering Heat Shock Response (HSR) and elevated levels of HSP70 to compensate for the activity of HSP90α, ultimately leading to increased chemoresistance. PCR transcription data have shown that *Hsp70* and *Hsp90α* are highly expressed in glioma cell lines and almost undetected in normal cell lines. Also, cell viability or toxicity of HSP inhibitors was previously measured on non-cancerous cell lines (Mehta *et al.,* 2011). Thus, NHA (normal cell line) was not included in further investigations. The

transcriptional activity level of *Hsp90α* was higher than *Hsp70* in glioma cell lines 1321N1, GOS-3 and U87-MG. Proteomic analysis data have shown that the inhibition of HSP90 can lead to the upregulation of HSP70. HSP70 is a potential target for treatment of glioma (Munje *et al.,* 2011; McConnell *et al.,* 2013). The present investigation focused mainly on the inhibition of the upregulated HSP70 and HSP90α, whereby dual targeting for both HSP70 and HSP90 were investigated using inhibitory drugs.

Benzoquinone ansamycin antibiotics which are known to be HSP90 inhibitors have the ability to inhibit multiple targets by specific binding to HSP90 N-terminal pocket. These include 17-allylamino-17-demethoxygeldanamycin (17-AAG), first geldanamycin analogue to enter clinical trials (Goetz *et al*., 2003). In the current study, 17-AAG was found to decrease glioma (U87-MG) cell viability at a dosage of 80 nM (IC_{50} concentration) after 48 h of incubation. 17-AAG appears to be effective at low levels due to its high affinity for the binding pocket in HSP90. It shows similar affinity in other cancer cells, such as breast cancer cell lines (Workman *et al*., 2004). In addition to 17-AAG as an HSP90 inhibitory compound, this study also investigated VER-155008 (VER), an HSP70 inhibitor. The inhibitory concentration (IC_{50}) of VER using U87-MG cell line over a 48 h period treatment was determined to be 13 µM. This concentration was used in all the experiments investigating the effect of VER. Similar IC_{50} values for VER have been previously reported in colon cancer cell lines (HCT16, HT29) and breast cancer cell lines (BT474, MDA-MB-468) (Massey *et al*., 2010). The inhibitory concentrations of 17-AAG and VER were also determined using 1321N1 and GOS-3 cell lines. The IC_{50} of 17-AAG for 1321N1 cell and GOS-3 cell lines was 100 nm. The IC_{50} of VER was found to be 12 µM for 1321N1 and GOS-3 cells lines. The IC_{50} demonstrates the efficacy of both drugs with all three cell lines. 17-AAG inhibits HSP90 activity by blocking ATPase binding pocket on N-terminal and is also proved as less toxic in vivo (Xia *et al.,* 2012). VER targets HSP70

with high affinity at lower concentrations and also it targets other members of HSP70 family (HSC70 and GRP78) and HSP90β at lower affinity (Massey *et al.,* 2010).

HSP90 has an array of client proteins regulating cell survival pathways and other signal transduction or apoptosis pathways (Goetz *et al.,* 2003). Some of these client proteins behave as oncoproteins. These client proteins include extracellular signal-regulated kinase (ERK) 1, GLUT-1, HER-2, Camp-dependent protein kinase, RAF-1, Akt and vascular endothelial growth factor (VEGF) expression (Picard *et al*., 2002). Akt is one of these client proteins that stabilises HSP90/70 multi-protein complex and it functions as a key modulator in apoptotic pathways. The active form of Akt is also stabilised by this intracellular complex with HSP90 along with CDC37 (client protein). The active Akt phosphorylates proapoptotic proteins such as BAD and transcription factors that suppress apoptotic activities. Therefore, Akt/PKB kinase assay was carried out to determine levels of Akt/PKB which directly helps to determine levels of HSP90 and HSP70 before and after treatment with inhibitory drugs (Basso *et al*., 2002; Zhang *et al.,* 2012a).

The Akt/PKB kinase activity assay data confirmed previous findings showing increased Akt kinase activity in glioma cell lines compared to normal cell lines (Mehta *et al.,* 2011). The significant increase in Akt activity in glioma cell lines have shown dependence on HSP70/90 complex stability. In 1321N1 cells, Akt activity with TMZ, 17-AAG and VER treated cells was reduced by 26, 8 and 62 %, respectively. In GOS-3 cells treated with TMZ, 17-AAG and VER showed reduced activity by 34, 41 and 78 %, respectively, while U87-MG cells have showed a reduction of 14, 26 and 17 %, respectively. In all three cell lines, Akt kinase activity was reduced on treatment with the inhibitory compounds. Theoretically, inhibition of HSP90 leads to disrupt interaction of Akt with the HSP90

complex. It also maintains unstable Akt and prevents formation of active Akt which interacts with other proapoptotic proteins in the apoptosis pathway, thereby, suppressing cell proliferation and regulating apoptosis of malignant cells. Therefore, mRNA quantification and Akt kinase activity data have shown reduced Akt kinase activity on treatment with inhibitory compounds which was consistent with previous studies (Mehta *et al.,* 2011). Therefore, the overexpression of HSP70/90 in cancer cell lines has emerged as molecular target (Zhang *et al*., 2012b).

In this study, Temozolomide (TMZ) was used as standard anti-cancer treatment. The inhibitory concentration of Temozolomide was determined and the IC_{50} values obtained were 135, 147 and 180 µM for the 1321N1, GOS-3 and U87-MG cell lines, respectively. With the concurrent assay, the cells were treated with all three drugs individually or in combination. For the sequential assay, the cell lines were treated separately with either 17-AAG, VER or TMZ and then incubated for a period of 48 h. In addition, the cell lines were treated either with 17-AAG or VER for 24 h, followed by TMZ for an additional 24 h. In the combination treatment using TMZ with 17-AAG and VER with 1321N1, showed cell viability reduced to 23 and 34 %, respectively, after 48 h. In addition, the combination treatment of TMZ with 17-AAG and VER using GOS-3 exhibited cell viability reduced to 17 and 31 %, respectively, after 48 h. In the concurrent assay using U87-MG cells, combination treatment of TMZ with 17-AAG and VER showed cell viability reduced to 43 and 32 %, respectively, after 48 h. Therefore, concurrent treatment using 1321N1, GOS-3 and U87-MG cells confirmed effectiveness of combinational treatment compared to the drugs treated individually. In all cell lines, the combination treatment using TMZ and VER was found to be the most significant, reducing 32%. Sequential assays have shown similar effects for combination treatment after 72 h. This reinforced that the use

of combinational treatment, enhances cell chemosensitivity towards standard treatment of TMZ.

This study has demonstrated the over-expression of *Hsp70* and *Hsp90*α in glioma cell lines by gene transcriptional analysis and Akt/PKB kinase activity. Chemosensitivity enhancement was monitored against standard treatment of Temozolomide using sequential and concurrent methods using 1321N1, GOS-3 and U87-MG cell lines. The most effective treatment was found to be with the U87-MG cell line. Interestingly, the activity of the inhibitory drugs was found to be significantly higher in the concurrent method. Therefore, transcriptional activity and kinase activity with combinations of the drugs was validated so as to establish the therapeutic importance and U87-MG cell line was used for the scheduled studies. The data demonstrated effectivity of treatment using U87-MG was most significant. Therefore, U87-MG was treated with the established IC50 of 17-AAG, VER and TMZ.

Recently, miRNAs have highlighted their importance as a novel class of tumour suppressor or oncogenic role. Dysregulation of miRNAs has been reported in various diseases. miR-21, for instance, is known as an anti-apoptotic miRNA linked to tumourigenesis. More than 2000 human miRNAs have been identified which makes it feasible to apply microarrays enabling miRNA expression analysis in large numbers of samples (Miska *et al*., 2004). miRNA microarrays have been useful in the classification of various cancers by defining miRNA markers predicting potential biomarkers (Esquela-Kerscher *et al.,* 2006; Caramuta *et al.,* 2013). Dysregulated miRNAs have been reported in glioma (Skalsky *et al.,* 2011). miRNA expression or function may be altered due to genetic mutations, epigenetic silencing and chromatin modifications (Cullen *et al*., 2008). Most importantly, these non-protein coding single stranded RNA molecules

regulate post-transcriptional gene expression. Understanding molecular mechanism of anti-cancer drugs is essential for determining efficient drug responses (Cullen *et al*., 2008, Skalsky *et al.,* 2011).

The cancer genome project was carried out involving a large panel of cancer cell lines which were screened by almost 138 drugs and contributed to the identification of mutated genes (Garnett *et al.,* 2012; Bateman *et al.,* 2014). Following this model, current research focuses on understanding the molecular mechanisms of treatment and to identify potential treatment particularly for glioma. Most important role of miRNA is to regulate multiple 3'UTR of the mRNA. The most commonly used miRNA profiling methods includes northern blotting, qPCR and high-throughput microarray technology. Among which northern blotting and qPCR methods are specific, but their low-throughput advents application of microarray technology form a more practical-approach to identify novel miRNAs (Chen *et al*., 2009).

miRNA microarray profiling is an efficient high through put method for identifying novel miRNA using a panel of miRNAs (Wang & Xi, 2013). In this study, miRNA microarray was carried out on duplicate samples of TMZ, 17-AAG and VER treated U87-MG. The quality of the extracted total RNA from U87-MG treated and untreated samples was assessed using Agilent 2100 Bioanalyzer confirmed excellent RNA integrity and also, electrophoresis verified ribosomal RNA degradation. The total RNA used for microarray experiments was of excellent quality. Each array was analysed using feature extraction software in order to carry out data normalisation to eliminate noise and multiple testing errors. Heat map verified correlation coefficient within and between the groups. Differential miRNA expression was obtained by comparing U87-MG treatment group including TMZ, 17-AAG and VER treated cells with U87-MG control (Untreated) as the

reference group. Each group was analysed using bioinformatics software. On application of stringent filtration, only VER-treated samples showed differential regulation with 9 upregulated and 4 downregulated, while the other sample group showed no regulation. Therefore, non-stringent filtering was applied to the data (uncorrected) to identify 154 miRNAs, 84 of which were upregulated. In order to determine potential targets, regulated miRNA obtained by non-stringent filtering data was also taken into consideration. Among which 12 upregulated miRNAs and 1 downregulated miRNA showed overlap between the treatments with VER and TMZ. Only one upregulated miRNA of 17-AAG treated sample appeared to overlap with VER and TMZ treated cells. Therefore, demonstrating that VER compared to 17-AAG, is a more efficient anti-chaperone.

miRNA target prediction algorithms follow varied models including seed match, conservation, free energy, and site accessibility. In order to determine the robustness of the algorithm for target prediction, this study further analysed the overlapped miRNAs with high fold difference or those subjected to stringent statistics for miRNA:mRNA target prediction using the statistical algorithms such as TargetScan Human 6.2, DIANA-microT and miRBD miRBaseV18. Interestingly, as shown in Table 3.7, Hsa-miR-194-5p, Hsa-miR-215, Hsa-miR-449a, Hsa-miR-744-5p and Hsa-miR-3161 showed a large fold change between treatments. In TMZ and VER treatment, Hsa-miR-194p was upregulated by 139 and 63 fold, respectively, Hsa-miR-215 was upregulated 165 and 61 fold, respectively, Hsa-miR-449a was upregulated by 62 and 77 fold, respectively and Hsa-miR-744-5p was upregulated by 63 and 43 fold, respectively. 17-AAG Vs Control data showed only one miRNA overlapping with VER Vs Control with 29 and 2 fold changes, respectively. Hsa-miR-4636 was the only downregulated miRNA in TMZ and VER treatment with a 32 and 33 fold change, respectively. Therefore, noticeable fold change

differences was reported in overlapping miRNAs between treatments. Also, reflecting similarity between miRNA regulation of TMZ and VER treatment and thereby regulating the same mRNA functions. Also, indicating probable similarity in mechanisms of action of both drugs TMZ and VER. miRNA targets more than one mRNAs, however, this study focused on the particular mRNAs that were validated and reported in cancer signalling pathways. The miRNA target prediction software identified upregulated Hsa-miR-194-5p, Hsa-miR-215, Hsa-miR-449a, Hsa-miR-744-5p and Hsa-miR-3161 correlating to *Dnmt3a, Alcam, Cdk4, Dnajc16 (Hsp40)* and *R-Ras2* genes, respectively. The targeted gene transcriptional levels were further validated using qRT-PCR in U87-MG treated and untreated cells.

miR-194-5p, located on chromosome 1 is involved in cell migration, invasion and metastasis (Meng *et al.,* 2010; Wu *et al.,* 2014). It has been shown to be highly induced in some cancers such as adenocarcinoma, gastric cancer and hepatic epithelial cells (Chen *et al*., 2013). However, it is downregulated in colorectal cancer cells (HCT116), colon cancer, CNS tumour cell line and nephroblastomas suggesting its tumour suppressor role (Gaur *et al*., 2007; Braun *et al*., 2008; Kahlert *et al.,* 2011). However, no study has been published to confirm if it only functions as tumour suppressor. In glioma, miR-194 was reported to downregulate during hypoxia conditions (Agrawal *et al*., 2014). A recent study reported the expression of miR-194 in endometrial cancer (EC) cells preventing epithelial mesenchymal transition (EMT) by inhibiting its target BMI-1 and also inhibited tumour invasion (Kahlert *et al.,* 2011). Likewise, it has been reported to be involved in TGF-β, ErbB signaling pathway and glioma and target DNMT3A (Nupur *et al*., 2012).

The present results show that miR-194-5p was found to be upregulated 139 and 63 fold in cells treated with TMZ and VER, respectively. However, its expression was not detected in 17-AAG treated cells. A study was carried out on miR-194-5p mRNA target *Dnmt3a* (DNA methyl transferase), where DNA methyl transferase (DNMT) family carried out DNA methylation at various stages to maintain gene expressions. DNMT1 maintains DNA methylation during DNA replication, while DNMT3A and DNMT3B are responsible for de novo DNA methylation. Aberrations in DNA methylation causes genomic instability by either hypermethylation or hypomethylation (Natsume *et al*., 2010; Koji *et al*., 2012). Transcriptional level of *Dnmt3a* shows no significant changes in TMZ and 17-AAG treated cells and marginal elevated expression in VER treatment. In colorectal cancer, DNMT3A levels did not show significant change compared to non-tumour (Meng *et al*., 2010; Zhao *et al*., 2014). However, previous data illustrated decreased expression of DNMT3A in glioma contributing to erratic DNA methylation (Fanelli *et al*., 2008). Therefore, VER demonstrates slight improvement in the condition.

Recent studies have shown that miR-215 is downregulated in several cancers such as oesophageal adenocarcinoma, colon cancer, nephroblastomas, multiple myeloma, demonstrating a tumour suppressor role (Deng *et al*., 2014), but other reports suggest overexpression in glioma and breast cancer (Roth *et al.,* 2011; Lee *et al.,* 2013). The elevated expression of miR-215 in breast cancer serum, osteosarcoma and colon cancer can lead to reduced cell proliferation, cell invasion and enhance cell cycle control (White *et al.,* 2011; van Schooneveld *et al.,* 2012; Khella *et al.,* 2013). miR-215 expression reported enhance chemosensitivity in osteosarcoma and colon cancer cells (Song *et al.,* 2010). miR-215 was upregulated by 165 and 61 fold in cells treated with TMZ and VER, respectively, and below the fold change detection in cells treated with 17-AAG. miR-215 located on chromosome 1q41 targeting adhesion molecule ALCAM reported to have

negative correlation in gastric epithelial cells (HFE145). They play a crucial role in carcinogenesis by p53 regulation and by inducing cell-cycle arrest (Jin *et al.,* 2011). ALCAM (CD166), a member of immunoglobulin superfamily, mediates cell-cell adhesion and is suggested to be involved in cell migration, progression and differentiation in melanoma, prostate, colorectal and breast cancers. ALCAM expression has been reported to be elevated in low grade tumours while reduced in high grade tumours (Kristiansen *et al.,* 2005; Hong *et al.,* 2010). Furthermore, studies illustrated in primary carcinoma, ALCAM degradation leads to break down of cellular network and thereby increases metastasis (Jin *et al.,* 2011). Reduced ALCAM expression has been associated with chemoresistance (Hong *et al.,* 2010). Moreover, ALCAM has been found to essential for the activation of metalloproteinase cascade, leading to cell invasion which forms crucial characteristics of GBM. Studies have shown the downregulation of ALCAM in glioblastoma, promoting cell invasion without affecting cell proliferation rates (Kijima *et al.,* 2012; Fujiwara *et al.,* 2014). In this study, *Alcam* levels were enhanced by 128.8, 14.4 and 2.6 fold in cells treated with TMZ, 17-AAG and VER, respectively. Although miRNA-215 and the target gene *Alcam* were both upregulated, there was no correlation in the level of induction. *Alcam* mRNA was detected in cells treated with 17-AAG, however, miRNA-215 was undetected in these cells. TMZ and 17-AAG treatment was most effective and VER appears to enhance *Alcam* expression in glioma.

miR-449 cluster located on chromosome 5 are highly conserved in humans and mice consist of three members, namely, miR-449a, miR-449b, miR-449c; these are simultaneously transcribed. miR-449 induces epithelial differentiation by inhibiting the Delta/Notch Pathway, whereas its inhibition reported defects in pulmonary epidermis differentiation. Increased levels of miR-449 has been reported in epithelial cell layer of choroid plexus in the brain (Feng *et al.,* 2010; Marcet *et al.,* 2011; Bao *et al.,* 2012).

Previous reports have suggested miR-449 transcriptionally regulated Cyclin Dependent Kinase 6 (CDK6) by inhibiting cell progression activity in cancer cells, but also indirectly regulated CDK4, as its 3'UTR is not exactly the same as the miR-449 seed sequence (Yang *et al.,* 2009). Reduced levels of CDK6 is associated with the inhibition of cell cycle progression (Feng *et al.,* 2010). miR-449 mainly targets regulators of cell damage responses, cell cycle arrest, inflammation and cancer pathways (Bou Kheir *et al.,* 2011).. Reduced expression of miR-449 has been observed in breast cancer MCF-7, lung carcinoma H1299, and noncancerous breast epithelial MCF-10A cells (Yang *et al.,* 2009). The Cyclin D–CDK4/6 complex is a central component of the G1/S-phase checkpoint (Bou Kheir *et al.,* 2011). miR-449 potently induces apoptosis and it also upregulates p53 activity (Lizé *et al.,* 2011). It suppresses tumour growth in bladder and prostate cancers (Noonan *et al.,* 2009; Chen *et al.,* 2012). The overexpression of miR-449 enhances chemosensitivity to cisplatin in gastric cancer cells (Hu *et al.,* 2014). In this study, miR-449a was induced by 62 and 77 fold in cells treated with TMZ and VER, respectively. *Cdk4*, mRNA was upregulated by 8.5, 3 and 3.5 fold in cells treated with TMZ, 17-AAG and VER, respectively. In contrast, *Cdk4* Gene was transcriptionally induced to similar levels when subjected to 17-AAG and VER. The miRNA-449a was found to be induced at the highest level with cells treated with VER and this was below the detection level with cells treated with 17-AAG. Elevated levels of CDK4 has been reported in U87-MG cell line (Lam *et al.,* 2000). CDKs play a role in cell cycle by interacting with cyclin-D and CDK4 to phosphorylate Rb which in turn activates E2F genes facilitating cell cycle progression through G1 phase. CDK4 overexpression is associated with tumour progression in osteosarcomas (Schmidt *et al.,* 2001) and gliomas (Masciullo *et al.,* 1997; Corrias *et al.,* 2010; Chen *et al.,* 2014). CDK4 and CDK6 proteins are associated with tumourigenesis and poor outcome in a variety of cancers. They are required for a cell to progress from

G1 to S phase (Schmidt *et al.,* 2001; Bradley *et al.,* 2014). miR-449a has been reported to be reduced in the U87-MG cell line acting as tumour suppressor by inhibiting cell growth and inducing apoptosis (Yao *et al.,* 2014). Previous studies have also shown the same tumour-suppressive function of miR-449a in bladder cancer, gastric adenocarcinoma, retinoblastoma and non-small cell lung cancer (Chen *et al.,* 2012; Luo *et al.,* 2013; Wei *et al.,* 2013). Inhibiting CDK4 radiosensitised breast cancer cells have been carried out by inducing apoptosis with altering cell cycle progression (Hagen *et al.,* 2013).

miR-744 is significantly deregulated in several cancers, including hepatocellular carcinoma (HCC) (Hou *et al.,* 2011), colon cancer (Dong *et al.,* 2013), breast cancer (Vislovukh *et al.,* 2013), and gastric cancer (Song *et al.,* 2012; Lin *et al.,* 2014). Recent studies suggest miR-744 is tumour biomarker since its levels are found to be stable in mouse serum while upregulated in gastric cancer (Vislovukh *et al.,* 2013). miR-744 lower levels in Multiple Myeloma (MM) patient serum are responsible for shorter survival patients (Kubiczkova *et al.,* 2014). miR-744 negatively regulates its target transforming growth factor beta-1 (TGF-b1), while other target cyclinB1 is known to be positively targeted (Huang *et al.,* 2011; Martin *et al.,* 2011). Furthermore, induction of miR-744 causes reduced cell proliferation via a transcription regulator c-Myc protein downregulation in HCC cell lines and cell cycle progression in HepG2 and SMMC-7721 cells (Lin *et al.,* 2014). In this study, miR-744-5p was enhanced on treatment with TMZ and VER by 63 and 43 fold, respectively. Therefore, miR expression after treatment may be contributing towards cancer progression and VER treatment shows an effective response similar to TMZ. As mentioned earlier, only two targets have been investigated to date. This study focused on *Dnajc16 (Hsp40)* as a target identified using miRNA target prediction software. DNAJ, also known as HSP40 is a molecular chaperone protein. It is

expressed in a wide variety of organisms from bacteria to humans. This family of proteins contains a 70 amino acid consensus sequence known as the J domain, which is known to interact with HSP70. The involvement of DNAJ family member Isoforms such as DNAJB2, DNAJB6, DNAJC5, DNAJC6, DNAJC13, and DNAJC26 in HSP70/90 chaperone machinery has been established (Heldens *et al.,* 2010). Identified target of miR-744, namely DNAJC16 belongs to the evolutionarily conserved DNAJ/HSP40 family of proteins (Qiu *et al.,* 2006). *Dnajc16* mRNA was found to be upregulated by 105.6, 17.4 and 5 fold on treatment with TMZ, 17-AAG and VER, respectively. Again, no correlation was found in miRNA and mRNA targets. As HSP40 family members act as a co-chaperone to HSP70 machinery, they would be favourable to disrupt the HSP70/90 complex in order to enhance chemotherapeutic effect. Data have shown efficacy of VER treatment by downregulating *Dnajc16* expression compared to 17-AAG and TMZ.

miR-3161, located on chromosome 11 has been documented in laryngeal cancer cells where it was downregulated using paclitaxel (Xu *et al.,* 2013). miR-3161 was the only miRNA that was found to be upregulated in cells treated with 17-AAG and VER by 29 and 2 fold, respectively. R-RAS2/TC21 activates PI3K/Akt and NFκB to facilitate cell survival (Arora *et al.,* 2008). It is also involved in several other cell regulatory functions such as cell adhesion, proliferation and migration. Limited studies carried out on R-RAS in brain tumours validates upregulation of RAS proteins in malignant gliomas (Nakada *et al.,* 2005). R-Ras was found to be over expressed in all CNS tumours and inversely proportional to tumour malignancy as it functions to stimulate cell survival and proliferation via PI3K pathway activation (Gutierrez-Erlandsson *et al.,* 2013). miR-3161 targets *R-Ras2*, located on chromosome 11p15.2, were elevated by 4.2, 7 and 8.7 fold in cells treated with TMZ, 17-AAG and VER, respectively. In this case, elevated *R-Ras2* is

unfavourable as it may result in adverse conditions. Furthermore, there was no correlation between the upregulation of miR-3161 and *R-Ras2* mRNA.

In this study, the overall integrated analysis of miRNA and their targets show no significant correlation. There are several factors which can be taken into account in order to provide an explanation for these finding. Studies have attempted to establish reliability of HSP70 and HSP90 inhibitory drugs for integrated analysis of miRNA. In HeLa, human embryonic kidney 293T, HepG2 cells and mouse embryo fibroblasts, they have illustrated that molecular chaperones can enhance efficacy of the process, but are not mandatory for RISC loading (Pare *et al.,* 2009). Other studies demonstrated the necessity of HSP70/90 requirement for RISC loading, on other hand, not for unwinding or target cleavage (Iwasaki *et al.,* 2010). They stabilise Argonaute (AGO2) protein and perform chaperoning role for conformational changes of the AGO2 protein by ATP hydrolysis allowing RISC loading by recruitment of miRNA duplex. Although inhibition of HSP70/90 affects AGO2 levels, miRNAs remain unaffected, nevertheless, it may play a role in the degradation of unloaded AGO2 (Martinez *et al.,* 2013).

Previous studies have illustrated the reliance of targeted mRNA expression on its complementarity. Moreover, mRNA degradation are outcome of perfect complementarity while silencing of protein translation, a consequence of partial complementarity. Despite of these, miRNA can bind onto microarray, screening miRNA existence in particular samples without justifying the process (Lim *et al.,* 2005). However, integrated analysis of miRNA and mRNA have shown that their association can only be determined if targeted mRNA is completely degraded (van Iterson *et al.,* 2013). Notably, miRNAs interact with 3'UTR region, but there are some exceptions showing binding sites in the protein coding in exons or 5'UTR regions. In some situations, RISC

complex necessary for mRNA degradation, is competed by ribosome-binding causing bridge miRNA-mediated regulation (Giraldez *et al.,* 2006; Bartel 2009; Fabian *et al.,* 2010). Both In vitro and In vivo studies have demonstrated a negative relationship between miRNA and their target mRNA. However, positive correlation has also been reported (Nunez *et al.,* 2013). Correlation studies of miRNA and their target mRNA inferred positive correlation may be due to the involvement of transcription factors and other regulating factor justifying increased expression levels in human and chimpanzee frontal cortex brain tissue samples (Dannemann *et al.,* 2012). A possible explanation is either the effects of miRNA are overriding by other miRNA networks or they are involved regulatory transcription factor demonstrating unpredictability of miRNA deregulation throughout. Although these studies were unable to identify correlation between miRNAs and their targets, perhaps, research described above can help to explain the behaviour of mRNAs. Even though, integrated analysis was unsuccessful, investigation of individual target may enhance understanding of the mechanisms of treatment.

The novel aspect of this study, as mentioned previously, was to compare the therapeutic efficacy of 17-AAG and VER compared to the chemotherapeutic agent, TMZ. Gene expression studies have been reported in breast cancer cell lines determining 17-AAG (HSP90) inhibitor response (Zajac *et al.,* 2010). Data from 17-AAG compared to control group have shown 4 upregulated and only 1 downregulated miRNA in non-stringent data, while VER compared to control data have shown 9 fold upregulation and 4 fold downregulation of miRNA on stringent filtering. Dysregulated miRNAs demonstrated overlapping of miRNAs in TMZ and VER treatment. 17-AAG and VER have a specific affinity towards HSP90 and HSP70, respectively. 17-AAG targets HSP90 by binding to nucleotide binding terminal and VER, an ATP-competitive inhibitor, selectively inhibits HSP70 by binding to nucleotide binding domain and also indirectly targets HSP90β. Data

obtained in selected mRNA transcription have reflected a close correlation in TMZ-treated and VER-treated cells. These data validate the previous chemosensitivity assay in which VER treatment was more effective compared to TMZ. However, *Hsp70* and *Hsp90* transcriptional data have shown that treatment with TMZ, 17-AAG and VER does not support Akt activity data. Experiments involving HSP70 and HSP90 ELISA were carried out to confirm expression of HSPs and moreover, to validate the effect of drugs. The results shows that HSP70 protein activity was inhibited by 13, 0 and 20 % in TMZ, 17-AAG and VER treatment respectively, while HSP protein was inhibited by 84, 43 and 65 % in TMZ, 17-AAG and VER treatment respectively. The treatment with 17-AAG shows significant inhibition of HSP90 target while VER targeted both HSP70 and HSP90. Protein expression data clearly confirm affinities of HSP70 and HSP90 inhibitors. The overall data suggest that targeting HSP70 can be a potential therapeutic biomarker for glioblastoma.

CHAPTER 5

CONCLUSION AND FUTURE WORK

5.1 Conclusion

This study has demonstrated the elevation of *Hsp70* and *Hsp90α* in glioma cell lines (1321N1, GOS-3 and U87-MG) by measuring transcriptional activity compared to control. Since there was no significant expression of *Hsp70* or *Hsp90*α reported in NHA (Normal Human Astrocytes), they were not used for further investigation. Initial results from this study reported induction of HSP70 on post-inhibition of HSP90 using 17-AAG. Therefore, HSP70 and HSP90 were targeted by VER-155008 and 17-AAG, respectively. Chemosensitivity was compared to standard treatment using the anticancer drug, Temozolomide. Furthermore, Akt kinase activity measured after treating cells with the relevant IC_{50} concentration of the drugs (TMZ, 17-AAG and VER), demonstrated of Akt kinase activity inhibition suggesting disruption of HSP70/90 complex. Concurrent and sequential chemosensitivity assays further validated the efficiency of inhibitor drugs. Interestingly, the activity of the inhibitory drugs was reported to be significantly higher in the concurrent method suggesting the ability of the drug to enhance chemosensitivity in glioma. Therefore, further investigations were carried out on Grade IV glioma cell line U87-MG.

In order to understand the molecular mechanisms of the heat shock protein inhibitors. miRNA are small regulatory RNAs known to regulate several mRNAs simultaneously. Thereby, miRNA microarray analysis was carried out and their mRNA targets were determined to identify novel molecular biomarkers. miRNA microarray identified 154 miRNAs including stringent and non-stringent data suggesting the role of miRNAs in glioma biology. However, no correlation was documented in miRNA and their target mRNA *Dnmt3a, Alcam*, *Dnajc16* (*Hsp40)*, *Cdk4 and R-Ras2*. Therefore, the application of miRNA technology is somewhat limited in being appropriate in predicting targets.

Nevertheless, the transcriptional level of selected mRNA authenticates effectivity of 17-AAG and VER treatment. 17-AAG targets HSP90, whereas VER targets both HSP70 and HSP90β. HSP70 and HSP90 protein expression data confirmed the efficacy of VER and 17-AAG. The overall data suggest that HSP90 is a softer target and HSP70 is a therapeutic target for treatment of glioma.

The main findings of this study are summarised:

1. Established that there are enhanced *Hsp70* and *Hsp90* transcriptional levels in glioma cell lines confirmed by decreased Akt kinase activity.
2. The chemosensitivity cell viability assay demonstrated overcome resistance in 17-AAG and VER treatment and the combinational effect was most effective in U87-MG.
3. Integrated analysis of miRNA: mRNA have shown no correlation in untreated and heat shock protein inhibitory drug treated U87-MG cell lines.
4. VER-155008 enhances chemosensitivity in U87-MG cells.
5. HSP70 can be a therapeutic target for glioma.

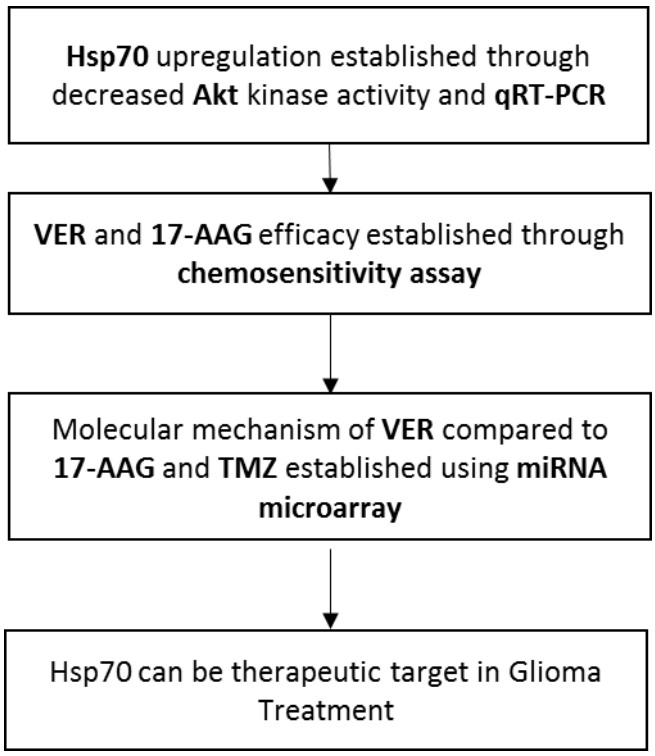

Figure 5.1: Summary of the project main findings

5.2 Future work

The study established HSP70 as a chemotherapeutic target in glioma. Moreover, VER-155008, an HSP70 inhibitor, has proven to be powerful cancer therapeutic agent. A recent publication also supports VER-155008 as a possible therapy in non-small-cell lung cancer (NSCLC) (Wen *et al.,* 2014). A report has shown its ability to induce apoptosis in BT474 breast cancer cells and HCT166 colon cancer cells (Massey *et al.,* 2010). Therefore, measuring apoptosis using different parameters such as cytochrome-C caspase3/9 could be beneficial. Also, its featured ability in indirectly targeting HSP90β would be worth investigating. Therefore, detailed analysis of VER-155008 mode of action and mechanism is required in other types of cancers apart from glioma. This study investigated the chemotherapeutic effect of 17-AAG and VER-155008 at the molecular level by identifying deregulated miRNA, however, it was established that there is no significant correlation between miRNA and their targets. Therefore questioning the reliability of miRNA:mRNA integrated analysis for determining potential biomarkers. miRNA and their target mRNA expressions need to be verified using an anti-miR inhibition method. miRNA binding is proceeded irrespective of the perfect match of seed sequence. Thereby, it is essential to validate whether the regulation of mRNA could be carried out by different miRNA families. Identifying regulatory pathways involved can enhance understanding of miRNA regulation.

CHAPTER 6

REFERENCES

Agrawal, R., Pandey, P., Jha, P., Dwivedi, V., Sarkar, C. & Kulshreshtha, R. (2014). Hypoxic signature of microRNAs in glioblastoma: insights from small RNA deep sequencing, *BMC Genomics*, **15**(686), 1-16.

Aghdassi, A., Phillips, P., Dudeja, V., Dhaulakhandi, D., Sharif, R., Dawra, R., Lerch, M.M. & Saluja, A. (2007). Heat shock protein 70 increases tumorigenicity and inhibits apoptosis in pancreatic adenocarcinoma, *Cancer Research,* **67**(2), 616-625.

Ahner, A., Whyte, F.M. & Brodsky, J.L. (2005). Distinct but overlapping functions of Hsp70, Hsp90, and an Hsp70 nucleotide exchange factor during protein biogenesis in yeast, *Archives of Biochemistry & Biophysics,* **435**(1), 32-41.

An, W.G., Schulte, T.W. & Neckers, L.M. (2000). The heat shock protein 90 antagonist geldanamycin alters chaperone association with p210(bcr-abl) and v-src proteins before their degradation by the proteasome, *Cell Growth & Differentiation,* **11**(7), 355-360.

Appin, C.L., Gao, J., Chisolm, C., Torian, M., Alexis, D., Vincentelli, C., Schniederjan, M.J., Hadjipanayis, C., Olson, J.J., Hunter, S., Hao, C. & Brat, D.J. (2013). Glioblastoma with oligodendroglioma component (GBM-O): molecular genetic and clinical characteristics, Brain pathology, 23(4), 454-461.

Arora, S., Wang, Y., Jia, Z., Vardar-Sengul, S., Munawar, A., Doctor, K.S., Birrer, M., McClelland, M., Adamson, E. & Mercola, D. (2008). Egr1 regulates the coordinated expression of numerous EGF receptor target genes as identified by ChIP-on-chip, *Genome Biology,* **9**(11), R166.1- R166.14.

Assanga, S., Gil-Salido, A., Lujan, M., Rosas-Durazo, A., Acosta-Silva, L., Rivera-Castañeda, G. & Rubio-Pino, L. (2013). Cell growth curves for different cell lines and their

relationship with biological activities, *International Journal of Biotechnology and Molecular Biology Research,* **4**(4), 60-70.

Bao, J., Li, D., Wang, L., Wu, J., Hu, Y., Wang, Z., Chen, Y., Cao, X., Jiang, C., Yan, W. & Xu, C. (2012). Microrna-449 and microrna-34b/c Function Redundantly in Murine Testes by Targeting E2F Transcription Factor-Retinoblastoma Protein (E2F-prb) Pathway, *Journal of Biological Chemistry,* **287**(26), 21686-21698.

Bardelli, A. & Siena, S. (2010). Molecular mechanisms of resistance to cetuximab and panitumumab in colorectal cancer, *Journal of clinical oncology : official journal of the American Society of Clinical Oncology,* **28**(7), 1254-1261.

Barnes, J.A., Dix, D.J., Collins, B.W., Luft, C. & Allen, J.W. (2001). Expression of inducible Hsp70 enhances the proliferation of MCF-7 breast cancer cells and protects against the cytotoxic effects of hyperthermia, *Cell Stress & Chaperones,* **6**(4), 316-325.

Bartel, D.P. (2009). MicroRNAs: target recognition and regulatory functions, *Cell,* **136**(2), 215-233.

Bartel, D.P. (2004). MicroRNAs: genomics, biogenesis, mechanism, and function, *Cell,* **116**(2), 281-297.

Bartels, C.L. & Tsongalis, G.J. (2009). Micrornas: novel biomarkers for human cancer, *Clinical Chemistry,* **55**(4), 623-631.

Basso, A.D., Solit, D.B., Chiosis, G., Giri, B., Tsichlis, P. & Rosen, N. (2002). Akt forms an intracellular complex with heat shock protein 90 (hsp90) and cdc37 and is destabilized by inhibitors of hsp90 function, *Journal of Biological Chemistry,* **277**(42), 39858-39866.

Bateman, A.R., El-Hachem, N., Beck, A.H., Aerts, H.J.W.L. & Haibe-Kains, B. (2014). Importance of collection in gene set enrichment analysis of drug response in cancer cell lines, *Sci Rep*, **4**, 1-10.

Beere, H.M., Wolf, B.B., Cain, K., Mosser, D.D., Mahboubi, A., Kuwana, T., Tailor, P., Morimoto, R.I., Cohen, G.M. & Green, D.R. (2000). Heat-shock protein 70 inhibits apoptosis by preventing recruitment of procaspase-9 to the Apaf-1 apoptosome, *Nature Cell Biology,* **2**(8), 469-475.

Bisht, K.S., Bradbury, C.M., Mattson, D., Kaushal, A., Sowers, A., Markovina, S., Ortiz, K.L., Sieck, L.K., Isaacs, J.S., Brechbiel, M.W., Mitchell, J.B., Neckers, L.M. & Gius, D. (2003). Geldanamycin and 17-allylamino-17-demethoxygeldanamycin potentiate the in vitro and in vivo radiation response of cervical tumor cells via the heat shock protein 90-mediated intracellular signaling and cytotoxicity, *Cancer Research*, **63**(24), 8984-8995.

Bolstad, B.M., Irizarry, R.A., Åstrand, M. & Speed, T.P. (2003). A comparison of normalization methods for high density oligonucleotide array data based on variance and bias, *Bioinformatics,* **19**(2), 185-193.

Bou Kheir, T., Futoma-Kazmierczak, E., Jacobsen, A., Krogh, A., Bardram, L., Hother, C., Gronbaek, K., Federspiel, B., Lund, A. & Friis-Hansen, L. (2011). miR-449 inhibits cell proliferation and is down-regulated in gastric cancer, *Molecular Cancer,* **10**(1), 29-41.

Bradley, B., Loftus, J., Mielke, C. & Dinu, V. (2014). Differential expression of microRNAs as predictors of glioblastoma phenotypes, *BMC Bioinformatics,* **15**(21), 1-11.

Braun, C.J., Zhang, X., Savelyeva, I., Wolff, S., Moll, U.M., Schepeler, T., Ørntoft, T.F., Andersen, C.L. & Dobbelstein, M. (2008). P53-responsive micrornas 192 and 215 are capable of inducing cell cycle arrest, *Cancer Research,* **68**(24), 10094-10104.

Buckner, J.C., Brown, P.D., O'Neill, B. P., Meyer, F. B., Wetmore, C.J. & Uhm, J.H. (2007). Central nervous system tumors, *Mayo Clinic proceedings,* **82**(10), 1271-1286.

Calderwood, S.K., Khaleque, M.A., Sawyer, D.B. & Ciocca, D.R. (2006). Heat shock proteins in cancer: chaperones of tumorigenesis, *Trends in Biochemical Sciences,* **31**(3), 164-172.

Caramuta, S., Lee, L., Ozata, D.M., Akcakaya, P., Georgii-Hemming, P., Xie, H., Amini, R., Lawrie, C.H., Enblad, G., Larsson, C., Berglund, M. & Lui, W. (2013). Role of microRNAs and microRNA machinery in the pathogenesis of diffuse large B-cell lymphoma, *Blood Cancer Journal,* **3**, e152-164.

Centenera, M.M., Fitzpatrick, A.K., Tilley, W.D. & Butler, L.M. (2013). Hsp90: Still a viable target in prostate cancer, *Biochimica et Biophysica Acta (BBA) - Reviews on Cancer,* **1835**(2), 211-218.

Chan, J.A., Krichevsky, A.M. & Kosik, K.S. (2005). MicroRNA-21 is an antiapoptotic factor in human glioblastoma cells, *Cancer Research,* **65**, 6029-6033.

Chatterjee, M., Andrulis, M., St++hmer, T., M++ller, E., Hofmann, C., Steinbrunn, T., Heimberger, T., Schraud, H., Kressmann, S., Einsele, H. & Bargou, R.C. (2012). The PI3K/Akt signalling pathway regulates the expression of Hsp70, which critically contributes to Hsp90-chaperone function and tumor cell survival in multiple myeloma, *Haematologica*, **1**(1), 1-32**.**

Chen, G., Shen, Z.L., Wang, L., Lv, C.Y., Huang, X.E. & Zhou, R.P. (2013). Hsa-miR-181a-5p expression and effects on cell proliferation in gastric cancer, *Asian Pacific journal of cancer prevention: APJCP,* **14**(6), 3871-3875.

Chen, H., Lin, Y., Mao, Y., Wu, J., Liu, Y., Zheng, X. & Xie, L. (2012). MicroRNA-449a acts as a tumor suppressor in human bladder cancer through the regulation of pocket proteins, *Cancer Letters,* **320**(1), 40-47.

Chen, T., Lee, S., Lin, L., Lin, C., Chang, K. & Li, C. (2014). Cyclin-dependent kinase 4 overexpression is mostly independent of gene amplification and constitutes an independent prognosticator for nasopharyngeal carcinoma, *Tumor Biology,* **35**(7), 7209-7216.

Chen, Y., Gelfond, J., McManus, L. and Shireman, P. (2009). Reproducibility of quantitative RT-PCR array in miRNA expression profiling and comparison with microarray analysis, *BMC Genomics,* **10**(407), 1-10.

Chou, J., Lin, J.H., Brenot, A., Kim, J., Provot, S. & Werb, Z. (2013). GATA3 suppresses metastasis and modulates the tumour microenvironment by regulating microRNA-29b expression, *Nature Cell Biology,* **15**(2), 201-213.

Ciafre, S.A., Galardi, S., Mangiola, A., Ferracin, M., Liu, C.G., Sabatino, G., Negrini, M., Maira, G., Croce, C.M. & Farace, M.G. (2005). Extensive modulation of a set of microRNAs in primary glioblastoma, *Biochem Biophys Res Commun,* **334**, 1351-1358.

Ciocca, D.R. & Calderwood, S.K. (2005). Heat shock proteins in cancer: diagnostic, prognostic, predictive, and treatment implications, *Cell Stress & Chaperones,* **10**(2), 86-103.

Corrias, M.V., Gambini, C., Gregorio, A., Croce, M., Barisione, G., Cossu, C., Rossello, A., Ferrini, S. & Fabbi, M. (2010). Different subcellular localization of ALCAM molecules in neuroblastoma: association with relapse, *Cellular Oncology,* **32**(1-2), 77-86.

Cruickshanks, N., Shervington, L., Patel, R., Munje, C., Thakkar, D. & Shervington, A. (2010). Can hsp90alpha-targeted siRNA combined with TMZ be a future therapy for glioma?, *Cancer Investigation,* **28**(6), 608-614.

Cullen, P.J. (2008). Endosomal sorting and signalling: an emerging role for sorting nexins, *Nat Rev Mol Cell Biol*, **9**(7), 574-582.

Cummins, J.M. & Velculescu, V.E. (2006). Implications of micro-RNA profiling for cancer diagnosis, *Oncogene,* **25**(46), 6220-6227.

Cutress, R.I., Townsend, P.A., Brimmell, M., Bateman, A.C., Hague, A. & Packham, G. (2002). BAG-1 expression and function in human cancer, *British Journal of Cancer,* **87**(8), 834-839.

Dannemann, M., Prufer, K., Lizano, E., Nickel, B., Burbano, H.A. & Kelso, J. (2012). Transcription factors are targeted by differentially expressed miRNAs in primates, *Genome Biology and Evolution*, **4**(4), 552-564.

Davis.A.L, Cabello.C.M, Qiao.S, Azimian.S & Wondrak. G.T. (2013). Phenotypic identification of the redox dye methylene blue as an antagonist of heat shock response gene expression in metastatic melanoma cells, *Molecular Sciences,* **14**(1), 4185-4202.

Demidenko, Z.N., Vivo, C., Halicka, H.D., Li, C.J., Bhalla, K., Broude, E.V. & Blagosklonny, M.V. (2006). Pharmacological induction of Hsp70 protects apoptosis-prone cells from

doxorubicin: comparison with caspase-inhibitor- and cycle-arrest-mediated cytoprotection, *Cell Death and Differentiation,* **13**(9), 1434-1441.

Deng, Y.,Huang, Z.,Xu, Y.,Jin, J.,Zhuo, W.,Zhang, C.,Zhang, X.,Shen, M.,Yan, X.,Wang, L.,Wang, X.,Kang, Y.,Si, J. & Zhou, T. (2014). MiR-215 modulates gastric cancer cell proliferation by targeting RB1, *Cancer Letters,* **342**(1), 27-35.

Dong, Y., Zhao, J., Wu, C., Zhang, L., Liu, X., Kang, W., Leung, W., Zhang, N., Chan, F. & Sung, J. (2013). Tumor suppressor functions of mir-133a in colorectal cancer, *Mol Cancer Res,* **11**, 1051-1060.

Elisa Zorzi, P.B. (2011). Inducible hsp70 in the regulation of cancer cell survival: analysis of chaperone induction, expression and activity, *Cancers,* **3**(4), 3921-3956.

Esquela-Kerscher, A. and Slack, F.J. (2006). Oncomirs--microRNAs with a role in cancer, *Nat Rev Cancer,* **6**, 259-269.

Fabbri, M., Garzon, R., Cimmino, A., Liu, Z., Zanesi, N., Callegari, E., Liu, S., Alder, H., Costinean, S., Fernandez-Cymering, C., Volinia, S., Guler, G., Morrison, C.D., Chan, K.K., Marcucci, G., Calin, G.A., Huebner, K. & Croce, C.M. (2007). MicroRNA-29 family reverts aberrant methylation in lung cancer by targeting DNA methyltransferases 3A & 3B, *PNAS USA,* **104**(40), 15805-15810.

Fabian, M.R., Sonenberg, N. & Filipowicz, W. (2010). Regulation of mRNA translation and stability by microRNAs, *Annual Review of Biochemistry*, **79**, 351-379.

Fan, C.Y., Lee, S. & Cyr, D.M. (2003). Mechanisms for regulation of Hsp70 function by Hsp40, *Cell Stress & Chaperones,* **8**(4), 309-316.

Fanelli, M., Caprodossi, S., Ricci-Vitiani, L., Porcellini, A., Tomassoni-Ardori, F., Amatori, S., Andreoni, F., Magnani, M., De Maria, R., Santoni, A., Minucci, S. & Pelicci, P.G. (2008). Loss of pericentromeric DNA methylation pattern in human glioblastoma is associated with altered DNA methyltransferases expression and involves the stem cell compartment, *Oncogene,* **27**(3), 358-365.

Fawzy. A, Attia.H, Khalaf.A, Sameea.A, Tahawy.M.A.E, Farag.M & Younis.F. (2013). Heat shock protein-70 and -27 expressions as parameters of early diagnosis and disease progression in hepatocellular carcinoma, *Life Sciences Journal,* **10**(1), 262-268.

Feng, M. & Yu, Q. (2010). miR-449 regulates CDK-Rb-E2F1 through an auto-regulatory feedback circuit, *Cell Cycle*, **9**, 213-214.

Fujiwara, K.,Ohuchida, K.,Sada, M.,Horioka, K.,Ulrich III, C.D.,Shindo, K.,Ohtsuka, T.,Takahata, S.,Mizumoto, K.,Oda, Y.&Tanaka, M. (2014). CD166/ALCAM expression is characteristic of tumorigenicity and invasive and migratory activities of pancreatic cancer cells, *PlosOne,* **9**(9), el07247 (1-11).

Gallerne, C., Prola, A. & Lemaire, C. (2013). Hsp90 inhibition by PU-H71 induces apoptosis through endoplasmic reticulum stress and mitochondrial pathway in cancer cells and overcomes the resistance conferred by Bcl-2, *Biochemica et Biophysica Acta (BBA) - Molecular Cell Research,* **1833**(6), 1356-1366.

Gao, X., Zhang, R., Qu, X., Zhao, M., Zhang, S., Wu, H., Li Jianyong & Chen, L. (2012). MiR-15a, miR-16-1 and miR-17-92 cluster expression are linked to poor prognosis in multiple myeloma, *Leukemia Research,* **36**(12), 1505-1509.

Garnett, M.J., Edelman, E.J., Heidorn, S.J., Greenman, C.D., Dastur, A., Lau, K.W., Greninger, P., Thompson, I.R., Luo, X., Soares, J., Liu, Q., Iorio, F., Surdez, D., Chen, L., Milano, R.J., Bignell, G.R., Tam, A.T., Davies, H., Stevenson, J.A., Barthorpe, S., Lutz, S.R., Kogera, F., Lawrence, K., McLaren-Douglas, A., Mitropoulos, X., Mironenko, T., Thi, H., Richardson, L., Zhou, W., Jewitt, F., Zhang, T., O'Brien, P., Boisvert, J.L., Price, S., Hur, W., Yang, W., Deng, X., Butler, A., Choi, H.G., Chang, J.W., Baselga, J., Stamenkovic, I., Engelman, J.A., Sharma, S.V., Delattre, O., Saez-Rodriguez, J., Gray, N.S., Settleman, J., Futreal, P.A., Haber, D.A., Stratton, M.R., Ramaswamy, S., McDermott, U. & Benes, C.H. (2012). Systematic identification of genomic markers of drug sensitivity in cancer cells, *Nature*, **483**(7391), 570-575.

Gaur, A., Jewell, D.A., Liang, Y., Ridzon, D., Moore, J.H., Chen, C., Ambros, V.R. & Israel, M.A. (2007). Characterization of microRNA expression levels and their biological correlates in human cancer cell lines, *Cancer Research*, **67**(6), 2456-2468.

Giraldez, A.J., Mishima, Y., Rihel, J., Grocock, R.J., Van Dongen, S., Inoue, K., Enright, A.J. & Schier, A.F. (2006). Zebrafish MiR-430 promotes deadenylation and clearance of maternal mRNAs, *Science*, **312**(5770), 75-79.

Gaspar, N.,Marshall, L.,Perryman, L.,Bax, D.,Little, S.,Viana-Pereira, M.,SHarp, S.,Vassal, G.,Pearson, A.,Reis, R.,Hargrave, D.,Workman, P.&Jone, C., (2010). MGMT-independent temozolomide resistance in pediatric glioblastoma cells associated with a PI3-kinase-mediated HOX/STEM cell gene signature, *Cancer Res,* **70 (22),** 9243-9252.

Gaspar, N., Sharp, S.Y., Pacey, S., Jones, C., Walton, M., Vassal, G., Eccles, S., Pearson, A. & Workman, P. (2009). Acquired resistance to 17-Allylamino-17-

Demethoxygeldanamycin (17-AAG, Tanespimycin) in glioblastoma cells, *Cancer Research,* **69**(5), 1966-1975.

Gava, L.M. & Ramos, C.H.I. (2009). Human 90kda heat shock protein hsp90 as a target for cancer therapeutics, *Current Chemical Biology,* **3**(1)**,** 10-21.

Giraldez, A.J., Mishima, Y., Rihel, J., Grocock, R.J., Van Dongen, S., Inoue, K., Enright, A.J. & Schier, A.F. (2006). Zebrafish MiR-430 promotes deadenylation and clearance of maternal mRNAs, *Science,* **312**(5770), 75-79.

Goetz, M.P., Toft, D.O., Ames, M. & Erlichman, C. (2003). The Hsp90 chaperone complex as a novel target for cancer therapy, *Annals of Oncology,* **14**(8), 1169-1176.

Goloudina, A.R., Demidov, O.N. & Garrido, C. (2012). Inhibition of HSP70: A challenging anti-cancer strategy, *Cancer Letters,* **325**(2), 117-124.

Graner, M.W. & Bigner, D.D. (2005). Chaperone proteins and brain tumors: potential targets and possible therapeutics, *Neurooncology,* **7**(3), 260-277.

Grbovic, O.M., Basso, A.D., Sawai, A.F., Ye, Q.F., Friedlander, P.F., Solit, D.F. & Rosen, N. (2006). V600E B-Raf requires the Hsp90 chaperone for stability and is degraded in response to Hsp90 inhibitors, *PNAS,* **103** (1), 57-62.

Griffiths-Jones, S., Saini, H.K., van Dongen, S. & Enright, A.J. (2008). miRBase: tools for microRNA genomics, *Nucleic Acids Research,* **36**, D154-158.

Griffiths-Jones, S. (2006). MiRBase: The MicroRNA sequence database, *Methods in Molecular Biology,* **342**, 129-138.

Guan, Y., Mizoguchi, M., Yoshimoto, K., Hata, N., Shono, T., Suzuki, S.O., Araki, Y., Kuga, D., Nakamizo, A., Amano, T., Ma, X., Hayashi, K. & Sasaki, T. (2010). MiRNA-196 is upregulated in glioblastoma but not in anaplastic astrocytoma and has prognostic significance, *Clinical Cancer Research,* **16**(16), 4289-4297.

Guo, F., Rocha, K., Bali, P., Pranpat, M., Fiskus, W., Boyapalle, S., Kumaraswamy, S., Balasis, M., Greedy, B., Armitage, E.S.M., Lawrence, N. & Bhalla, K. (2005). Abrogation of heat shock protein 70 induction as a strategy, to increase antileukemia activity of heat shock protein 90 inhibitor 17-allylamino-demethoxy geldanamycin, *Cancer Research,* **65**(22), 10536-10544.

Gutierrez-Erlandsson, S., Herrero-Vidal, P., Fernandez-Alfara, M., Hernandez-Garcia, S., Gonzalo-Flores, S., Mudarra-Rubio, A., Fresno, M. & Cubelos, B. (2013). R-RAS2 overexpression in tumours of the human central nervous system, *Molecular Cancer,* **12**(1), 127-137.

Hagen, K., Zeng, X., Lee, M., Tucker Kahn, S., Harrison Pitner, M., Zaky, S., Liu, Y., O'Regan, R., Deng, X. & Saavedra, H. (2013). Silencing CDK4 radiosensitizes breast cancer cells by promoting apoptosis, *Cell Division*, **8**(10), 1-17.

Hanahan, D. & Weinberg, R.A. (2011). Hallmarks of Cancer: The Next Generation, *Cell,* **144**(5), 646-674.

He, L., Thomson, J.M., Hemann, M.T., Hernando-Monge, E., Mu, D., Goodson, S., Powers, S., Cordon-Cardo, C., Lowe, S.W., Hannon, G.J. & Hammond, S.M. (2005). A microRNA polycistron as a potential human oncogene, *Nature,* **435**, 828-833.

Heldens, L., Dirks, R.P., Hensen, S.M., Onnekink, C., van Genesen, S.T., Rustenburg, F. & Lubsen, N.H. (2010). Co-chaperones are limiting in a depleted chaperone network, *Cellular and molecular life sciences: CMLS*, **67**(23), 4035-4048.

Hong, X., Michalski, C.W., Kong, B., Zhang, W., Raggi, M.C., Sauliunaite, D., De Oliveira, T., Friess, H. & Kleeff, J. (2010). ALCAM is associated with chemoresistance and tumor cell adhesion in pancreatic cancer, *Journal of Surgical Oncology,* **101**(7), 564-569.

Hou, J., Lin, L., Zhou, W., Wang, Z., Ding, G., Dong, Q., Qin, L., Wu, X., Zheng, Y. & Yang, Y. (2011). Identification of miRNomes in human liver and hepatocellular carcinoma reveals miR-199a/b-3p as therapeutic target for hepatocellular carcinoma, *Cancer Cell,* **19**, 232-243.

Houry, W.A. (2001). Chaperone-assisted protein folding in the cell cytoplasm, *Current Protein & Peptide Science,* **2**(3), 227-244.

Hu, J., Fang, Y., Cao, Y., Qin, R. and Chen, Q. (2014). miR-449a Regulates proliferation and chemosensitivity to cisplatin by targeting cyclin D1 and BCL2 in SGC7901 cells, *Digestive Diseases and Sciences,* **59**(2), 336-345.

Huang, V., Place, R.F., Portnoy, V., Wang, J., Qi, Z., Jia, Z., Yu, A., Shuman, M., Yu, J. & Li, L. (2011). Upregulation of Cyclin B1 by miRNA and its implications in cancer, *Nucleic Acids Res,* **40**, 1695-1707.

Huse, J.T., Brennan, C., Hambardzumyan, D., Wee, B., Pena, J., Rouhanifard, S.H., Sohn-Lee, C., le Sage, C., Agami, R., Tuschl, T. & Holland, E.C. (2009). The PTEN-regulating microRNA miR-26a is amplified in high-grade glioma and facilitates gliomagenesis in vivo, *Genes & Development,* **23**(11), 1327-1337.

Iorio, M.V., Ferracin, M., Liu, C.G., Veronese, A., Spizzo, R., Sabbioni, S., Magri, E., Pedriali, M., Fabbri, M. & Campiglio, M. (2005). MicroRNA gene expression deregulation in human breast cancer, *Cancer Res,* **65**, 7065-7070.

Iwasaki, S., Kobayashi, M., Yoda, M., Sakaguchi, Y., Katsuma, S., Suzuki, T. & Tomari, Y. (2010). Hsc70/Hsp90 Chaperone Machinery Mediates ATP-Dependent RISC Loading of Small RNA Duplexes, *Molecular Cell,* **39**(2), 292-299.

Javeri, A., Ghaffarpour, M., Taha, M.F. & Houshmand, M. (2013). Downregulation of miR-34a in breast tumors is not associated with either p53 mutations or promoter hypermethylation while it correlates with metastasis, *Medical Oncology,* **30**(1), 413.

Javid, B., MacAry, P.A. & Lehner, P.J. (2007). Structure and function: heat shock proteins and adaptive immunity, *The Journal of Immunology,* **179**(4), 2035-2040.

Jego, G., Hazoumé, A., Seigneuric, R. & Garrido, C. (2010). Targeting heat shock proteins in cancer, *Cancer Letters,* **1**(1), 1-11.

Jin, Z., Selaru, F.M., Cheng, Y., Kan, T., Agarwal, R., Mori, Y., Olaru, A.V., Yang, J., David, S., Hamilton, J.P., Abraham, J.M., Harmon, J., Duncan, M., Montgomery, E.A. and Meltzer, S.J. (2011). MicroRNA-192 and -215 are upregulated in human gastric cancer in vivo and suppress ALCAM expression in vitro, *Oncogene*, **30**(13), 1577-1585.

Jolly, C. & Morimoto, R. (2000). Role of the heat shock response and molecular chaperones in oncogenesis and cell death, *Journal of the National Cancer Institute,* **92**(19), 1564-1572.

Kahlert, C., Klupp, F., Brand, K., Lasitschka, F., Diederichs, S., Kirchberg, J., Rahbari, N., Dutta, S., Bork, U., Fritzmann, J., Reissfelder, C., Koch, M. & Weitz, J. (2011). Invasion

front-specific expression and prognostic significance of microRNA in colorectal liver metastases, *Cancer Science,* **102**(10), 1799-1807.

Kaiser, M., Kuehnl, A., Reins, J., Fischer, S., Ortiz-Tanchez, J., Schlee, C., Mochmann, L.H., Heesch, S., Benlasfer, O., Hofmann, W., Thiel, E. & Baldus, C.D. (2011). Antileukemic activity of the HSP70 inhibitor pifithrin-μ in acute leukemia, *Blood Cancer Journal,* **1**(7), e28.

Karaayvaz, M., Zhai, H. & Ju, J. (2013). miR-129 promotes apoptosis and enhances chemosensitivity to 5-fluorouracil in colorectal cancer, *Cell Death & Disease,* **4** (6), e659.

Khella, H.W.Z., Bakhet, M., Allo, G., Jewett, M.A.S., Girgis, A.H., Latif, A., Girgis, H., Von Both, I., Bjarnason, G.A. & Yousef, G.M. (2013). miR-192, miR-194 and miR-215: a convergent microRNA network suppressing tumor progression in renal cell carcinoma, *Carcinogenesis,* **34**(10), 2231-2239.

Kijima, N., Hosen, N., Kagawa, N., Hashimoto, N., Nakano, A., Fujimoto, Y., Kinoshita, M., Sugiyama, H. & Yoshimine, T. (2012). CD166/Activated leukocyte cell adhesion molecule is expressed on glioblastoma progenitor cells and involved in the regulation of tumor cell invasion, *Neurooncology,* **14**(10), 1254-1264.

Kim, H., Huang, W., Jiang, X., Pennicooke, B., Park, P.J. & Johnson, M.D. (2010). Integrative genome analysis reveals an oncomir/ oncogene cluster regulating glioblastoma survivorship, *PNAS USA,* **107**(5), 2183-2188.

Kim, Y., Nobusawa, S., Mittelbronn, M., Paulus, W., Brokinkel, B., Keyvani, K., Sure, U., Wrede, K., Nakazato, Y., Tanaka, Y., Vital, A., Mariani, L., Stawski, R., Watanabe, T., De

Girolami, U., Kleihues, P. & Ohgaki, H. (2010). Molecular Classification of Low-Grade Diffuse Gliomas, *The American Journal of Pathology,* **177**(6), 2708-2714.

Kluiver, J., Poppema, S., de Jong, D., Blokzijl, T., Harms, G., Jacobs, S., Kroesen, B.J. & van den Berg, A. (2005). BIC and miR-155 are highly expressed in hodgkin, primary mediastinal and diffuse large B cell lymphomas, *Journal of Pathology,* **207**(2), 243-249.

Koji, Y., Masahiro, M., Nobuhiro, H., Toshiyuki, A., Akira, N. & Tomio, S. (2012). Molecular biomarkers of glioblastoma: current targets and clinical implications, *Current Biomarker Findings,* **2**(0), 63-73.

Kosaka, N., Iguchi, H., Yoshioka, Y., Takeshita, F., Matsuki, Y. & Ochiya, T. (2010). Secretory mechanisms and intercellular transfer of micrornas in Living Cells, *Journal of Biological Chemistry,* **285**(23), 17442-17452.

Kota, J., Chivukula, R.R., O'Donnell, K.A., Wentzel, E.A., Montgomery, C.L., Hwang, H.W., Chang, T.C., Vivekanandan, P., Torbenson, M., Clark, K.R., Mendell, J.R. & Mendell, J.T. (2009). Therapeutic microRNA delivery suppresses tumorigenesis in a murine liver cancer model, *Cell,* **137**(6), 1005-1017.

Kozomara, A. & Griffiths-Jones, S. (2014). miRBase: annotating high confidence microRNAs using deep sequencing data, *Nucleic Acids Research,* **42**(D1), D68-D73.

Krichevsky, A.M., King, K.S., Donahue, C.P., Khrapko, K. & Kosik, K.S. (2003). A microRNA array reveals extensive regulation of microRNAs during brain development, *RNA,* **9**(10), 1274-1281.

Kristiansen, G., Pilarsky, C., Wissmann, C., Kaiser, S., Bruemmendorf, T., Roepcke, S., Dahl, E., Hinzmann, B., Specht, T., Pervan, J., Stephan, C., Loening, S., Dietel, M. & Rosenthal, A. (2005). Expression profiling of microdissected matched prostate cancer samples reveals CD166/MEMD and CD24 as new prognostic markers for patient survival, *Journal of Pathology*, **205**(3), 359-376.

Kubiczkova, L., Kryukov, F., Slaby, O., Dementyeva, E., Jarkovsky, J., Nekvindova, J., Radova, L., Greslikova, H., Kuglik, P., Vetesnikova, E., Pour, L., Adam, Z., Sevcikova, S. & Hajek, R. (2014). Circulating serum microRNAs as novel diagnostic and prognostic biomarkers for multiple myeloma and monoclonal gammopathy of undetermined significance, *Haematologica,* **99**(3), 511-518.

Lagos-Quintana, M., Rauhut, R., Yalcin, A., Meyer, J., Lendeckel, W. & Tuschl, T. (2002). Identification of tissue-specific microRNAs from mouse, *Current Biology,* **12**(9), 735-739.

Lam, P.Y., Di Tomaso, E., Ng, H.K., Pang, J.C., Roussel, M.F. & Hjelm, N.M., 2000. Expression of p19INK4d, CDK4, CDK6 in glioblastoma multiforme, *British Journal of Neurosurgery,* **14**(1), 28-32.

Lee, C.H., Kuo, W.H., Lin, C.C., Oyang, Y.J., Huang, H.C. & Juan, H.F., 2013. MicroRNA-regulated protein-protein interaction networks and their functions in breast cancer, *International Journal of Molecular Sciences,* **14**(6), 11560-11606.

Li, C., Lee, J., Ko, Y., Kim, J. & Seo, J. (2000). Heat shock protein 70 inhibits apoptosis downstream of cytochrome c release and upstream of caspase-3 activation, *Journal of Biological Chemistry,* **275**(33), 25665-25671.

Li, P., Grgurevic, S., Liu, Z., Harris, D., Rozovski, U., Calin, G.A., Keating, M.J. & Estrov, Z. (2013). Signal Transducer and Activator of Transcription-3 Induces microrna-155 Expression in Chronic Lymphocytic Leukemia, *Plos One,* **8**(6), e64678.

Lim, L.P., Lau, N.C., Garrett-Engele, P., Grimson, A., Schelter, J.M., Castle, J., Bartel, D.P., Linsley, P.S. & Johnson, J.M. (2005). Microarray analysis shows that some microRNAs downregulate large numbers of target mRNAs, *Nature,* **433**(7027), 769-773.

Lim, S.O., Park, S.G., Yoo, J., Park, Y.M., Kim, H., Jang, K., Cho, J.W., Yoo, B.C., Jung, G. & Park, C.K. (2005). Expression of heat shock proteins (HSP27, HSP60, HSP70, HSP90, GRP78, GRP94) in hepatitis B virus-related hepatocellular carcinomas and dysplastic nodules, *World Journal of Gastroenterology,* **11**(14), 2072-2079.

Lin, F., Ding, R., Zheng, S., Xing, D., Hong, W., Zhou, Z. & Shen, J. (2014). Decrease expression of microRNA-744 promotes cell proliferation by targeting c-Myc in human hepatocellular carcinoma, *Cancer Cell International,* **14**(1), 58-62.

Liu, B., Qu, L. & Tao, H. (2009). Cyclo-oxygenase 2 up-regulates the effect of multidrug resistance, *Cell Biology International,* **34**(1), 21-25.

Lizé, M., Klimke, A. & Dobbelstein, M. (2011). MicroRNA-449 in cell fate determination, *Cell Cycle,* **10**(17), 2874-2882.

Lopez-Chavez, A., Carter, C.A. & Giaccone, G. (2009). The role of KRAS mutations in resistance to EGFR inhibition in the treatment of cancer, *Current Opinion in Investigational Drugs,* **10**(12), 1305-1314.

Louis, D. N., Ohgaki, H., Wiestler, O.D. & Cavanee, W. K. (2007). WHO classification of tumours of the central nervous system, Acta Neuropathology, **114**(2), 97–109.

Lu, J., Getz, G., Miska, E.A., Alvarez-Saavedra, E., Lamb, J., Peck, D., Sweet-Cordero, A., Ebert, B.L., Mak, R.H., Ferrando, A.A., Downing, J.R., Jacks, T., Horvitz, H.R. & Golub, T.R. (2005). MicroRNA expression profiles classify human cancers, *Nature,* **435**, 834-838.

Ma, L., Sato, F., Sato, R., Matsubara, T., Hirai, K., Yamasaki, M., Shin, T., Shimada, T., Nomura, T., Mori, K., Sumino, Y. & Mimata, H. (2014). Dual targeting of heat shock proteins 90 and 70 promotes cell death and enhances the anticancer effect of chemotherapeutic agents in bladder cancer, *Oncology Reports,* **31**(6), 2482-2492.

Macias, A.T., Williamson, D.S., Allen, N., Borgognoni, J., Clay, A., Daniels, Z., Dokurno, P., Drysdale, M.J., Francis, G.L., Graham, C.J., Howes, R., Matassova, N., Murray, J.B., Parsons, R., Shaw, T., Surgenor, A.E., Terry, L., Wang, Y., Wood, M. & Massey, A.J. (2011). Adenosine-derived inhibitors of 78 kDa glucose regulated protein (grp78) ATPase: insights into isoform selectivity, *Journal of Medicinal Chemistry,* **54**(12), 4034-4041.

Mahalingam, D., Swords, R., Carew, J.S., Nawrocki, S.T., Bhalla, K. & Giles, F.J. (2009). Targeting HSP90 for cancer therapy, *British Journal of Cancer,* **100**(10), 1523-1529.

Malzkorn, B., Wolter, M., Liesenberg, F., Grzendowski, M., Stühler, K., Meyer, H.E. & Reifenberger, G. (2010). Identification and functional characterization of microRNAs involved in the malignant progression of gliomas, *Brain Pathology,* **20**(3), 539-550.

Marchesi, F., Turriziani, M., Tortorelli, G., Avvisati, G., Torino, F. & De Vecchis, L. (2007). Triazene compounds: mechanism of action and related DNA repair systems, *Pharmacological Research,* **56**(4), 275-287.

Marcet, B., Chevalier, B., Luxardi, G., Coraux, C., Zaragosi, L., Cibois, M., Robbe-Sermesant, K., Jolly, T., Cardinaud, B., Moreilhon, C., Giovannini-Chami, L., Nawrocki-

Raby, B., Birembaut, P., Waldmann, R., Kodjabachian, L. & Barbry, P. (2011). Control of vertebrate multiciliogenesis by miR-449 through direct repression of the Delta/Notch pathway, *Nature Cell Biology*, **13**(6), 693-699.

Martin, J., Jenkins, R.H., Bennagi, R., Krupa, A., Phillips, A.O., Bowen, T. & Fraser, D.J. (2011). Post-Transcriptional regulation of transforming growth factor beta-1 by MicroRNA-744, *PLoS ONE*, **6**(10), e25044.

Martinez, N.J. & Gregory, R.I. (2013). Argonaute2 expression is post-transcriptionally coupled to microRNA abundance, *RNA*, **19**(5), 605-612.

Masciullo, V., Scambia, G., Marone, M., Giannitelli, C., Ferrandina, G., Bellacosa, A., Benedetti Panici, P. & Mancuso, S. (1997). Altered expression of cyclin D1 and CDK4 genes in ovarian carcinomas, *International Journal of Cancer*, **74**(4), 390-395.

Massey, A.J., Williamson, D.S., Browne, H., Murray, J.B., Dokurno, P., Shaw, T., Macias, A.T., Daniels, Z., Geoffroy, S., Dopson, M., Lavan, P., Matassova, N., Francis, G.L., Graham, C.J., Parsons, R., Wang, Y., Padfield, A., Comer, M., Drysdale, M.J. & Wood, M. (2010). A novel, small molecule inhibitor of Hsc70/Hsp70 potentiates Hsp90 inhibitor induced apoptosis in HCT116 colon carcinoma cells, *Cancer Chemotherapy and Pharmacology,* **66**(3), 535-545.

McConnell, J.R. & McAlpine, S.R. (2013). Heat shock proteins 27, 40, and 70 as combinational and dual therapeutic cancer targets, *Bioorganic & Medicinal Chemistry Letters,* **23**(7), 1923-1928.

Mehta, A., Shervington, A., Howl, J., Jones, S. & Shervington, L. (2013). Can RNAi-mediated hsp90alpha knockdown in combination with 17-AAG be a therapy for glioma?, *FEBS Open Bio,* **3**, 271-278.

Mehta, A., Shervington, L., Munje, C. & Shervington, A. (2011). A novel therapeutic strategy for the treatment of glioma,combining chemical and molecular targeting of Hsp90, *Cancers,* **3**, 4228-4244.

Meng, Z., Fu, X., Chen, X., Zeng, S., Tian, Y., Jove, R., Xu, R. & Huang, W. (2010). miR-194 is a marker of hepatic epithelial cells and suppresses metastasis of liver cancer cells in mice, *Hepatology,* **52**(6), 2148-2157.

Michael, M.Z., O'Connor, S.M., Pellekaan, N.G.V., Young, G.P. & James, R.J. (2003). Reduced accumulation of specific microRNAs in colorectal neoplasia, *Molecular Cancer Research,* **1**(12), 882-891.

Miska, E.A., Alvarez-Saavedra, E., Townsend, M., Yoshii, A., Sestan, N., Rakic, P., Constantine-Paton, M. & Horvitz, H.R. (2004). Microarray analysis of microRNA expression in the developing mammalian brain, *Genome Biology,* **5**(9), R68.

Mohammed, K. & Shervington, A. (2008). Can CYP1A1 siRNA be an effective treatment for lung cancer?, *Cellular & Molecular Biology Letters,* **13**(2), 240-249.

Munje, C., Shervington, L., Mehta, A., Khan, Z. & Shervington, A. (2011). Validating the efficacy of shrna vs. sirna in silencing hsp90α in gliomas, *Bioanalysis and Biomedicine,* **1**(1), 1-5.

Nakada, M., Niska, J.A., Tran, N.L., McDonough, W.S. & Berens, M.E. (2005). EphB2/R-Ras signaling regulates glioma cell adhesion, growth, and invasion, *The American Journal of Pathology,* **167**(2), 565-576.

Natsume, A., Kondo, Y., Ito, M., Motomura, K., Wakabayashi, T. & Yoshida, J. (2010). Epigenetic aberrations and therapeutic implications in gliomas, *Cancer Science,* **101**(6), 1331-1336.

Negrini, M. & Calin, G.A. (2008). Breast cancer metastasis: a microRNA story. *Breast Cancer Research: BCR,* **10**(2), 203-203.

Nicolaı, A., Senet, P., Delarue, P. & Ripoll, D.R. (2010). Human Inducible Hsp70: structures, dynamics, and interdomain communication from all-atom molecular dynamics simulations, *Journal of Chemical Theory and Computation,* **6**(8), 2501-2519.

Noonan, E.J., Place, R.F., Pookot, D., Basak, S., Whitson, J.M., Hirata, H., Giardina, C. & Dahiya, R. (2009). miR-449a targets HDAC-1 and induces growth arrest in prostate cancer, *Oncogene,* **28**, 1714-1724.

Nylandsted, J., Rohde, M., Brand, K., Bastholm, L., Elling, F. & Jaattela, M. (2000). Selective depletion of heat shock protein 70 (Hsp70) activates a tumor-specific death program that is independent of caspases and bypasses Bcl-2, *PNAS USA,* **97**(14), 7871-7876.

Nunez, Y., Truitt, J., Gorini, G., Ponomareva, O., Blednov, Y., Harris, R. & Mayfield, R. (2013). Positively correlated miRNA-mRNA regulatory networks in mouse frontal cortex during early stages of alcohol dependence, *BMC Genomics,* **14**(1), 725-750.

Nupur, S. & Alok, M. (2012). In silico mining identifies tumor suppressor gene's expression regulating DNA methyl transferases (DNMT) as miRNA targets in cancer, *International Journal of Advanced Life Sciences (IJALS),* **5**(2277), 758X.

Nylandsted, J., Gyrd-Hansen, M., Danielewicz, A., Fehrenbacher, N., Lademann, U., Høyer-Hansen, M., Weber, E., Multhoff, G., Rohde, M. & Jäättelä, M. (2004). Heat Shock Protein 70 promotes cell survival by inhibiting lysosomal membrane permeabilization, *The Journal of experimental medicine,* **200**(4), 425-435.

O'Carroll, D. & Schaefer, A. (2013). General principals of miRNA biogenesis and regulation in the brain, *Neuropsychopharmacology,* **38**(1), 39-54.

Ohba, S.F.,Hirose, Y.F.,Yoshida, K.F.,Yazaki, T.F.&Kawase, T. (2010). Inhibition of 90-kD heat shock protein potentiates the cytotoxicity of chemotherapeutic agents in human glioma cells, *Journal Nerosurg,* **112**(1), 33-42.

Ohgaki, H., Dessen, P., Jourde, B. (2004). Genetic pathways to glioblastoma: a population-based study, *Cancer Research*, **64,** 6892–6899.

Ohgaki, H., Kleihues, P. (2005) Population-based studies on incidence, survival rates, and genetic alterations in astrocytic and oligodendroglial gliomas, Journal Neuropathology Experiment Neurology, **64**, 479–489.

Pan, Q., Yang, X.J., Wang, H.M., Dong, X.T., Wang, W., Li, Y. & Li, J.M. (2012a). Chemoresistance to temozolomide in human glioma cell line U251 is associated with increased activity of O6-methylguanine-DNA methyltransferase and can be overcome by metronomic temozolomide regimen, *Cell Biochemistry and Biophysics,* **62**(1), 185-191.

Papagiannakopoulos, T., Shapiro, A. & Kosik, K.S. (2008). MicroRNA-21 targets a network of key tumor-suppressive pathways in glioblastoma cells, *Cancer Research,* **68**(19), 8164-8172.

Pare, J.M., Tahbaz, N., Lopez-Orozco, J., LaPointe, P., Lasko, P. & Hobman, T.C. (2009). Hsp90 regulates the function of argonaute 2 and its recruitment to stress granules and P-bodies, *Molecular Biology of the Cell,* **20**(14), 3273-3284.

Parsons, D.W., Jones, S., Zhang, X. (2008). An integrated genomic analysis of human glioblastoma multiforme, *Science,* **321,** 1807–1812.

Patel, R., Shervington, L., Lea, R. & Shervington, A. (2008). Epigenetic silencing of telomerase and a non-alkylating agent as a novel therapeutic approach for glioma, *Brain Research,* **1188**(0), 173-181.

Pearl, L.H. & Prodromou, C. (2006). Structure and mechanism of the Hsp90 molecular chaperone machinery, *Annual Review of Biochemistry,* **75**, 271-294.

Pellegrino, L., Stebbing, J., Braga, V.M., Frampton, A.E., Jacob, J., Buluwela, L., Jiao, L.R., Periyasamy, M., Madsen, C.D., Caley, M.P., Ottaviani, S., Roca-Alonso, L., El-Bahrawy, M., Coombes, R.C., Krell, J. & Castellano, L. (2013). miR-23b regulates cytoskeletal remodeling, motility and metastasis by directly targeting multiple transcripts, *Nucleic Acids Research,* **41**(10), 5400-5412.

Picard, D. (2002). Heat-shock protein 90, a chaperone for folding and regulation, *Cellular and Molecular Life Sciences,* **59**(10), 1640-1648.

Powers, M.V., Jones, K., Barillari, C., Westwood, I., Montfort, R.L.M. & Workman, P. (2010). Targeting HSP70: The second potentially druggable heat shock protein and molecular chaperone?, *Cell Cycle,* **9**(8), 1542-1550.

Qiu, X., Shao, Y., Miao, S. & Wang, L., 2006. The diversity of the DnaJ/Hsp40 family, the crucial partners for Hsp70 chaperones, *Cellular and Molecular Life Sciences: CMLS,* **63**(22), 2560-2570.

Rao, S.A.M., Santosh, V. & Somasundaram, K. (2010). Genome-wide expression profiling identifies deregulated miRNAs in malignant astrocytoma, *Modern Pathology,* **23**(10), 1404-1417.

Rerole, A., Gobbo, J., De Thonel, A., Schmitt, E., de Barros, J.P.P., Hammann, A., Lanneau, D., Fourmaux, E., Deminov, O., Micheau, O., Lagrost, L., Colas, P., Kroemer, G. & Garrido, C. (2011). Peptides and aptamers targeting HSP70: a novel approach for anticancer chemotherapy, *Cancer Research,* **71**(2), 484-495.

Ritossa, F. (1962). A new puffing pattern induced by temperature shock and DNP in drosophila, *Experientia*, **18**(12), 571-573.

Roth, P., Wischhusen, J., Happold, C., Chandran, P.A., Hofer, S., Eisele, G., Weller, M. & Keller, A. (2011). A specific miRNA signature in the peripheral blood of glioblastoma patients, *J Neurochemistry,* **118**(3), 449-457.

Rozovski, U., Calin, G.A., Setoyama, T., D'Abundo, L., Harris, D.M., Li, P., Liu, Z., Grgurevic, S., Ferrajoli, A., Faderl, S., Burger, J.A., O'Brien, S., Wierda, W.G., Keating, M.J. & Estrov, Z. (2013). Signal transducer and activator of transcription (STAT)-3 regulates microRNA gene expression in chronic lymphocytic leukemia cells, *Molecular Cancer,* **12**(50), 1-2.

Samantarrai, D., Dash, S., Chhetri, B. & Mallick, B. (2013). Genomic and epigenomic cross-talks in the regulatory landscape of mirnas in breast cancer, *Molecular Cancer Research,* **11**(4), 315-328.

Sato, S., Fujita, N. & Tsuruo, T. (2000). Modulation of Akt kinase activity by binding to Hsp90, *PNAS,* **97**(20), 10832-10837.

Schmidt, B.A., Rose, A., Steinhoff, C., Strohmeyer, T., Hartmann, M. & Ackermann, R. (2001). Up-regulation of cyclin-dependent kinase 4/cyclin d2 expression but down-regulation of cyclin-dependent kinase 2/cyclin e in testicular germ cell tumors, *Cancer Research,* **61**(10), 4214-4221.

Schramedei, K., Morbt, N., Pfeifer, G., Lauter, J., Rosolowski, M., Tomm, J.M., von Bergen, M., Horn, F. & Brocke-Heidrich, K. (2011). MicroRNA-21 targets tumor suppressor genes ANP32A and SMARCA4, *Oncogene,* **30**(26), 2975-2985.

Schroeder, A., Mueller, O., Stocker, S., Salowsky, R., Leiber, M., Gassmann, M., Lightfoot, S., Menzel, W., Granzow, M. & Ragg, T. (2006). The RIN: an RNA integrity number for assigning integrity values to RNA measurements, *BMC Molecular Biology*, **7**(1), 3.

Shervington, A., Cruickshanks, N., Lea, R., Roberts, G., Dawson, T. & Shervington, L. (2008). Can the lack of HSP90alpha protein in brain normal tissue and cell lines, rationalise it as a possible therapeutic target for gliomas?, *Cancer Investigation,* **26**(9), 900-904.

Shiiba, M., Shinozuka, K., Saito, K., Fushimi, K., Kasamatsu, A., Ogawara, K., Uzawa, K., Ito, H., Takiguchi, Y. & Tanzawa, H. (2013). MicroRNA-125b regulates proliferation and

radioresistance of oral squamous cell carcinoma, *British Journal of Cancer,* **108**(9), 1817-1821.

Silber, J., Lim, D., Petritsch, C., Persson, A., Maunakea, A., Yu, M., Vandenberg, S., Ginzinger, D., James, C.D., Costello, J., Bergers, G., Weiss, W., Alvarez-Buylla, A. & Hodgson, J.G. (2008). miR-124 and miR-137 inhibit proliferation of glioblastoma multiforme cells and induce differentiation of brain tumor stem cells, *BMC Medicine,* **6**(1), 14-24.

Skalsky, R.L. & Cullen, B.R. (2011). Reduced expression of brain-enriched microrna s in glioblastomas permits targeted regulation of a cell death gene, *PLoS ONE,* **6**(9), e24248.

Smoll, N.R., Gautschi, O.P., Schatlo, B., Schaller, K. & Weber, D.C. (2012). Relative survival of patients with supratentorial low-grade gliomas, Neuro-oncology, 14(8), 1062-1069.

Solit, D.B., Zheng, F.F., Drobnjak, M., Münster, P.N., Higgins, B., Verbel, D., Heller, G., Tong, W., Cordon-Cardo, C., Agus, D.B., Scher, H.I. & Rosen, N. (2002). 17-Allylamino-17-demethoxygeldanamycin induces the degradation of androgen receptor and her-2/neu and inhibits the growth of prostate cancer xenografts, *Clinical Cancer Research,* **8**(5), 986-993.

Song, B., Wang, Y., Titmus, M.A., Botchkina, G., Formentini, A., Kornmann, M. & Ju, J. (2010). Molecular mechanism of chemoresistance by miR-215 in osteosarcoma and colon cancer cells, *Molecular Cancer*, **9**(96), 1-10.

Song, M., Pan, K., Su, H., Zhang, L., Ma, J., Li, J., Yuasa, Y., Kang, D., Kim, Y.S. & You, W. (2012). Identification of serum microRNAs as novel non-invasive biomarkers for early detection of gastric cancer, *PLoS One*, **7**, e33608.

Soo, E.T., Yip, G.W., Lwin, Z.M., Kumar, S.D. & Bay, B.H. (2008). Heat shock proteins as novel therapeutic targets in cancer, *In vivo,* **22**(3), 311-315.

Sreedhar, A.S. & Csermely, P. (2004). Heat shock proteins in the regulation of apoptosis: new strategies in tumor therapy - A comprehensive review, *Pharmacology & Therapeutics,* **101**(3), 227-257.

Srinivasan, S., Patric, I.R.P. & Somasundaram, K. (2011). A ten-microrna expression signature predicts survival in glioblastoma, *PLoS ONE,* **6**(3).

Stephanou, S. & Latchman, D.S. (2011). Transcriptional modulation of heat-shock protein gene expression, *Biochemistry Research International,* **1**(1), 1-8.

Stupp, R., Mason, W.P., van den, B. (2005). Radiotherapy plus concomitant and adjuvant temozolomide for glioblastoma, *New England Journal of Medicine,* **352**(10), 987-996.

Su, Y., Li, X., Ji, W., Sun, B., Xu, C., Li, Z., Qian, G. & Su, C. (2014). Small molecule with big role: microrna s in cancer metastatic microenvironments, *Cancer Letters,* **344**(2), 147-156.

Takamizawa, J., Konishi, H., Yanagisawa, K., Tomida, S., Osada, H., Endoh, H., Harano, T., Yatabe, Y., Nagino, M. & Nimura, Y. (2004). Reduced expression of the let-7 microRNAs in human lung cancers in association with shortened postoperative survival, *Cancer Res,* **64**, 3753-3756.

Thakkar, D., Shervington, L. & Shervington, A. (2011). Proteomic studies coupled with RNAi methodologies can shed further light on the downstream effects of telomerase in glioma, *Cancer Investigation,* **29**(2), 113-122.

Townsend, P.A., Stephanou, A., Packham, G. & Latchman, D.S. (2005). BAG-1: a multi-functional pro-survival molecule, *International Journal of Biochemistry & Cell Biology,* **37**(2), 251-259.

Van Schooneveld, E., Wouters, M.C., Van der Auwera, I., Peeters, D.J., Wildiers, H., Van Dam, P.A., Vergote, I., Vermeulen, P.B., Dirix, L.Y. & Van Laere, S.J. (2012). Expression profiling of cancerous and normal breast tissues identifies microRNAs that are differentially expressed in serum from patients with (metastatic) breast cancer and healthy volunteers, *Breast Cancer Research: BCR,* **14**(1), R34.

Vislovukh, A., Kratassiouk, G., Porto, E., Gralievska, N., Beldiman, C., Pinna, G., El'skaya, A., Harel-Bellan, A., Negrutskii, B. & Groisman, I. (2013). Proto-oncogenic isoform A2 of eukaryotic translation elongation factor eEF1 is a target of miR-663 and miR-744, *British Journal of Cancer,* **108**(11), 2304-2311.

Volinia, S., Calin, G.A., Liu, C.G., Ambs, S., Cimmino, A., Petrocca, F., Visone, R., Iorio, M., Roldo, C. & Ferracin, M. (2006). A microRNA expression signature of human solid tumors defines cancer gene targets, *PNAS,* **103**, 2257-2261.

Wang, B. and Xi, Y. (2013). Challenges for MicroRNA Microarray Data Analysis, *Microarrays,* **2**(2), 1- 10.

Wei, B., Song, Y., Zhang, Y. & Hu, M. (2013). microRNA-449a functions as a tumor-suppressor in gastric adenocarcinoma by targeting Bcl-2, *Oncology Lletters,* **6**(6), 1713-1718.

Wen, W., Liu, W., Shao, Y. & Chen, L. (2014). VER-155008, a small molecule inhibitor of HSP70 with potent anti-cancer activity on lung cancer cell lines, *Experimental Biology and Medicine,* **239**(5), 638-645.

Wesseling, P., van, d.B. & Perry, A. (2015). Oligodendroglioma: pathology, molecular mechanisms and markers, *Acta Neuropathologica,* **129**(6), 809-827.

White, N.M.A., Khella, H.W.Z., Grigull, J., Adzovic, S., Youssef, Y.M., Honey, R.J., Stewart, R., Pace, K.T., Bjarnason, G.A., Jewett, M.A.S., Evans, A.J., Gabril, M. & Yousef, G.M. (2011). miRNA profiling in metastatic renal cell carcinoma reveals a tumour-suppressor effect for miR-215, *British Journal of Cancer,* **105**(11), 1741-1749.

Whitesell, L. & Lindquist, S.L. (2005). HSP90 and the chaperoning of cancer, *Nature reviews, Cancer,* **5**(10), 761-772.

Workman, P. (2004). Altered states: selectively drugging the Hsp90 cancer chaperone, *Trends in Molecular Medicine,* **10**(2), 47-51.

Wu, X., Liu, T., Fang, O., Leach, L.J., Hu, X. & Luo, Z. (2014). miR-194 suppresses metastasis of non-small cell lung cancer through regulating expression of BMP1 and p27kip1, *Oncogene,* **33**(12), 1506-1514.

Xia, Y., Rocchi, P., Iovanna, J.L. & Peng, L. (2012). Targeting heat shock response pathways to treat pancreatic cancer, *Drug Discovery Today,* **17**(1), 35-43.

Xiao, L., Lu, X. & Ruden, D.M. (2006). Effectiveness of hsp90 inhibitors as anti-cancer drugs, *Mini Reviews In Medicinal Chemistry,* **6**(10), 1137-1143.

Xu, C.Z., Xie, J., Jin, B., Chen, X.W., Sun, Z.F., Wang, B.X. & Dong, P. (2013). Gene and microRNA expression reveals sensitivity to paclitaxel in laryngeal cancer cell line, *International Journal of Clinical and Experimental Pathology,* **6**(7), 1351-1361.

Xu, J., Liao, X. & Wong, C. (2010). Downregulations of B-cell lymphoma 2 and myeloid cell leukemia sequence 1 by microRNA-153 induce apoptosis in a glioblastoma cell line DBTRG-05MG, *International Journal of Cancer,* **126**(4), 1029-1035.

Yang, X., Feng, M., Jiang, X., Wu, Z., Li, Z., Aau, M. & Yu, Q. (2009). miR-449a and miR-449b are direct transcriptional targets of E2F1 and negatively regulate pRb-E2F1 activity through a feedback loop by targeting CDK6 and CDC25A, *Genes Dev,* **23**, 2388-2393.

Yao, Y., Ma, J., Xue, Y., Wang, P., Li, Z., Li, Z., Hu, Y., Shang, X. & Liu, Y. (2014). MiR-449a exerts tumor-suppressive functions in human glioblastoma by targeting Myc-associated zinc-finger protein, *Molecular Oncology,* **1**(0), 1-17.

Yamazaki, H., Chijiwa, T., Inoue, Y., Abe, Y., Suemizu, H., Kawai, K., Wakui, M., Furukawa, D., Mukai, M., Kuwao, S., Saegusa, M. & Nakamura, M. (2012). Overexpression of the miR-34 family suppresses invasive growth of malignant melanoma with the wild-type p53 gene, *Experimental and Therapeutic Medicine,* **3**(5), 793-796.

Yoshino, A., Ogino, A., Yachi, K., Ohta, T., Fukushima, T., Watanabe, T., Katayama, Y., Okamoto, Y., Naruse, N., Sano, E. & Tsumoto, K. (2010). Gene expression profiling predicts response to temozolomide in malignant gliomas, *International Journal of Oncology,* **36**(6), 1367-1377.

Zajac, M., Gomez, G., Benitez, J. & Martinez-Delgado, B., 2010. Molecular signature of response and potential pathways related to resistance to the HSP90 inhibitor, 17AAG, in breast cancer, *BMC Medical Genomics,* **3**(1), 44.

Zhang, L., Hou, D., Chen, X., Li, D., Zhu, L., Zhang, Y., Li, J., Bian, Z., Liang, X., Cai, X., Yin, Y., Wang, C., Zhang, T., Zhu, D., Zhang, D., Xu, J., Chen, Q., Ba, Y., Liu, J., Wang, Q., Chen, J., Wang, J., Wang, M., Zhang, Q., Zhang, J., Zen, K. & Zhang, C. (2012). Exogenous plant MIR168a specifically targets mammalian LDLRAP1: evidence of cross-kingdom regulation by microRNA, *Cell Research,* **22**(1), 107-126.

Zhang, S., Sun, Y., Yuan, Z., Li, Y., Li, X., Gong, Z. & Peng, Y. (2012b). Heat shock protein 90β inhibits apoptosis of intestinal epithelial cells induced by hypoxia through stabilizing phosphorylated Akt, *BMB Reports,* **46**(1), 47-52.

Zhang, Y., Yan, L.X., Wu, Q.N., Du, Z.M., Chen, J., Liao, D.Z., Huang, M.Y., Hou, J.H., Wu, Q.L., Zeng, M.S., Huang, W.L., Zeng, Y.X. & Shao, J.Y. (2011). miR-125b is methylated and functions as a tumor suppressor by regulating the ETS1 proto-oncogene in human invasive breast cancer, *Cancer Research,* **71**(10), 3552-3562.

Zhang, Y., Liu, D., Chen, X., Li, J., Li, L., Bian, Z., Sun, F., Lu, J., Yin, Y., Cai, X., Sun, Q., Wang, K., Ba, Y., Wang, Q., Wang, D., Yang, J., Liu, P., Xu, T., Yan, Q., Zhang, J., Zen, K. & Zhang, C. (2010). Secreted monocytic mir-150 enhances targeted endothelial cell migration, *Molecular Cell,* **39**(1), 133-144.

Zhao, H., Ren, L., Wang, Z., Sun, T., Yu, Y., Wang, Y., Yan, T., Zou, W., He, J., Zhang, Y., Hong, J. & Fang, J. (2014). MiR-194 Deregulation contributes to colorectal carcinogenesis via targeting AKT2 pathway, *Theranostics,* **4**(12), 1193-1208.

Zhu, H. & Fan, G.C., (2011). Extracellular/circulating microRNAs and their potential role in cardiovascular disease, *American Journal of Cardiovascular Disease,* **1**(2), 138-14.

Zylicz, M., King, F.W. & Wawrzynow, A. (2001). Hsp70 interactions with the p53 tumour suppressor protein, *The EMBO Journal,* **20**(17), 4634-4638.

https://www.phe-culturecollections.org.uk/technical/ccp/cellcounting.aspx

http://lifescience.roche.com/shop/products/mrna-isolation-kit

CHAPTER 7

APPENDIX

7.1 Gene expression in glioma cell lines

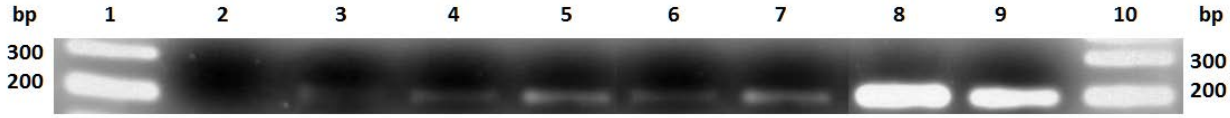

Figure 7.1: Transcriptional activity of *Hsp70* and *Hsp90α* glioma cell lines. Lane 1 and 10 represents molecular marker, lane 2 and 3 represents *Hsp70* and *Hsp90* expression in NHA respectively, Lane 4 and 5 represents *Hsp70* and *Hsp90*expression in 1321N1 respectively, Lane 6 and 7 represents *Hsp70* and *Hsp90*expression in U87-MG respectively, Lane 8 and 9 represents *Hsp70* and *Hsp90* expression in GOS-3 respectively.

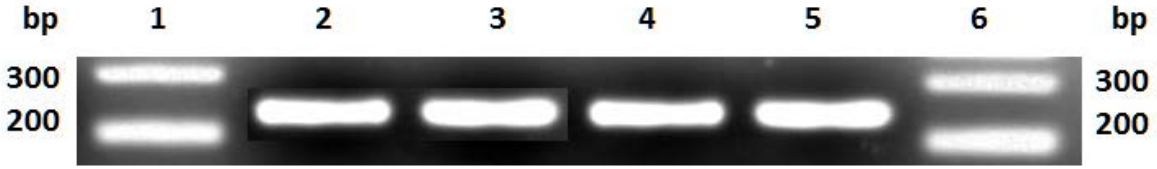

Figure 7.2: Transcriptional activity of *GAPDH*. Lane 1 and 6 represents molecular marker, lane 2-5 represents *GAPDH* expression in NHA, 1321N1, GOS-3 and U87-MG.

7.2 miRNA microarray raw data

Table 7.1: miRNAs up/down-regulated in treatment group TMZ Vs Control.

Systematic name	FC	Regulation	p (Corr)	p	mirbase accession No	Chr	Strand	Start	Stop	Active sequence
hsa-miR-215	165	up	0.06	0.000	MIMAT0000272	chr1	+	220291241	220291222	GTCTGTCAATTCATAGGTCAT
hsa-miR-194-5p	139	up	0.08	0.001	MIMAT0000460	chr1	+	220291534	220291519	TCCACATGGAGTTGCT
hsa-miR-550a-3p	65	up	0.33	0.003	MIMAT0003257	chr7	-	30295999	30296016	ATGTGCCTGAGGGAGTAA
hsa-miR-769-5p	64	up	0.06	0.000	MIMAT0003886	chr19	-	46522223	46522240	AGCTCAGAACCCAGAGGTC
hsa-miR-744-5p	63	up	0.08	0.001	MIMAT0004945	chr17	-	11985234	11985247	TGCTGTTAGCCCTA
hsa-miR-449a	62	up	0.38	0.005	MIMAT0001541	chr5	+	54502153	54502134	ACCAGCTAACAATACACTGC
hsa-miR-101-3p	49	up	0.61	0.021	MIMAT0000099	chr1	+	65524183	65524164	TTCAGTTATCACAGTACTGT
hsa-miR-200c-3p	33	up	0.13	0.001	MIMAT0000617	chr12	-	7072913	7072927	TCCATCATTACCCGG
hsa-miR-652-3p	29	up	0.17	0.002	MIMAT0003322	chrX	-	109298623	109298637	CACAACCCTAGTGGC
hsa-miR-7-1-3p	23	up	0.61	0.032	MIMAT0004553	chr9	+	86584749	86584731	TATGGCAGACTGTGATTTG
hsa-miR-4521	23	up	0.61	0.050	MIMAT0019058	chr17	-	8090273	8090287	CTGAGCACAGGACTTC
hsa-miR-500a-3p	19	up	0.06	0.000	MIMAT0002871	chrX	-	49659834	49659851	CAGAATCCTTGCCCAGGT
hsa-miR-4758-3p	19	up	0.53	0.008	MIMAT0019904	chr20	+	60907610	60907598	GAGGGTGGTCAGCA
hsa-miR-557	18	up	0.06	0.000	MIMAT0003221	chr1	-	168344830	168344844	AGACAAGGCCCACCCG

hsa-miR-382-5p	16	up	0.61	0.037	MIMAT0000737	chr14	-	101520659	101520674	CGAATCCACCACGAAC
hsa-miR-192-5p	5	up	0.61	0.028	MIMAT0000222	chr11	+	64658652	64658634	GGCTGTCAATTCATAGGTC
hsa-miR-324-5p	2	up	0.61	0.037	MIMAT0000761	chr17	+	7126653	7126638	ACACCAATGCCCTAGGG
hsa-miR-331-3p	2	up	0.54	0.010	MIMAT0000760	chr12	-	94226389	94226407	TTCTAGGATAGGCCCAGGG
hsa-miR-148b-3p	2	up	0.61	0.040	MIMAT0000759	chr12	-	54731065	54731083	ACAAAGTTCTGTGATGCAC
hsa-miR-3654	-73	down	0.13	0.001	MIMAT0018074	chr7	+	132719675	132719661	TTCCTCAGCTTGTCCA
hsa-miR-335-3p	-70	down	0.52	0.008	MIMAT0004703	chr7	-	130136003	130136024	GGTCAGGAGCAATAATGAAAAA
hsa-miR-3620-5p	-50	down	0.61	0.032	MIMAT0022967	chr1	-	228284997	228285007	GGCCCAGCCCAG
hsa-miR-431-3p	-42	down	0.61	0.018	MIMAT0004757	chr14	-	101347411	101347427	AGAAGCCCTGCAAGACG
hsa-miR-4636	-32	down	0.61	0.018	MIMAT0019693	chr5	+	9053958	9053942	CTAAAGGCTTTGAACACG
hsa-miR-193a-5p	-2	down	0.38	0.005	MIMAT0004614	chr17	-	29887045	29887056	TCATCTCGCCCGC
hsa-miR-4697-5p	-2	down	0.38	0.004	MIMAT0019791	chr11	+	133768429	133768416	CACGTCAGTGACTGC

Table 7.2: miRNAs up/down-regulated in treatment group 17-AAG Vs Control.

Systematic name	FC	Regulation	p (Corr)	p	mirbase accession No	Chr	Strand	Start	Stop	Active sequence
hsa-miR-3161	29	up	0.67	0.007	MIMAT0015035	chr11	-	48118351	48118365	ATCTGGGCCTCTGTTC
hsa-miR-557	19	up	0.09	0.000	MIMAT0003221	chr1	-	1.68E+08	1.68E+08	AGACAAGGCCCACCCG
hsa-miR-3692-5p	18	up	0.67	0.009	MIMAT0018121	chr6	-	1.58E+08	1.58E+08	CAGTATCCACTCCTGAC
hsa-miR-664b-5p	17	up	0.17	0.001	MIMAT0022271	chrX	-	1.54E+08	1.54E+08	TACCCAATCATCTCCCT
hsa-miR-345-5p	-2	down	0.67	0.033	MIMAT0000772	chr14	-	1.01E+08	1.01E+08	GAGCCCTGGACTAG

Table 7.3: miRNAs upregulated in treatment group VER Vs Control.

Systematic name	FC	Regulation	p (Corr)	p	mirbase accession No	Chr	Strand	Start	Stop	Active sequence
hsa-let-7e-5p	2	up	0.21	0.012	MIMAT0000066	chr19	-	52196049	52196067	AACTATACAACCTCCTACC
hsa-let-7g-5p	2	up	0.30	0.028	MIMAT0000414	chr3	+	52302319	52302299	AACTGTACAAACTACTACCTC
hsa-miR-103a-3p	3	up	0.15	0.005	MIMAT0000101	chr5	+	167987970	167987953	TCATAGCCCTGTACAATG
hsa-miR-107	2	up	0.17	0.008	MIMAT0000104	chr10	+	91352575	91352557	TGATAGCCCTGTACAATGCT
hsa-miR-1180	24	up	0.30	0.027	MIMAT0005825	chr17	+	19247880	19247869	ACACACCCACGCG
hsa-miR-125a-5p	3	up	0.15	0.005	MIMAT0000443	chr19	-	52196527	52196544	TCACAGGTTAAAGGGTCTC
hsa-miR-128	3	up	0.22	0.013	MIMAT0000424	chr2	-	136423018	136423036	AAAGAGACCGGTTCACTGT
hsa-miR-1285-3p	2	up	0.34	0.038	MIMAT0005876	chr2	+	70480122	70480106	AGGTCTCACTTTGTTGC
hsa-miR-1306-3p	2	up	0.25	0.016	MIMAT0005950	chr22	-	20073639	20073652	CACCACCAGAGCCA
hsa-miR-148b-3p	2	up	0.36	0.048	MIMAT0000759	chr12	-	54731065	54731083	ACAAAGTTCTGTGATGCAC
hsa-miR-152	3	up	0.12	0.002	MIMAT0000438	chr17	+	46114600	46114586	CCAAGTTCTGTCATGC
hsa-miR-185-5p	2	up	0.26	0.018	MIMAT0000455	chr22	-	20020681	20020697	TCAGGAACTGCCTTTCT
hsa-miR-194-5p	63	up	0.12	0.003	MIMAT0000460	chr1	+	220291534	220291519	TCCACATGGAGTTGCT
hsa-miR-1972	2	up	0.29	0.025	MIMAT0009447	chr16	-	70064304	70064317	TGAGCCACTGTGCC
hsa-miR-204-5p	2	up	0.30	0.030	MIMAT0000265	chr9	+	73424944	73424925	AGGCATAGGATGACAAAGGG

hsa-miR-215	61	up	0.04	0.000	MIMAT0000272	chr1	+	220291241	220291222	GTCTGTCAATTCATAGGTCAT
hsa-miR-23b-3p	2	up	0.08	0.001	MIMAT0000418	chr9	-	97847551	97847567	GGTAATCCCTGGCAATG
hsa-miR-26a-5p	2	up	0.15	0.006	MIMAT0000082	chr3	-	38010911	38010925	AGCCTATCCTGGATT
hsa-miR-30c-2-3p	2	up	0.29	0.023	MIMAT0004550	chr6	+	72086730	72086712	AGAGTAAACAGCCTTCTCC
hsa-miR-30d-5p	2	up	0.29	0.026	MIMAT0000245	chr8	+	135817145	135817132	CTTCCAGTCGGGGA
hsa-miR-30e-3p	2	up	0.19	0.010	MIMAT0000693	chr1	-	41220089	41220106	GCTGTAAACATCCGACTG
hsa-miR-3152-3p	2	up	0.30	0.029	MIMAT0015025	chr9	-	18573350	18573369	TTATTGCCCCTATTCTAACA
hsa-miR-3158-5p	2	up	0.28	0.021	MIMAT0019211	chr10	-	103361192	103361206	GAAGGGCTTCCTCTC
hsa-miR-3161	2	up	0.30	0.031	MIMAT0015035	chr11	-	48118351	48118365	ATCTGGGCCTCTGTTC
hsa-miR-324-5p	2	up	0.19	0.010	MIMAT0000761	chr17	+	7126653	7126638	ACACCAATGCCCTAGGG
hsa-miR-342-3p	3	up	0.11	0.002	MIMAT0000753	chr14	-	100576060	100576074	ACGGGTGCGATTTCTG
hsa-miR-3617-5p	61	up	0.04	0.000	MIMAT0017997	chr20	+	44333771	44333755	CCCATCTTGCAACTATG
hsa-miR-374b-5p	2	up	0.34	0.038	MIMAT0004955	chrX	+	73438413	73438395	CACTTAGCAGGTTGTATTA
hsa-miR-379-5p	54	up	0.04	0.000	MIMAT0000733	chr14	-	101488413	101488428	CCTACGTTCCATAGTC
hsa-miR-382-5p	58	up	0.15	0.005	MIMAT0000737	chr14	-	101520659	101520674	CGAATCCACCACGAAC
hsa-miR-432-5p	2	up	0.30	0.031	MIMAT0002814	chr14	-	101350838	101350855	CCACCCAATGACCTACTC
hsa-miR-4443	3	up	0.30	0.027	MIMAT0018961	chr3	-	48238065	48238078	AAAACCCACGCCTCC
hsa-miR-4458	93	up	0.12	0.002	MIMAT0018980	chr5	-	8461049	8461064	TTCTTCCACACCTACCT

hsa-miR-4484	3	up	0.12	0.002	MIMAT0019018	chr10	-	127508379	127508391	TGGGGCTTCTCCCG
hsa-miR-449a	77	up	0.15	0.005	MIMAT0001541	chr5	+	54502153	54502134	ACCAGCTAACAATACACTGC
hsa-miR-449c-5p	43	up	0.30	0.031	MIMAT0010251	chr5	+	54468130	54468115	ACAGCCGCTAGCAATA
hsa-miR-4506	43	up	0.12	0.003	MIMAT0019042	chr14	+	94414641	94414628	TTGCCTCAGACCACC
hsa-miR-4521	56	up	0.13	0.004	MIMAT0019058	chr17	-	8090273	8090287	CTGAGCACAGGACTTC
hsa-miR-4710	39	up	0.32	0.035	MIMAT0019815	chr14	+	105144057	105144044	AACCACCTGCCCTCA
hsa-miR-4726-5p	2	up	0.31	0.032	MIMAT0019845	chr17	-	36875954	36875966	CCACTCCAGGCTCC
hsa-miR-486-5p	23	up	0.30	0.029	MIMAT0002177	chr8	-	41637127	41637140	CTCGGGGCAGCTCA
hsa-miR-493-5p	18	up	0.13	0.003	MIMAT0002813	chr14	-	101335414	101335433	AATGAAAGCCTACCATGTAC
hsa-miR-497-5p	2	up	0.35	0.043	MIMAT0002820	chr17	+	6921273	6921256	ACAAACCACAGTGTGCTG
hsa-miR-498	2	up	0.20	0.012	MIMAT0002824	chr19	-	54177491	54177506	GAAAAACGCCCCCTGGC
hsa-miR-500a-3p	17	up	0.04	0.000	MIMAT0002871	chrX	-	49659834	49659851	CAGAATCCTTGCCCAGGT
hsa-miR-5010-5p	18	up	0.05	0.001	MIMAT0021043	chr17	-	40666231	40666247	AATTTTGCTCTGCCATCC
hsa-miR-502-3p	33	up	0.04	0.000	MIMAT0004775	chrX	-	49779264	49779278	TGAATCCTTGCCCAGG
hsa-miR-5196-5p	37	up	0.28	0.021	MIMAT0021128	chr19	-	35836453	35836465	CCCAACCCTCGTCC
hsa-miR-520c-3p	2	up	0.30	0.031	MIMAT0002846	chr19	-	54210763	54210781	ACCCTCTAAAAGGAAGCACT
hsa-miR-532-3p	3	up	0.36	0.048	MIMAT0004780	chrX	-	49767818	49767831	TGCAAGCCTTGGGTG
hsa-miR-550a-3p	81	up	0.14	0.005	MIMAT0003257	chr7	-	30295999	30296016	ATGTGCCTGAGGGAGTAA

hsa-miR-6134	2	up	0.30	0.031	MIMAT0024618	chrX	+	28513760	28513744	TCTACATCCTACCACCTC
hsa-miR-652-3p	41	up	0.11	0.002	MIMAT0003322	chrX	-	109298623	109298637	CACAACCCTAGTGGC
hsa-miR-7-1-3p	61	up	0.15	0.005	MIMAT0004553	chr9	+	86584749	86584731	TATGGCAGACTGTGATTTG
hsa-miR-744-5p	43	up	0.04	0.000	MIMAT0004945	chr17	-	11985234	11985247	TGCTGTTAGCCCTA
hsa-miR-758-5p	3	up	0.15	0.005	MIMAT0022929	chr14	-	101492379	101492392	GTGTGCTCTCTGGTC
hsa-miR-769-5p	48	up	0.13	0.004	MIMAT0003886	chr19	-	46522223	46522240	AGCTCAGAACCCAGAGGTC
hsa-miR-885-5p	29	up	0.04	0.000	MIMAT0004947	chr3	+	10436204	10436189	AGAGGCAGGGTAGTGTA
hsa-miR-9-5p	2	up	0.34	0.040	MIMAT0000441	chr1	+	156390170	156390152	TCATACAGCTAGATAACCA
hsa-miR-98-5p	3	up	0.34	0.038	MIMAT0000096	chrX	+	53583226	53583206	AACAATACAACTTACTACCTC

Table 7.4: miRNAs downregulated in treatment group VER Vs Control.

Systematic name	FC	Regulation	p (Corr)	p	mirbase accession No	Chr	Strand	Start	Stop	Active sequence
dmr_285	-2	down	0.0	0.000						
hsa-miR-10b-3p	-31	down	0.1	0.006	MIMAT0004556	chr2	-	177015099	177015117	ATTCCCCTAGAATCGAATC
hsa-miR-1225-5p	-3	down	0.1	0.003	MIMAT0005572	chr16	+	2140217	2140208	CCCCCCACTGG
hsa-miR-1227-5p	-3	down	0.1	0.006	MIMAT0022941	chr19	+	2234077	2234067	CCACCGCCTGGC
hsa-miR-1234-3p	-3	down	0.3	0.018	MIMAT0005589	chr8	+	145625557	145625547	GTGGGGTGGGT
hsa-miR-1234-5p	-2	down	0.2	0.008	MIMAT0022944	chr8	+	145625513	145625504	CGGCCCCCCCC
hsa-miR-135a-3p	-5	down	0.2	0.009	MIMAT0004595	chr3	+	52328311	52328299	CGCCACGGCTCCA
hsa-miR-138-2-3p	-3	down	0.2	0.006	MIMAT0004596	chr16	-	56892492	56892507	AACCCTGGTGTCGTGA
hsa-miR-139-3p	-4	down	0.1	0.001	MIMAT0004552	chr11	+	72326171	72326157	ACTCCAACAGGGCCG
hsa-miR-1469	-10	down	0.0	0.000	MIMAT0007347	chr15	-	96876502	96876511	GGAGCCCGCGC
hsa-miR-1587	-2	down	0.3	0.025	MIMAT0019077	chrX	-	39696824	39696835	CCCAACCCAGCCC
hsa-miR-1915-3p	-3	down	0.2	0.016	MIMAT0007892	chr10	+	21785556	21785546	CCCGCCGCGTC
hsa-miR-197-5p	-2	down	0.3	0.026	MIMAT0022691	chr1	-	110141534	110141545	CCTCCCACTGCCC
hsa-miR-2861	-3	down	0.2	0.008	MIMAT0013802	chr9	-	130548259	130548268	CCGCCCACCGC
hsa-miR-3137	-2	down	0.2	0.010	MIMAT0015005	chr3	+	194855264	194855251	ACCCCATTGCTCCCA

hsa-miR-3188	-2	down	0.3	0.030	MIMAT0015070	chr19	-	18392950	18392961	CCCCGTATCCGCA
hsa-miR-3196	-3	down	0.1	0.004	MIMAT0015080	chr20	-	61870146	61870157	GAGGCCCCTGCCG
hsa-miR-3663-3p	-2	down	0.3	0.029	MIMAT0018085	chr10	+	118927268	118927259	GCGCCCGGCCT
hsa-miR-371b-5p	-3	down	0.2	0.008	MIMAT0019892	chr19	+	54290958	54290945	AAAGTGCCGCCATCT
hsa-miR-3940-5p	-2	down	0.3	0.024	MIMAT0019229	chr19	+	6416462	6416452	CAGAGCCCGCCC
hsa-miR-4428	-3	down	0.2	0.016	MIMAT0018943	chr1	-	237634473	237634485	GCTCCATGTTCCCG
hsa-miR-4430	-3	down	0.3	0.040	MIMAT0018945	chr2	-	33643591	33643603	CTCCGCTCACTCCA
hsa-miR-4446-3p	-3	down	0.3	0.041	MIMAT0018965	chr3	-	113313773	113313786	ACCCATGTCACTGCC
hsa-miR-4462	-3	down	0.4	0.045	MIMAT0018986	chr6	+	37523197	37523185	TTCCCAAGCCACCC
hsa-miR-4478	-2	down	0.1	0.004	MIMAT0019006	chr9	+	124882381	124882368	CTCCTCAGCTCAGCC
hsa-miR-4505	-2	down	0.1	0.006	MIMAT0019041	chr14	-	74225458	74225469	TCCGTCCCAGCCC
hsa-miR-4507	-2	down	0.3	0.024	MIMAT0019044	chr14	+	106324343	106324333	CCCAGCCCAGCC
hsa-miR-4515	-2	down	0.3	0.021	MIMAT0019052	chr15	-	83736112	83736122	GGGCTGCCGGGA
hsa-miR-4530	-3	down	0.1	0.001	MIMAT0019069	chr19	+	39900312	39900301	CGCTCCCGTCCTG
hsa-miR-4532	-2	down	0.1	0.001	MIMAT0019071	chr20	-	56470462	56470471	CGCCGGGCTCC
hsa-miR-4538	-2	down	0.3	0.028	MIMAT0019081					TCAGCCCAGCTCATC
hsa-miR-4634	-3	down	0.3	0.022	MIMAT0019691	chr5	-	174178755	174178764	CCCCGGGCCGG
hsa-miR-4636	-33	down	0.3	0.019	MIMAT0019693	chr5	+	9053958	9053942	CTAAAGGCTTTGAACACG

hsa-miR-4647	-26	down	0.1	0.004	MIMAT0019709	chr6	+	44221975	44221961	TTCCTCAGCACAGCAC
hsa-miR-4656	-2	down	0.3	0.036	MIMAT0019723	chr7	+	4828227	4828215	ACAGGCCTCCTGCC
hsa-miR-4665-5p	-3	down	0.1	0.002	MIMAT0019739	chr9	-	6007846	6007857	GCTCGCGCTCACG
hsa-miR-4721	-2	down	0.1	0.003	MIMAT0019835	chr16	+	28855320	28855308	CCACCGTCACCTGG
hsa-miR-4728-5p	-2	down	0.1	0.002	MIMAT0019849	chr17	-	37882758	37882771	TGCTTGCTGCCTCTC
hsa-miR-4739	-2	down	0.3	0.035	MIMAT0019868	chr17	+	77681018	77681007	AGGGCCCCTCCGC
hsa-miR-4741	-2	down	0.1	0.003	MIMAT0019871	chr18	-	20513381	20513392	AGCCGACCCCTCC
hsa-miR-4767	-42	down	0.2	0.011	MIMAT0019919	chrX	-	7065923	7065932	GGCGGCGGCCA
hsa-miR-4787-3p	-37	down	0.0	0.000	MIMAT0019957	chr3	-	50712575	50712584	GCGCGGGGCAG
hsa-miR-4787-5p	-3	down	0.1	0.003	MIMAT0019956	chr3	-	50712535	50712545	GGGATGCCGCCG
hsa-miR-5001-5p	-2	down	0.2	0.008	MIMAT0021021	chr2	+	233415227	233415216	AGCTCCGCCGCTG
hsa-miR-5006-5p	-2	down	0.4	0.046	MIMAT0021033	chr13	+	42142462	42142449	TTCCACCTCCTGCCC
hsa-miR-503-5p	-52	down	0.3	0.022	MIMAT0002874	chrX	+	133680385	133680368	CTGCAGAACTGTTCCCGC
hsa-miR-513a-5p	-3	down	0.0	0.000	MIMAT0002877	chrX	+	146295034	146295019	ATGACACCTCCCTGTG
hsa-miR-513b	-3	down	0.1	0.004	MIMAT0005788	chrX	+	146280596	146280579	ATAAATGACACCTCCTTGT
hsa-miR-513c-5p	-3	down	0.1	0.004	MIMAT0005789	chrX	+	146271256	146271238	ATAAACGACACCTCCTTGA
hsa-miR-548q	-126	down	0.1	0.003	MIMAT0011163	chr10	+	12767281	12767267	CCGCCATTACTTTTGC
hsa-miR-5585-3p	-96	down	0.1	0.006	MIMAT0022286	chr1	-	32552594	32552608	ACCTGTAGTCCCAGCT

hsa-miR-575	-4	down	0.1	0.003	MIMAT0003240	chr4	+	83674568	83674552	GCTCCTGTCCAACTGGCT
hsa-miR-6068	-4	down	0.1	0.002	MIMAT0023693	chr1	+	63792616	63792606	CCACCGCCGGAG
hsa-miR-6089	-3	down	0.3	0.028	MIMAT0023714	chrX	-	2527283	2527293	CCGCCCCGCCC
hsa-miR-6090	-2	down	0.3	0.021	MIMAT0023715	chr11	-	128392334	128392343	GCCCCGCCCCT
hsa-miR-6125	-3	down	0.1	0.004	MIMAT0024598	chr12	-	62654208	62654218	TCCGCCGCTCCG
hsa-miR-638	-3	down	0.3	0.019	MIMAT0003308	chr19	-	10829107	10829119	AGGCCGCCACCCGC
hsa-miR-650	-15	down	0.4	0.047	MIMAT0003320	chr22	-	23165291	23165305	GTCCTGAGAGCGCTGC
hsa-miR-6722-3p	-2	down	0.3	0.042	MIMAT0025854	chr9	+	139641412	139641402	CCTGGCCCACCC
hsa-miR-718	-9	down	0.3	0.036	MIMAT0012735	chrX	+	153285432	153285423	CGACGCCCGGC
hsa-miR-921	-6	down	0.4	0.044	MIMAT0004971	chr1	+	166124005	166123990	GAATCCTGGTTCTGTCC
hsa-miR-940	-4	down	0.3	0.020	MIMAT0004983	chr16	-	2321817	2321827	GGGGAGCGGGGG

7.3 Primer Design

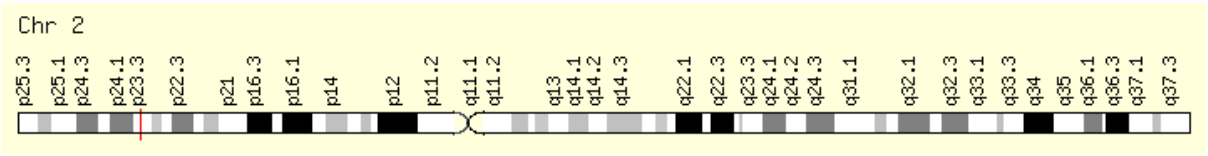

Figure 7.3: Gene location of *Dnmt3a* using GeneCards database. Red bar represents location of *Dnmt3a.*

1251	tggtggccag	gccgcattgt	gtcttggtgg	atgacgggcc	ggagccgagc
1301	agctgaaggc	acccgctggg	tcatgtggtt	cggagacggc	aaattctcag
1351	tggtgtgtgt	tgagaagctg	atgccgctga	gctcgttttg	cagtgcgttc
1401	caccaggcca	cgtacaacaa	gcagcccatg	taccgcaaag	ccatctacga
1451	ggtcctgcag	gtggccagca	gccgcgcggg	gaagctgttc	ccggtgtgcc
1501	acgacagcga	tgagagtgac	actgccaagg	ccgtggaggt	gcagaacaag
1551	cccatgattg	aatgggccct	gggggggcttc	cagccttctg	gccctaaggg
1601	cctggagcca	ccagaagaag	agaagaatcc	ctacaaagaa	gtgtacacgg
1651	acatgtgggt	ggaacctgag	gcagctgcct	acgcaccacc	tccaccagcc
1701	aaaaagcccc	ggaagagcac	agcggagaag	cccaaggtca	aggagattat
1751	tgatgagcgc	acaagagagc	ggctggtgta	cgaggtgcgg	cagaagtgcc
1801	ggaacattga	ggacatctgc	atctcctgtg	ggagcctcaa	tgttaccctg
1851	gaacaccccc	tcttcgttgg	aggaatgtgc	caaaactgca	agaactgctt
1901	tctggagtgt	gcgtaccagt	acgacgacga	cggctaccag	tcctactgca
1951	ccatctgctg	tgggggccgt	gaggtgctca	tgtgcggaaa	caacaactgc
2001	tgcaggtgct	tttgcgtgga	gtgtgtggac	ctcttggtgg	ggccgggggc
2051	tgcccaggca	gccattaagg	aagacccctg	gaactgctac	atgtgcgggc
2101	acaagggtac	ctacgggctg	ctgcggcggc	gagaggactg	gccctcccgg
2151	ctccagatgt	tcttcgctaa	taaccacgac	caggaatttg	accctccaaa
2201	ggtttaccca	cctgtcccag	ctgagaagag	gaagcccatc	cgggtgctgt
2251	ctctctttga	tggaatcgct	acagggctcc	tggtgctgaa	ggacttgggc
2301	attcaggtgg	accgctacat	tgcctcggag	gtgtgtgagg	actccatcac
2351	ggtgggcatg	gtgcggcacc	aggggaagat	catgtacgtc	ggggacgtcc

Figure 7.4: mRNA sequence of *Dnmt3a* & the locations of the primers using NCBI database. Primer locations have been highlighted in blues and yellow indicating sense and antisense primers, respectively.

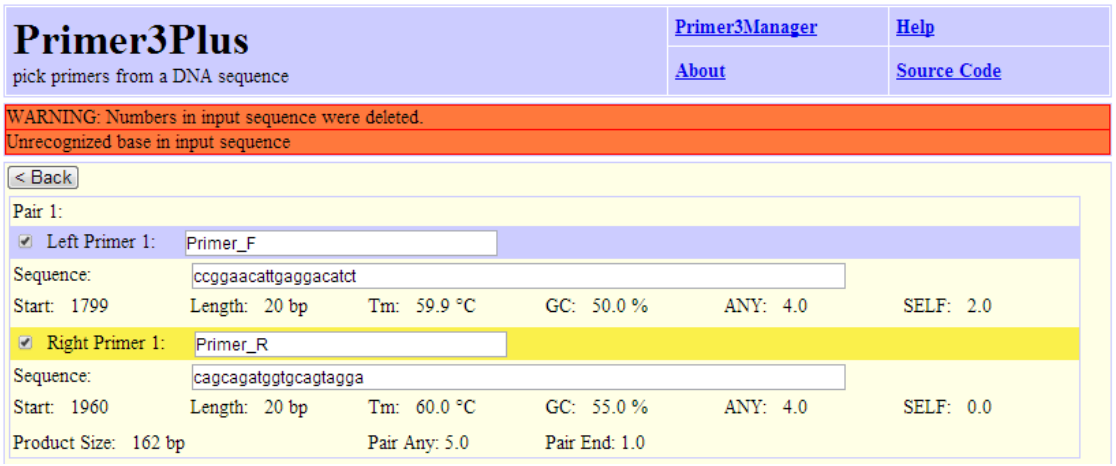

Figure 7.5: Primer design of *Dnmt3a* gene using Primer3Plus. The output page of Primer3 provides the right and the left primers.

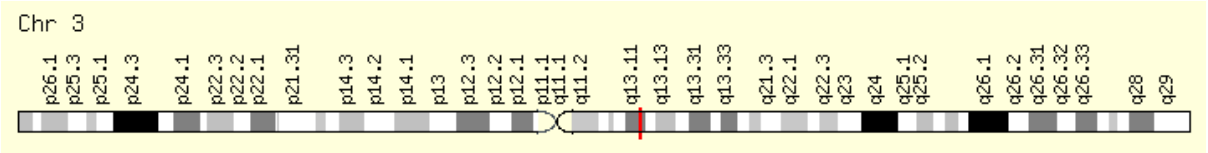

Figure 7.6: Gene location of *Alcam* using GeneCards database. Red bar represents location of *Alcam*.

301	acctggcgtt	tcatgcacat	tgccactgcc	attattatta	tcattccaat
351	acaaggaaaa	taaaagaaga	taccagcgaa	aagaaccgct	tacacctttc
401	cgaattactc	aagtgtctcc	tggaaacaga	gggtcgttgt	ccccggagga
451	gcagccgaag	ggcccgtggg	ctggtgttga	ccgggaggga	ggaggagttg
501	ggggcattgc	gtggtggaaa	gttgcgtgcg	gcagagaacc	gaaggtgcag
551	cgccacagcc	caggggacgg	tgtgtctggg	agaagacgct	gcccctgcgt
601	cgggacccgc	cagcgcgcgg	gcaccgcggg	gcccgggacg	acgccccctc
651	ctgcggcgtg	gactccgtca	gtggcccacc	aagaaggagg	aggaatatgg
701	aatccaaggg	ggccagttcc	tgccgtctgc	tcttctgcct	cttgatctcc
751	gccaccgtct	tcaggccagg	ccttggatgg	tatactgtaa	attcagcata
801	tggagatacc	attatcatac	cttgccgact	tgacgtacct	cagaatctca
851	tgtttggcaa	atggaaatat	gaaaagcccg	atggctcccc	agtatttatt
901	gccttcagat	cctctacaaa	gaaaagtgtg	cagtacgacg	atgtaccaga
951	atacaaagac	agattgaacc	tctcagaaaa	ctacactttg	tctatcagta
1001	atgcaaggat	cagtgatgaa	aagagatttg	tgtgcatgct	agtaactgag
1051	gacaacgtgt	ttgaggcacc	tacaatagtc	aaggtgttca	gtaagtagtc
1101	tgcagcagtg	tcactgctaa	gtgggattga	tggccagtac	cagaccatgt
1151	tctttagaaa	gaagactgaa	ctctctgtag	tgtctctata	gcaggtatct
1201	atataagggg	acttaaagag	atcttcattc	tgctcatata	tactatcagc
1251	aaagaaaaca	aagagtatga	aattcaaata	ggagatttgc	agtgaggaac
1301	taaaataata	ttctctgtta	ctttgtcatg	taaaaatgtc	gtgagctatg
1351	aagtactact	actgataact	agcaggtgat	cttaattttt	actgacatgt
1401	acaaataagt	gttgtgtgat	acatacatag	atatatgata	tatatgtaat
1451	catgtatatc	acgcatacat	atacatgtat	ttggctgaac	caaatgaaat
1501	tgccattttg	ctgcataata	aaaaaatata	agcaaattca	aactatattt
1551	taacagaggt	ataaattttc	catttatata	tatccacata	tataaatatc

Figure 7.7: mRNA sequence of *Alcam* & the locations of the primers using NCBI database. Primer locations have been highlighted in blues and yellow indicating sense and antisense primers, respectively.

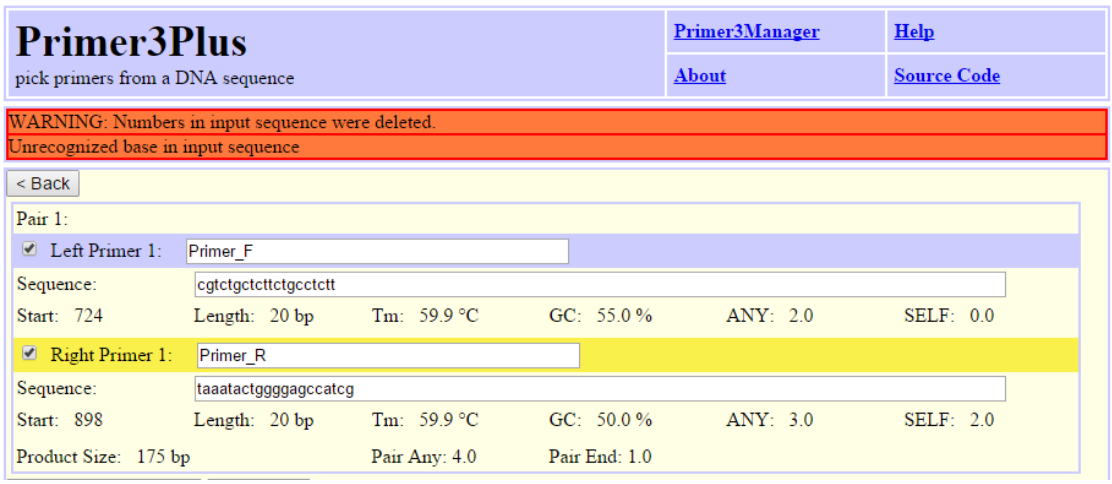

Figure 7.8: Primer design of *Alcam* gene using Primer3Plus. The output page of Primer3 provides the right and the left primers.

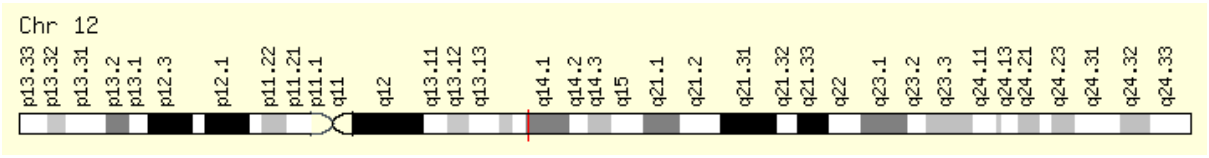

Figure 7.9: Gene location of *Cdk4* using GeneCards database. Red bar represents location of *Cdk4*.

```
401    gtgagagtcc  ccaatggagg  aggaggtgga  ggaggccttc  ccatcagcac
451    agttcgtgag  gtggctttac  tgaggcgact  ggaggctttt  gagcatccca
501    atgttgtccg  gctgatggac  gtctgtgcca  catcccgaac  tgaccgggag
551    atcaaggtaa  ccctggtgtt  tgagcatgta  gaccaggacc  taaggacata
601    tctggacaag  gcacccccac  caggcttgcc  agccgaaacg  atcaaggatc
651    tgatgcgcca  gtttctaaga  ggcctagatt  tccttcatgc  caattgcatc
701    gttcaccgag  atctgaagcc  agagaacatt  ctggtgacaa  gtggtggaac
751    agtcaagctg  gctgactttg  gcctggccag  aatctacagc  taccagatgg
801    cacttacacc  cgtggttgtt  acactctggt  accgagctcc  cgaagttctt
851    ctgcagtcca  catatgcaac  acctgtggac  atgtggagtg  ttggctgtat
901    ctttgcagag  atgtttcgtc  gaaagcctct  cttctgtgga  aactctgaag
951    ccgaccagtt  gggcaaaatc  tttgacctga  ttgggctgcc  tccagaggat
1001   gactggcctc  gagatgtatc  cctgccccgt  ggagcctttc  cccccagagg
1051   gccccgccca  gtgcagtcgg  tggtacctga  gatggaggag  tcgggagcac
1101   agctgctgct  ggaaatgctg  acttttaacc  cacacaagcg  aatctctgcc
1151   tttcgagctc  tgcagcactc  ttatctacat  aaggatgaag  gtaatccgga
1201   gtgagcaatg  gagtggctgc  catggaagga  agaaaagctg  ccatttccct
1251   tctggacact  gagagggcaa  tctttgcctt  tatctctgag  gctatggagg
1301   gtcctcctcc  atctttctac  agagattact  ttgctgcctt  aatgacattc
1351   ccctcccacc  tctccttttg  aggcttctcc  ttctccttcc  catttctcta
1401   cactaagggg  tatgttccct  cttgtccctt  tccctacctt  tatatttggg
1451   gtccttttt  atacaggaaa  aacaaaacaa  agaaataatg  gtctttttt
1501   tttttttaat  gtttcttcct  ctgtttggct  ttgccattgt  gcgatttgga
1551   aaaaccactt  ggaagaaggg  actttcctgc  aaaaccttaa  agactggtta
1601   aattacaggg  cctaggaagt  cagtggagcc  ccttgactga  caaagcttag
```

Figure 7.10: mRNA sequence of *Cdk4* & the locations of the primers using NCBI database. Primer locations have been highlighted in blues and yellow indicating sense and antisense primers, respectively.

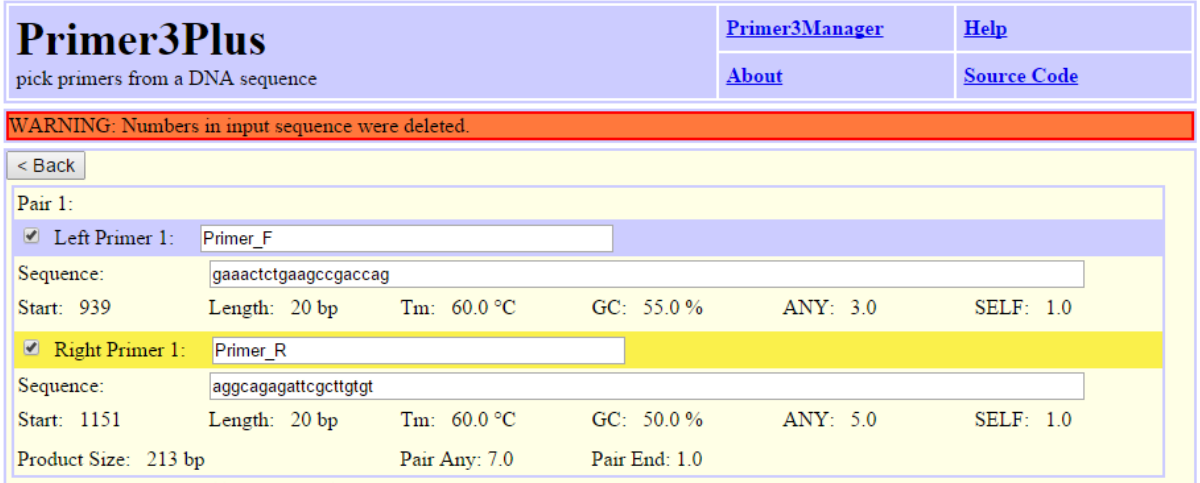

Figure 7.11: Primer design of *Cdk4* gene using Primer3Plus. The output page of Primer3 provides the right and the left primers.

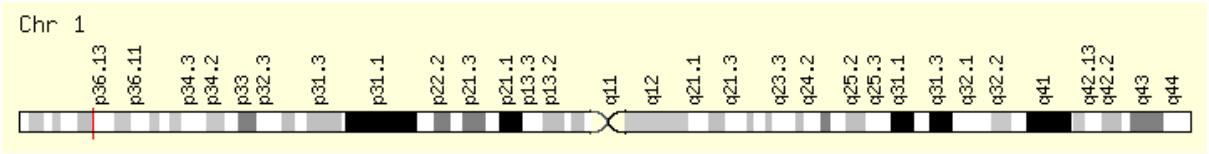

Figure 7.12: Gene location of *Dnajc16 (Hsp40)* using GeneCards database. Red bar represents location of *Dnajc16(Hsp40).*

3951	agacagagtt	tcactcttgt	tgcccaggct	ggagtgaaat	ggtgcgatct
4001	cggttcaccg	caacctccac	atcccaggtt	caagtgattc	tcctgcctca
4051	gcctcctgag	tagctaggat	tacaggcatg	tgccaccatg	taattagccc
4101	ggctaatttt	gtatttttag	tagagacggg	atttctccat	gttgatcagg
4151	ctggtcatga	actcctgacc	tcaggtgatc	tgcctgcctc	agcctcccaa
4201	agtgctgctg	ggattacagg	cgtgagccac	cactcccggc	taagttagta
4251	tttctttaat	cttaatgctt	taaactaagc	cacttggatc	ctgaataatt
4301	taaatcttga	gctacattgg	taagtaataa	attatttaag	gccaggaatt
4351	cctgtagttt	tcatggagtc	tgtagcttta	ttaaaaaata	aatcactgcc
4401	aggcttcatt	cttccatatg	atcctctaaa	aatggacact	tcctctgaat
4451	gctgtatctc	atggcacctg	gtccaactag	aaatggtcaa	ggaattcatt
4501	tggctccttg	atacatcagt	cctcaatatt	actttctagg	tattttatgg
4551	ccagattgct	tatatgagtg	gtcttttggt	ttggtagtag	gtttttattt
4601	ttaatttctg	tactaatgaa	attcctgact	ttaatttctg	aaaaccaaaa
4651	actctccaag	tgtatttatt	tatatttttt	ttaatagaga	cgaggtcttg
4701	ctatgttgcc	caggctggtc	ccaaactcct	ggcctcaagc	agtccttcca
4751	ccttggcctc	ccaaagtgct	gggattatca	atatgagcca	ccatgccaga
4801	tttgttcatt	tttaaacatt	tttatctctt	caagtcatct	tttgatcttt
4851	taaaaagcac	cttcaaacag	ctgcaccttc	catttgcact	aggaaatgaa
4901	ggtagtgatg	ggattggcaa	tgttcctggc	agatgtttca	gcccaaaagc
4951	tcttctacag	accggtttag	agctggtgcc	ctatgagaat	attagggagc

Figure 7.13: mRNA sequence of *Dnajc16 (Hsp40)* & the locations of the primers using NCBI database. Primer locations have been highlighted in blues and yellow indicating sense and antisense primers, respectively.

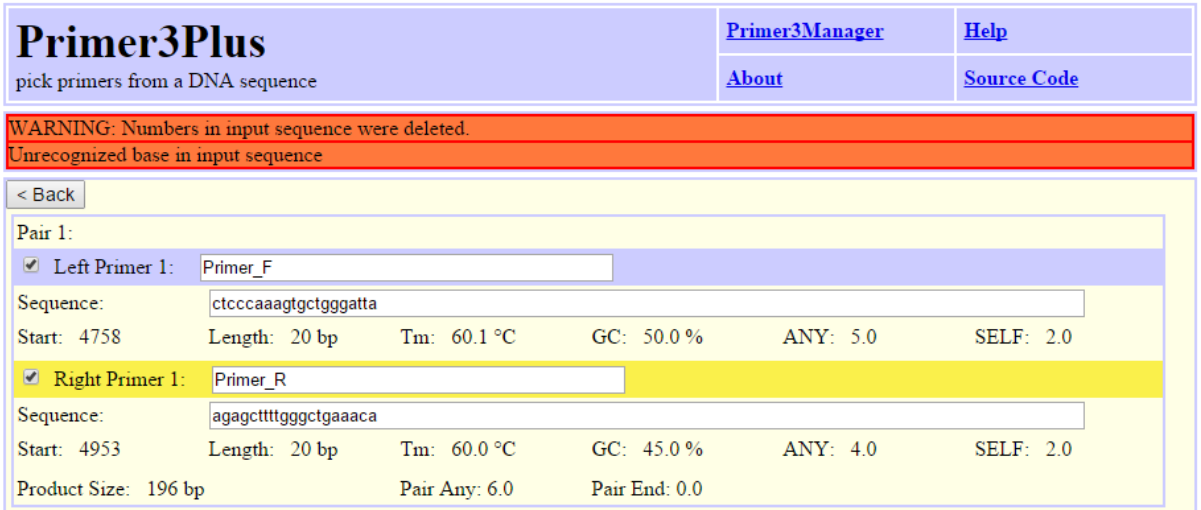

Figure 7.14: Primer design of *Dnajc16 (Hsp40)* gene using Primer3Plus. The output page of Primer3 provides the right and the left primers.

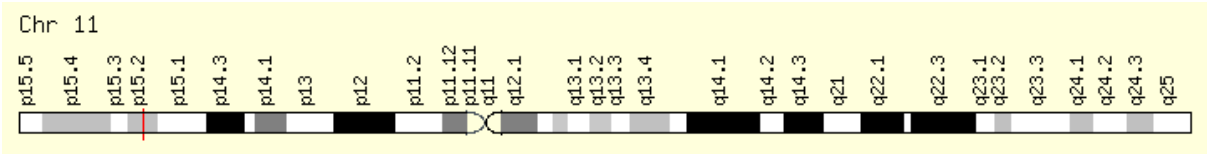

Figure 7.15: Gene location of *R-Ras2* using GeneCards database. Red bar represents location of *R-Ras2*.

```
301   tctgtagcgt  ccccatggcc  gcggccggct  ggcgggacgg  ctccggccag
351   gagaagtacc  ggctcgtggt  ggtcggcggg  ggcggcgtgg  gcaagtcggc
401   gctcaccatc  cagttcatcc  agtcctattt  tgtaacggat  tatgatccaa
451   ccattgaaga  ttcttacaca  aagcagtgtg  tgatagatga  cagagcagcc
501   cggctagata  ttttggatac  agcaggacaa  gaagagtttg  gagccatgag
551   agaacagtat  atgaggactg  gcgaaggctt  cctgttggtc  ttttcagtca
601   cagatagagg  cagttttgaa  gaaatctata  agtttcaaag  acagattctc
651   agagtaaagg  atcgtgatga  gttcccaatg  attttaattg  gtaataaagc
701   agatctggat  catcaaagac  aggtaacaca  ggaagaagga  caacagttag
751   cacggcagct  taaggtaaca  tacatggagg  catcagcaaa  gattaggatg
801   aatgtagatc  aagctttcca  tgaacttgtc  cgggttatca  ggaaatttca
851   agagcaggaa  tgtcctcctt  caccagaacc  aacacggaaa  gaaaaagaca
901   agaaaggctg  ccattgtgtc  attttctaga  atcccttcag  ttttagctac
951   caacggccag  gaaaagccct  catcttctct  ttctctcctc  agtttacatc
1001  ttgttggtac  ctttctagcc  ttagacaaat  gatcaccatg  ttagccttag
1051  acgaagaagc  tggctagtcc  tttctgtgaa  gctaatacaa  tggtcatttc
1101  cagacaaatt  taaaggaaac  actaaggctg  cttcaaagat  tatctgattc
1151  ctttaaaata  tatgtctata  tacacagaca  tgctcttttt  ttaagtgctt
1201  acatttttaat  agagatgaat  cagttttgga  atctaagctg  tttgccaagc
1251  tgaagctaca  ggttgtgaaa  taatttttaa  cttttgggat  catactgcct
```

Figure 7.16: mRNA sequence of *R-Ras2* & the locations of the primers using NCBI database. Primer locations have been highlighted in blues and yellow indicating sense and antisense primers, respectively.

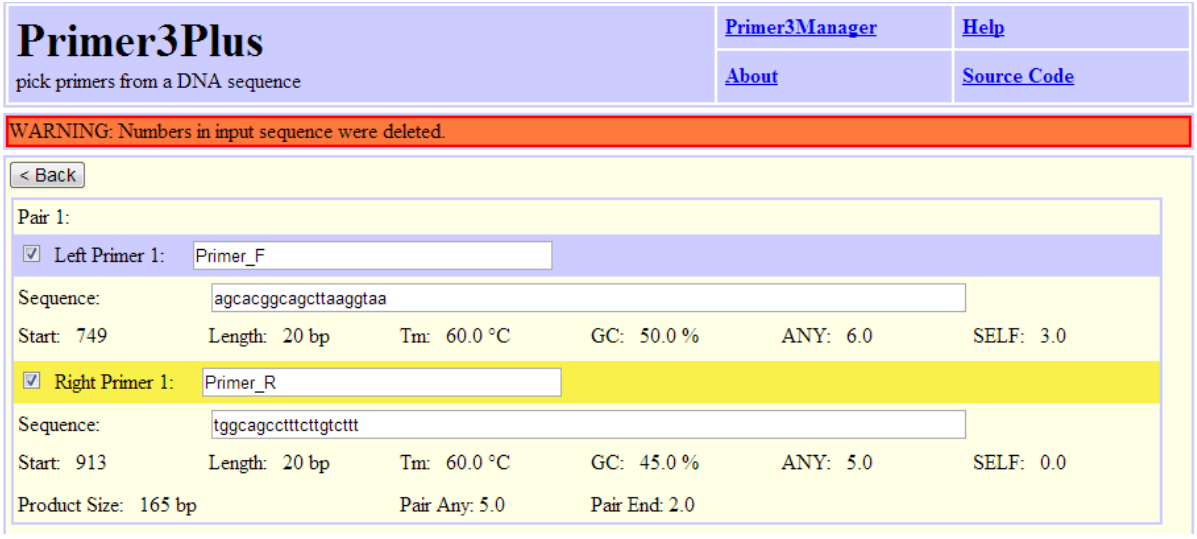

Figure 7.17: Primer design of *R-Ras2* gene using Primer3Plus. The output page of Primer3 provides the right and the left primers.

7.4 Gene expression of predicted target mRNA

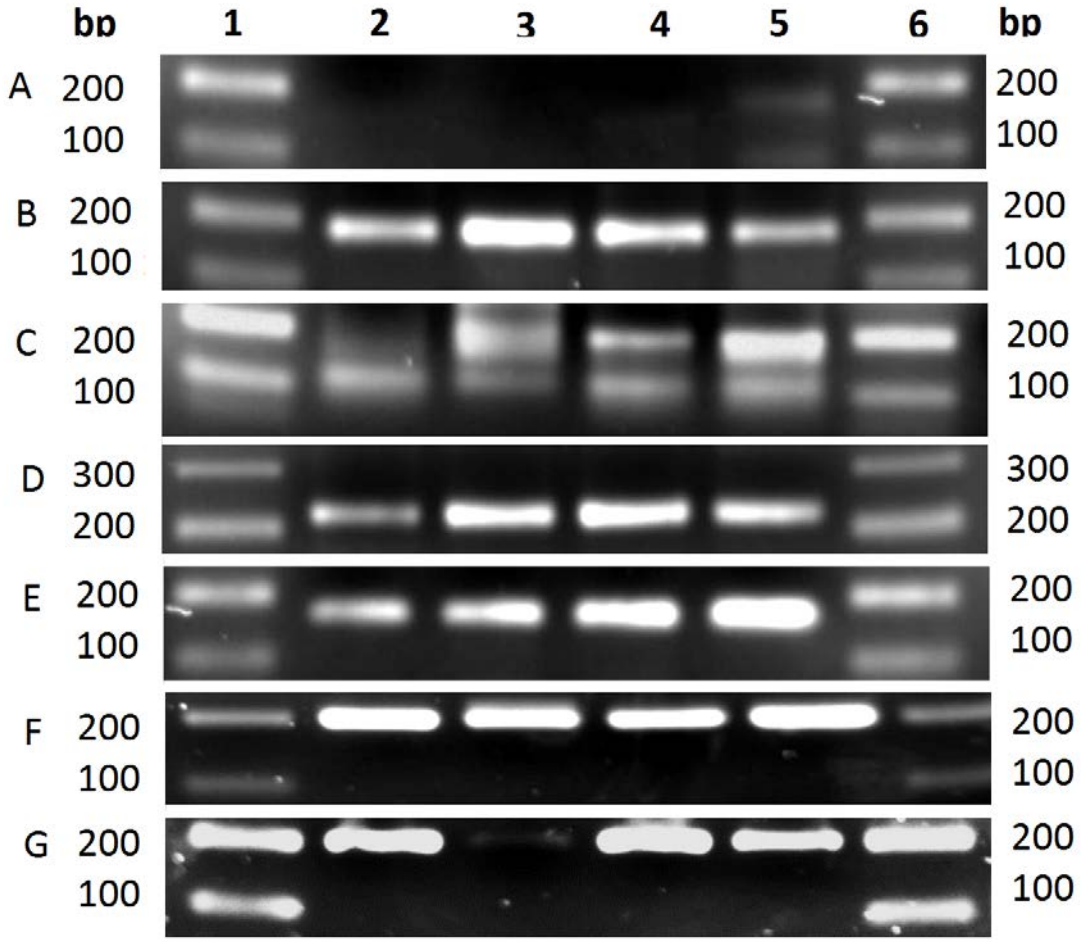

Figure 7.18: Agarose gel electrophoresis of predicted miRNA targets. lane 1 and 6 represents the 100 bp molecular marker, lane 2 represents Untreated control, lane 3 TMZ-treated U87-MG, lane 4 represents 17-AAG-treated U87-MG and lane 5 represents VER-treated U87-MG. (A) *Dnmt3a* (B) *Alcam* (C) *Cdk4* (D) *Dnajc16 (Hsp40)* (E) *R-Ras2* (F) *Hsp70* (G) *Hsp90α.*

CHAPTER 8

PUBLICATIONS AND PRESENTATIONS

8.1 CONFERENCES AND SEMINARS

Sydney Driscoll Neuroscience Foundation annual lectures, Royal Preston Hospital, May 2013 & 2014, Preston, UK.

Annual Research Conference, University of Central Lancashire, 2012, 2013 & 2014, Preston

BTNW annual research meeting, December 2012, 2013 & 2014, Preston, UK.

Biochemical Journal Symposium 2014: Human Therapeutics: Where Biology Meets Chemistry, 20th March 2014, London, UK.

School of Pharmacy and Biomedical sciences seminar series, UCLan, Preston.

Complementary approaches to combat multidrug resistance in Gram-negative bacteria by Dr Roger Draheim on 26th February 2014.

Targeted nanomedicines: role of targeting ligands by Prof Gert Storm on 28th April 2014.

Dual drugs loaded functional solid lipid nanoparticles for synergistic antitumor effects on melanoma stem-like cells by Prof Xun Sun on 22nd October 2014.

The Importance of Native Protein Hierarchy Levels of Structural Organization for Amyloidogenesis: Toward comprehension of biochemical and biophysical aspects underlying misfolding and disease by Dr Alex Quintas on 18th January 2013.

New insights into the roles of metalloproteinases in cancer growth and metastasis by Prof Dylan Edwards on 25th January 2013

Apoptosis impairment in colorectal cancer: Lessons learnt from Systems Modelling by reggfDr Heinrich Huber on 3rd May 2013.

In silico analysis, synthesis and in vitro evaluation of novel anticancer agents by Prof Annie Joubert on 27th September 2013.

8.2 SELECTED ABSTRACTS & PROCEEDINGS

1. Patil, H., Shervington, A., & Shervington, L. (2013) Can Hsp70 be a therapeutic target for Glioma? BNOS annual meeting, Durham,UK.

2. Patil, H., Shervington, A., & Shervington, L. (2013) Can Hsp70 be therapeutic biomarker for treatment of glioma?. UCLan research student conference, Preston, UK.

3. Patil, H, Khan Z, Shervington A, & Shervington L (2012). Can Hsp70/90 be the magic bullet for cancer treatment? UCLan research student conference, Preston, UK.